2013

MODELING EFFECT OF MICROSTRUCTURE ON THE PERFORMANCE OF FIBROUS HEAT INSULATION

Raghu Arambakam
Virginia Commonwealth University

School of Engineering
Virginia Commonwealth University

This is to certify that the dissertation prepared by Raghu Raja Simha Arambakam entitled MODELING EFFECT OF MICROSTRUCTURE ON THE PERFORMANCE OF FIBROUS HEAT INSULATION has been approved by his or her committee as satisfactory completion of the thesis or dissertation requirement for the degree of Doctor of Philosophy

Dr. Hooman V. Tafreshi, School of Engineering

Dr. P. Worth Longest, School of Engineering

Dr. Gary C. Tepper, School of Engineering

Dr. Umit Ozgur, School of Engineering

Dr. Vamsi K. Yadavalli, School of Engineering

Dr. Barbara D. Boyan, Dean of the School of Engineering

Dr. F. Douglas Boudinot, Dean of the School of Graduate Studies

September 20, 2013

MODELING EFFECT OF MICROSTRUCTURE ON THE PERFORMANCE OF FIBROUS HEAT INSULATION

A dissertation submitted in partial fulfillment of the requirements for the degree of Doctor of Philosophy at Virginia Commonwealth University.

by

RAGHU RAJA SIMHA ARAMBAKAM
M. S. in Mechanical and Aerospace Engineering, Oklahoma State University, 2010
B. Tech. in Mechanical Engineering, Jawaharlal Nehru Tech. University, India, 2008

Director: DR. HOOMAN VAHEDI TAFRESHI
ASSOCIATE PROFESSOR, MECHANICAL AND NUCLEAR ENGINEERING

Virginia Commonwealth University
Richmond, Virginia
December 2013

Acknowledgement

I would like to express my sincere gratitude to my advisor, Dr. Hooman Vahedi Tafreshi, for his guidance and support of my PhD study. His immense knowledge, patience and mentorship steered me this far and will always be appreciated. I cannot imagine having a better advisor for my PhD study.

I would also like to thank the members of my committee Dr. P. Worth Longest, Dr. Gary C. Tepper, Dr. Umit Ozgur and Dr. Vamsi K. Yadavalli for their thoughtful suggestions and comments which enriched the quality of this work.

My sincere thanks also go to Dr. Karla Mossi for her mentorship and support throughout my PhD study at VCU.

This work was supported by The Nonwovens Institute at NC State University. Their financial support is gratefully acknowledged.

For their gift of life, love and learning I am truly thankful to my parents Mani and Krishna. I am not capable of expressing enough gratitude to them.

This acknowledgement would not be complete without thanking my other family and friends for their love, support and advice: especially Himaja Arambakam, Venugopal Arambakam, Usha Arambakam, Shashikanth Muthyala, Dr. Ramakrishna Reddy, Nava Davuluri, Sareen Suryadevara, Dr. Pavani Davuluri, Vasudha Surampudi, Dr. Vijender Chaitankar, Bhanu Kamapanthula and maybe Tom Bucher.

Table of Contents

Page

List of Tables

Page

List of Figures

Page

Abstract

MODELING EFFECT OF MICROSTRUCTURE ON THE PERFORMANCE OF FIBROUS HEAT INSULATION

By Raghu Raja Simha Arambakam, M.S.

A dissertation submitted in partial fulfillment of the requirements for the degree of Doctor of Philosophy at Virginia Commonwealth University.

Virginia Commonwealth University, 2013

Major Director: Dr. Hooman Vahedi Tafreshi
Associate Professor, Mechanical and Nuclear Engineering

Heat insulation is the process of blocking the transfer of thermal energy between objects at different temperatures. Heat transfer occurs due to conduction, convection, or radiation, as well as any combination of these three mechanisms. Fibrous insulations can completely suppress the convective mode of heat transfer for most applications, and also help to reduce the conductive and radiative modes to some extent. In this study, an attempt has been made to computationally predict the effects of microstructural parameters (e.g., fiber diameter, fiber orientation and porosity) on the insulation performance of fibrous

materials. The flexible simulation method developed in this work can potentially be used to custom-design optimal multi-component fibrous insulation media for different applications.

With regards to modeling conductive heat transfer, a computationally-feasible simulation method is developed that allows one to predict the effects of each microstructural parameter on the transfer of heat across a fibrous insulation. This was achieved by combining analytical calculations for conduction through interstitial fluid (e.g., air) with numerical simulations for conduction through fibrous structures.

With regards to modeling radiative heat transfer, both Monte Carlo Ray Tracing and Electromagnetic Wave Theory were implemented for our simulations. The modeling methods developed in this work are flexible to allow simulating the performance of media made up of different combinations of fibers with different materials or dimensions at different operating temperatures. For example, our simulations demonstrate that fiber diameter plays an important role in blocking radiation heat transfer. In particular, it was shown that there exists an optimum fiber diameter for which maximum insulation against radiative transfer is achieved. The optimum fiber diameter is different for fibers made of different materials and also depends on the mean temperature of the media.

The contributions of conduction and radiation heat transfer predicted using the above techniques are combined to define a total thermal resistance value for media with different microstructures. Such a capability can be of great interest for design and optimization of the overall performance of fibrous media for different applications.

Chapter 1 General Introduction

1.1 Background Information

Heat insulation is the process of blocking transfer of thermal energy between objects at different temperatures. Heat transfer occurs due conduction, convection, or radiation as well as any combination of these three mechanisms. Conduction can be reduced by eliminating the physical contact between the objects. Convection can be suppressed by suppressing the fluid motion (via friction for instance), and radiation can be minimized by minimizing the view factor between the surfaces. Fibrous insulations can reduce conductive and radiative heat transfer between surfaces. More importantly, they can efficiently eradicate convective mode of heat transfer for most applications, thanks to the significant friction that is caused by their constituent fibers against natural convection (Nield and Bejan, 1998).

Contribution of conduction or radiation to the overall rate of heat transfer through a fibrous medium can vary depending on the physical properties of the fibers and the operating temperature of the surfaces. In addition, for choosing a suitable insulation material for a given application, one has to consider many other factors such as the available space between the walls or the structural stability of the media for the given

environment etc. Therefore, it is important to be able to custom-design optimal insulations for different applications. For such a design process to be effective, it must be based on a mathematical platform that provides quantitative predictions of the contribution of each and every microstructural parameter of constituent fibers to the heat transfer through the media. While the physics of heat transfer in porous media has been studied in numerous studies in the past, an accurate, but yet computationally-feasible, method for design and optimization of an actual product has not been proposed yet.

Insulation materials can be broadly classified into four different categories and the use of different materials depend on the application. The most common type of insulation is loose fill insulation. This type of insulation is usually made by loosely filling the insulation cavity with fibers made of fiber glass, mineral wool or cellulose. These insulations are commonly used as residential insulation. The second type of material is batt or blanket insulation. These are materials usually made of glass or mineral wool fibers which are laid down as blankets in the form of batts or rolls. The third kind of material is rigid board insulation. They are usually made of polystyrene, polyiso, polyurethane or fiber glass. This kind of material is usually preferred for applications where the strength of the insulation structure is crucial and also where the place available for insulation is limited. Another form of insulation material is the spray foam insulation. These insulations are usually obtained by spraying polystyrene, polyiso or polyurethane in molten form at the place of application directly. Also materials like aerogel are being used for high temperature insulations where place availability is limited. However it is not popular yet due to being more expensive than the other insulation materials.

Fiber-based materials represent the single largest mediator of heat insulation in residential and industrial applications. Application of fibrous media extends from ordinary building insulations to the expensive high-temperature insulation materials deployed in the aerospace industry, such as Alumina fibers used in reusable launch vehicles for reentry flights. The large surface area of the fibers provides enough friction to suppress the convection, leaving radiation and conduction to be the only modes of heat transfer in fibrous insulation materials. Contribution of the latter modes of heat transfer, of course, depends on the temperatures imposed on the material—conduction becomes almost negligible when working with high temperatures. While radiative heat transfer is generally important in high-temperature, conductive heat transfer is often the mechanism by which heat transfers through fibrous materials in temperatures near or below room temperature. The gist of most of the work in literature has been to treat the insulation material as a lumped system and study their heat insulation performance. Radiative transfer mostly occurs through the void spaces between the fibers in an insulation medium. The usual approach to such methods is to compute an effective thermal conductivity value which includes the contribution of conduction and radiation heat transfer, and to estimate the net heat transfer through the insulation material using Fourier's law treating the heat transfer as a diffusion process. The main drawback of using such approaches for the treatment of this coupled radiative – conductive heat transfer is its inability to predict the heat transfer of low SVF insulations. The heat transfer through the insulation materials decreases as the SVF of the material decreases, when predicted using the diffusion approximation. However experimental observations

report that as SVF decreases the heat transfer through the material first decreases till it reaches an optimum value and then increases. This is due to the fact that the contribution of radiative transfer increases non-linearly at low SVFs.

1.2 Heat Transfer in Insulation Materials

1.2.1 Convection Heat Transfer

When a temperature gradient is enforced between the opposite sides of a rectangular cavity in the direction of gravity, the colder (denser) fluid tends to move to the bottom of the enclosure (see Figure 1.1). This natural convection should overcome the viscous resistance of the fluid to motion. The relative importance of viscous and gravitational forces is often characterized by Rayleigh number. At low Rayleigh numbers, the viscous forces dominate the gravitational forces and free convection is suppressed. Free convection starts as Rayleigh number increases. Rayleigh number is given as:

$$Ra = \frac{g\beta\Delta TL^3}{\alpha\upsilon} \tag{1.1}$$

For the case of a rectangular cavity with $H / L >> 1$, the critical value of Rayleigh number above which advection becomes important is 1708. At Rayleigh numbers greater than 1708 counter-rotating flow circulation patterns commonly known as Rayleigh–Benard cells start to form (see Figure 1.2).

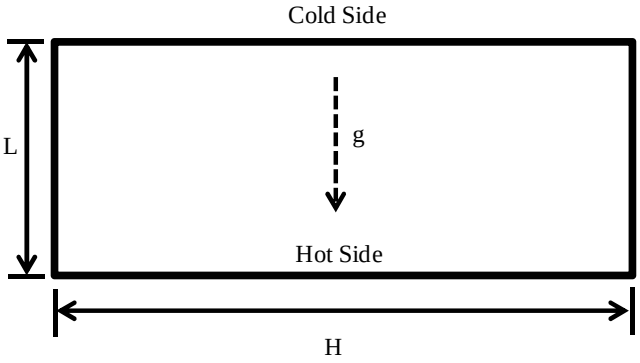

Figure 1.1: Rectangular cavity heated from below, Ra<1708. No convection takes place.

The terms stable and instable systems are also used to describe heat transfer in regime I (Ra<1708) and II (Ra>1708). In stable heat transfer system, convection does not take place.

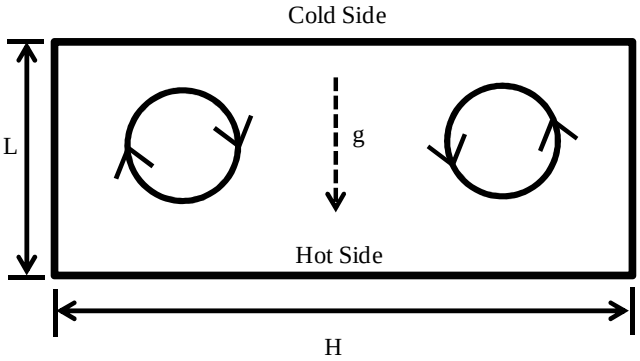

Figure 1.2: Rectangular cavity heated from below, Ra>1708. Benard cells start to appear.

For an empty rectangular cavity (no fibers included in the analysis) with a temperature difference of 900K across its thickness (T_h=1200 K and T_c=300 K) Rayleigh

number remains below 1708 for thicknesses up to about 1.1 cm, i.e., free convection is negligible even without the fibers as far as the thickness is less than 1.1 cm.

For free convection in porous media, the Rayleigh number is defined differently (Nield and Bejan, 1999):

$$Ra^{pm} = \frac{\rho g \beta K L \Delta T}{\mu \alpha_m} \tag{1.2}$$

where $\alpha_m = \frac{k_{eff}}{\rho c_p}$. For the geometry shown in Figure 1.1, when filled with porous media, The critical Rayleigh number for a porous medium, the Rayleigh number above which convection is expected to occur, is about $4\pi^2$ (Nield and Bejan, 1999). Performing an order of magnitude analysis for heat transfer between two walls with a temperature difference on the order of 100 K and a spacing on the order of 0.01 m filled with a fibrous insulation having a fiber diameter on the order of 10 µm, and SVF of about 1% (with air as the interstitial fluid), one obtains a Rayleigh number on the order of magnitude of 0.1. Therefore, one expects convective heat transfer to be negligible for such media as long as their thickness (spacing between the walls) is less than 1 m, on order of magnitude, which practically covers most applications of fibrous insulations. Note that in the above analysis permeability was obtained from the equations given by (Spielmann and Goren, 1968). Decreasing the fiber diameter or increasing the SVF reduces the permeability of a fibrous medium and therefore, suppresses the convection even further. Conversely, decreasing the SVF or increasing the fiber diameter increases the media's permeability and therefore reduces the thickness above which convection is no longer negligible.

1.2.2 Conduction Heat Transfer

Conductive heat transfer occurs through the fibers and the interstitial fluid. Therefore, an effective thermal conductivity, which includes the contributions of the solid and the interstitial fluid, is often defined and used in discussing the performance of an insulation material. The effective thermal conductivity of a fibrous material is greatly influenced by its microstructural parameters such as solid volume fraction (SVF), thermal conductivity of the solid fibers and the interstitial fluid, fiber diameter, and fiber orientation. Obviously, for media consisting of more than one type of fibers, i.e., composite insulation media, there are more parameters influencing the insulation performance (Mohammadi, 2003a)).

Conductive heat transfer through fibrous insulation materials has been studied analytically, numerically, and experimentally. Analytical models have been developed and compared with experiment to predict thermal insulation properties in terms of SVF and thermal conductivity of solid and interstitial phases by (Bankvall, 1973; Bhattacharya, 1980) amongst others. There are also analytical studies dealing with the effects of fiber orientation and fiber length on thermal conductivity (see for instance (Furmanski, 1991; Fu and Mai, 2003)). There are also numerous predominantly experimental studies reporting on the thermal insulation properties of different fibrous materials obtained, for instance, by a guarded hot plate apparatus (Mohammadi, 2003b; Vallabh, 2008). In such studies, performance of the material in blocking conductive and radiative heat transfer is often lumped together in the form of an effective conduction–radiation thermal conductivity (Mohammadi, 2003b; Vallabh, 2008). Improved testing

procedures and more advanced macroscale numerical simulations have also been developed for studying the combined conduction-radiation heat transfer through fibrous media with a specific attention to the effects of operating temperature and pressure on the performance of high-temperature insulations by (Zhang *et al.*, 2008a; Zhang *et al.*, 2008b).

1.2.3 Radiative Heat Transfer

Radiative heat transfer through fibrous insulation materials is often estimated using the Radiative Transfer Equation (RTE), in which the medium is assumed to be a pseudo-continuum (Walters and Buckius 1992). The RTE is a highly involved integro-differential equation that can only be solved numerically. The solution procedure for this equation may need Monte Carlo Ray Tracing (MCRT), experimental, and/or analytical calculations to obtain the radiative characteristics (e.g., scattering phase function) of the media under consideration. Two major approaches have often been considered for determining radiative properties of fibrous insulation media. The first approach is to analytically determine the radiative properties of each individual fiber (or particle) using, for instance, the Electromagnetic wave theory (e.g., Mie theory), and then generalize the properties for the whole medium accounting for its morphology (Larkin and Churchill 1959, Jeandel *et al.* 1993, Lee 1994, Cunnington and Lee 1996 and Lee 1998). The second approach is to experimentally obtain transmittance and reflectance values for the fibrous medium and extract its radiative properties via an inverse method for solving the RTE (Milandri *el al.* 2002, Nicolau *et al.* 1994 and Larkin and Churchill 1959). MCRT

has also been used to estimate the radiative properties of fibrous insulation media or to directly calculate the temperature or heat flux in a system in the absence of a continuum phase (i.e., the air entrapped between the fibers) (Coquard and Baillis 2005, Singh and Kaviany 2006, Coquard and Baillis 2004 and Kumar and Tien 1990).

An IR energy beam looses energy as it travels through a fibrous medium due to scattering and absorption, and gains energy due to in-scattering and fiber emission along its path. Equation for conservation of energy along a given path (direction) with which one can tally the change in energy in a given direction for a small wavelength interval is called Radiative Transfer Equation (RTE) (Howell *et al.*, 2011).

$$\frac{dI}{dS} = -\beta I + \kappa I_b + \frac{\sigma}{4\pi}\int_{\Omega=0}^{4\pi} I(\Omega)\Phi(\Omega)d\Omega \qquad (1.3)$$

The radiative heat that transfers across a fibrous insulation material can be estimated by solving the RTE. In order to obtain these properties both theoretical and experimental methods have been considered in the past. Inverse determination of the radiative properties of an insulation material has been considered using the heat transmittance data obtained from experiments (McKay *et al.*, 1984). The general approach in such studies has been to assume a common form of phase function like (e.g., Henyey–Greenstein phase function) and parametrically vary the scattering and absorption coefficients to make predictions of the RTE match experimental data (Milandri *et al.* 2002; Baillis and Sacadura, 2000).

According to the electromagnetic theory, fiber diameter and temperature are the most important parameters that the treatment of radiative transfer hinges upon. The

electromagnetic theory is well established and has been widely used to describe the interaction of an IR ray with cylindrical objects (Lind and Greenberg, 1966; Liou, 1972). A so-called *size parameter (x)* is defined to relate the radiation wavelength (i.e., temperature) to the fiber diameter (Howell *et al.*, 2011):

$$x = \frac{2\pi r}{\lambda} \tag{1.4}$$

Size parameter determines the nature of the interaction between IR radiation and a fiber in fibrous medium (see Table 1.1). For $x >> 1$, geometric optics can be used for modeling the IR–fiber interaction. Monte Carlo ray tracing which uses geometric optics treatment of IR can be used to predict the temperature or heat flux through a fibrous medium in the absence of the interstitial fluid (e.g., air). For $x \leq 1$, one needs to use the electromagnetic theory to predict the radiative properties of the insulation material and calculate the rate of heat transfer. For many common applications of fibrous insulations, the size parameter is about one ($x \approx 1$). For such cases, the Mie theory was previously used to predict the radiative properties of the insulation materials (Lee, 1989).

Table 1.1: Summary of modeling techniques based on size parameters

size parameter	**modeling technique**	**scattering treatment**	**assumption**
$x \geq 10$	MCRT	laws of geometric optics	wavelength smaller than fiber diameter
$10 > x \geq 0.1$	electromagnetic theory	Mie scattering theory	wavelength comparable to fiber diameter
$x < 0.1$	electromagnetic theory	Rayleigh scattering theory	wavelength greater than fiber diameter

When one of the above techniques is used to determine the radiative flux transmitted through the insulation media, another term called *transmittance* is defined, which is the ratio of total energy received by the sink and the total energy emitted by the source. In order to better describe the radiation process, extinction, scattering and absorption cross-sections and scattering phase functions need to be defined.

The *scattering cross-section* (C_{sca}) is a hypothetical area which describes the likelihood of radiation being scattered by a particle. The scattering cross-section is different from the geometrical cross-section of a particle and it depends on the wavelength of light, refractive index of the fiber, and fiber diameter. Similarly the *absorption cross-section* (C_{abs}) is a hypothetical area which describes the likelihood of radiation being scattered by a particle. The sum of absorption and scattering coefficients is called the extinction coefficient (C_{ext}). Phase function (Φ) is a non-dimensional parameter which is used to describe the angular distribution of scattered radiation (Howell *el al*. 2011 and Modest 2003). The values of radiative properties defined above are a function of temperature, refractive index of the material, fiber orientation, fiber diameter and fiber refractive index. The refractive index of the fibers' parent material is wavelength dependent. At a given temperature, there is a particular wavelength for the emitted IR which carries the greatest energy. This peak wavelength is computed using Planck's law. It is computationally very expensive to conduct the simulations at each and every wavelengths emitted at a given temperature. Therefore, the optical properties used for the simulations are obtained at the peak wavelength associated to the temperature. Impurities can also be important to determining the radiative properties of a substance. It

was recognized that impurities can affect the radiative behavior of a glass fiber (by altering the refractive index) as observed by (Larkin, 1957), for instance. However, this effect is not included in the current study.

When the scenario of heat transfer through fibrous insulation materials is studied, it is obvious that the radiative beam incident on the material heats up the fibers inside the insulation medium. When the fibers' temperatures change the fibers start to emit radiation too. In theory it is assumed that when the fibers are spaced at a certain distance from each other, it can be assumed that the rays emitted by the fibers do not affect the emission process by the neighboring fibers. Such an assumption is called *independent scattering assumption*. This assumption can be safely made for low SVF materials. On the other hand for high SVF materials this assumption breaks down and the interaction between the rays emitted by the fibers must be evaluated. Such cases where the IR interactions are not neglected are grouped as *dependent scattering* regime.

Another common assumption made in such studies is that the fibers are infinitely long. This assumption is made to avoid complicated computations involving the IR interaction with the sharp fiber edges when short fibers are considered. In spite of such assumptions being made the existing theory for computing the radiative properties are proved to make accurate predictions (Lee 1989).

1.3 Virtual Microstructures

To perform micro-scale simulation of heat transfer through fibrous materials, one needs to construct a computational domain that resembles the media's microstructure (see

Figure 1.3). The internal structure of disordered fibrous materials can be considered to fall into one of three main categories: unidirectional structures, where axes of all cylindrical fibers are parallel with one another (Spielman and Goren 1968), layered structures, where axes of cylindrical fibers lie randomly in parallel planes often perpendicular to a fluid flow (Wang *et al.* 2007), and three-dimensionally isotropic structures, where fibers axes can be randomly oriented in any direction in 3-D space (Clague and Phillips 1997) (see Figure 1.3). Fibers in the structures shown in Figure 1.3 a–d are allowed to have random in-plane orientations, but somewhat controlled through-plane orientations. These fibers have a zero mean through-plane orientation, but the standard deviation about this mean value varies from 0 to 45 degrees from one structure to another. Note that a standard deviation of 45 degrees represents a random through-plane orientation. Therefore, structures with through-plane standard deviation of 45 degrees are three-dimensionally isotropic (Figure 1.3d). The structures shown in Figure 1.3 e–h resemble fibrous media with layered microstructures (i.e., no through-plane orientations). The fibers in these structures have a zero mean in-plane orientation, but a standard deviation about this mean value that varies from 0 to 45 degrees from one structure to another. The media generation process is based on the so called μ-randomness algorithm (Pourdeyhimi *et al.* 2006). In the current study, a polydisperse fibrous structure was not used because it does not add any additional value to the methods developed here. Polydisperse fibrous structures can be simulated with the methods developed here at expense of extra CPU time. Polydisperse simulations will

require fiber diameter distributions to be empirically obtained and input to the model (case specific, lacking universality).

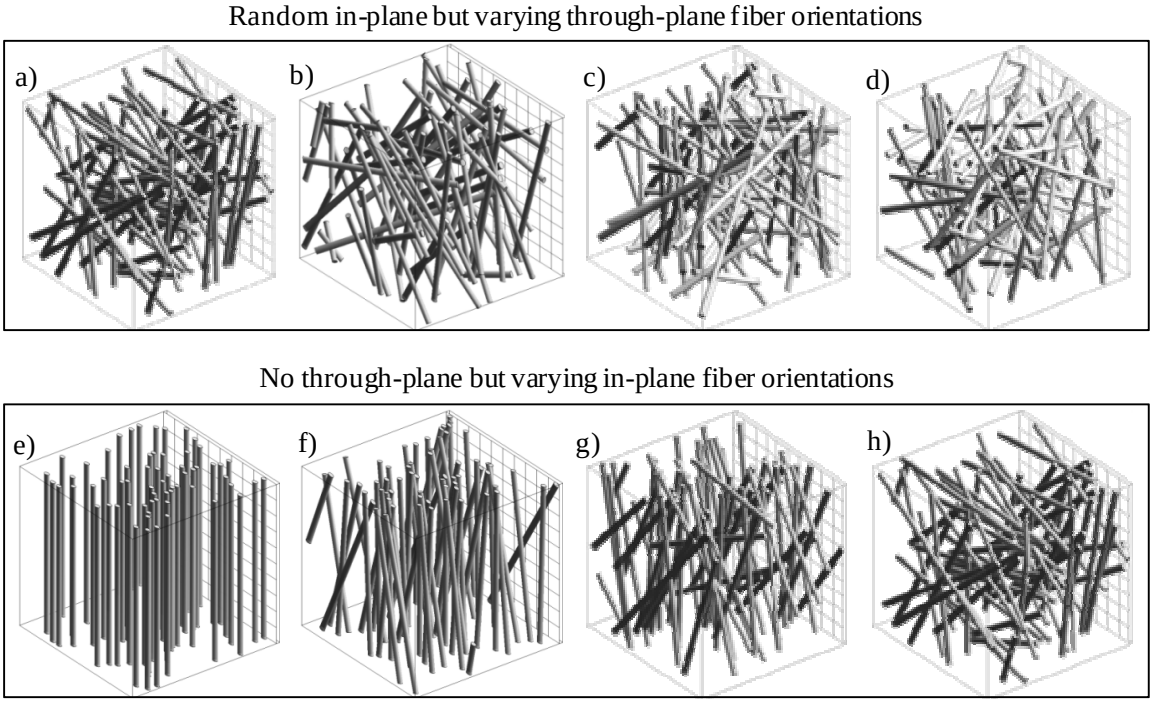

Figure 1.3: Fibrous media with random in-plane fiber orientations but different through-plane fiber orientations having standard deviations of 0 degree (a), 15 degrees (b), 30 degrees (c), and 45 degrees (d); fibrous media with zero through-plane fiber orientations but different in-plane fiber orientations having standard deviations of 0 degree (e), 15 degrees (f), 30 degrees (g), and 45 degrees (h).

1.4 Objective of the Work

The objective of this work is to build a design tool for insulation material development. A simulation method which can be used by insulation manufacturers to optimize the microstructure of an insulation material before manufacturing the material for a specific application (temperature range, thickness …) was developed.

In the current study, different modes of heat transfer were isolated and the material's microstructural parameters' influence on the heat transport through a fibrous structure is investigated at steady state. This study is focused on developing 3-D simulation algorithms for modeling radiative heat transfer via MCRT and Mie theory. The work also includes a study of the influence of geometrical parameters of a fibrous insulation on conductive heat transfer. The study also entails a comprehensive study on heat transfer through multi-component layered (i.e., composite) insulation materials. The proposed computational approach allows one to decouple the contributions of solid structure in the total conductive heat transfer from that of the interstitial fluid and study them separately.

In Chapter 2 numerical simulations to study the effective thermal conductivity of fibrous media with different microstructural parameters are presented. Assuming that the heat transfer through the interstitial fluid is independent of the geometrical parameters of the solid phase (for when the porosity is held constant), the energy equation was solved only for the solid structures, and the resulting values were used to predict the effective thermal conductivity of the whole media. This treatment allows the user to drastically reduce the computational cost of such simulations. Effect of different microstructural parameters on heat conduction was also studied.

In Chapter 3, a Monte Carlo Ray Tracing (MCRT) simulation technique is developed to study steady-state radiative heat transfer through fibrous insulation materials. Scattering within the realm of geometric optics is incorporated into the MCRT simulations using Snell's Law for ray refraction. Fibers' optical properties are obtained

from Fresnel's law and Beer's law based on the refractive index of the material. Two different treatments of "high" and "low" conductivities are considered for the fibers and their effects are discussed. A comprehensive parameter study was performed.

Chapter 4 focusses on development of a dual-scale computationally-feasible 3-D method to simulate the transfer of radiative heat through fibrous media comprised of fibers with different diameters and orientations. The radiative properties of the media are calculated using Mie theory and are used in the Radiative Transfer Equation (RTE) equation for computing the attenuation and augmentation of an InfraRed ray's energy as it travels through a fibrous medium.

In Chapter 5, the techniques developed in Chapter 2 and Chapter 4 are used to predict heat transfer through virtual multi-component fibrous insulations. The method involves computing the conduction and radiation resistance of the media individually and combining them using method of parallel resistances to obtain a total thermal resistance value.

In Chapter 6 the conclusions drawn from the work are presented followed by the author's recommendations for future study.

Chapter 2 Modeling Steady State Conduction in Fibrous Media[1]

2.1 Introduction

To better investigate the effects of microstructural parameters on the performance of fibrous insulation materials exposed to conductive heat flow, microscale 3-D simulations are developed. Such a simulation methodology is valuable as it allows one to isolate the effect of each individual parameter and study its influence on the performance of the whole media (i.e., the fibrous structure and the interstitial fluid). Since heat transfer through the interstitial fluid takes place independently from the geometrical parameters of the solid phase (for a given porosity), the energy equation was solved for the solid phase (fibrous structure) only. The conductivity values obtained for the solid structure can then be easily combined with the conductivity of the interstitial fluid to predict the effective thermal conductivity of the whole media if needed. This treatment allows us to significantly reduce the computational cost of such simulations (compared to the case where air is included in the simulations), and thereby to make a comprehensive parameter study feasible. In particular, with this treatment, one can consider much larger

[1] Contents of this section have been published in an article entitled "A simple simulation method for designing fibrous insulation materials", by R. Arambakam, H.V. Tafreshi, and B. Pourdeyhimi, *Materials and Design* **44**, 99 (2013).

computational domains for simulation to reduce the statistical errors associated with each simulation, and consequently produce a large simulation dataset.

2.2 Conduction in Fibrous Media

Conductive heat travels through both the fibers and the interstitial fluid (often air). Conductive heat transfer formulations for porous media are often developed considering heat flowing in parallel or series paths. When heat flow is assumed to occur in a series mode, then flow of thermal energy is assumed to occur in sequence through a series of layers. Conductive heat transfer is said to occur in parallel mode if the flow of heat is described through simultaneous parallel paths through the medium. In calculations the thermal conductance of each path is added to derive a total rate of heat flow through the entire medium (Bankvall, 1973; Bhattacharya, 1980). The most basic expression (Eq. (2.1)) for defining an effective thermal conductivity in porous media is developed based on a weighted average of the thermal conductivity values of the fibers and interstitial fluid (Bankvall, 1973; Bhattacharya, 1980), and heat transfer is assumed to occur in a parallel mode through solid and the interstitial fluid.

$$k_{eff} = \alpha k_f + (1-\alpha) k_g \tag{2.1}$$

The major problem with this equation is that it assumes the solid phase to act like a solid block connecting the heat source to the heat sink, neglecting the fact that heat has to flow through a number of small fiber-to-fiber contact areas before it can reach the sink. Therefore, one can expect that the term αk_f in the above equation significantly over-predicts the conductivity of the solid phase. The second term in the right-hand side of Eq.

(2.1), on the other hand, is expected to be quite accurate in predicting the conductivity of the fluid phase. This is because the interstitial fluid does connect the source and sink plates with no considerable bottle-necks in the heat flow path, at least for most practical fibrous structures (i.e., porous media with very low solid volume fractions).

2.2.1 Modeling Conductive Heat Transfer in Fibrous Media

An in-house MATLAB code was developed to generate fibrous structures with different structural parameters—virtual fibrous media with controlled porosity, thickness, and fiber diameter, as well as fibers in-plane and though-plane orientations (see Figure 1.3). Due to the randomness of the generation process, each simulation is repeated at least three times to reduce the statistical uncertainty of the results presented. After each fibrous structure is produced, a script file is produced for the GAMBIT software in which the actual SVF of the structure is measured and also is meshed using tetrahedral elements and exported to the Fluent code for heat transfer calculations.

The fibrous structures were considered to be sandwiched between a hot and cold plate as shown in Figure 2.1. A temperature gradient is imposed across the thickness of the media by assigning different temperatures to the hot and cold plates. The steady-state heat equation is solved for the flow of conductive heat through the fibers using the Fluent CFD code.

$$\frac{\partial^2 T}{\partial x^2}+\frac{\partial^2 T}{\partial y^2}+\frac{\partial^2 T}{\partial z^2}=0 \qquad (2.2)$$

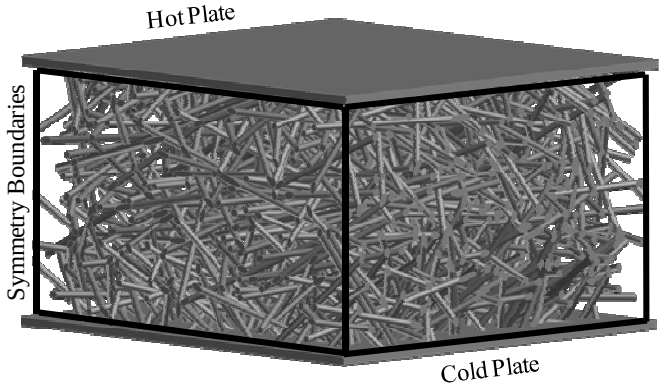

Figure 2.1: An example of the computational domains used in the study with corresponding boundary conditions. The fibrous structure shown here has a 3-D isotropic fiber orientation (i.e., three-dimensionally random fiber orientations).

Symmetry boundary condition has been considered for all lateral boundaries of the simulation domain. Although no plane of symmetry can actually exist in a disordered fibrous structure, the error associated with such a boundary condition is negligibly small when a large computational domain is considered for the simulations as the heat flow is mainly in the direction of the macroscopic temperature gradient (i.e., through-plane direction) (Wang *et al.*, 2007). The boundary conditions considered in the current simulations are shown in Figure 2.1. An arbitrary fiber thermal conductivity of 0.2 W/m-K (polypropylene) and a fiber diameter of 8μm were considered unless otherwise specified. The temperatures of the hot and cold plates are also arbitrarily chosen to be 330K and 300K, respectively. Since no air is considered in the calculations, heat transfer between the hot and cold plates is due only to conduction in the solid phase.

$$k_s = \frac{qL}{A\Delta T} \tag{2.3}$$

where q is the heat flux computed using Fluent, L is the thickness of the medium, A is the area of one of the heat plates and ΔT is the imposed temperature difference between the plates.

Thermal and electrical conductivities of a fibrous structure are greatly influenced by the fiber-to-fiber contact area at the fibers' crossover points (Faessel *et al.*, 2005; Zhang and Yi, 2008; Zhao *et al.*, 2009; Zhou *et al.*, 2012). Depending on the process by which a fibrous mat is produced, the fiber-to-fiber contact area may be negligibly small (e.g., when the fibers are perfectly cylindrical) or considerable large (e.g., when the fibers are at a melt state during the mat formation and fuse together at the crossover points, or bonded together via an adhesive). Accurate determination of the fiber-to-fiber contact area in fibrous mats is a challenge, as it depends on so many parameters such as material of the fibers and the fiber formation process (e.g., fiber spinning process) as well as the mat formation and mat consolidation processes, to name a few. It is therefore, unlikely that a universal correlation for the fiber-to-fiber contact area can be developed. To circumvent this problem when modeling the fibers which are perfectly round, the fibers were allowed to interpenetrate into one another (see Figure 2.2).

A restriction on the allowable distance between the axes of two fibers was placed at their crossover points to somehow control the extent of fiber-fiber interpenetration. The allowable distance between two fibers is non-dimensionalized using the fiber diameter d_f and is shown here with d^*. This simple treatment allows us to simulate a fibrous structure consisting of perfectly round fibers, but yet produce finite contact areas for the flow of conductive heat.

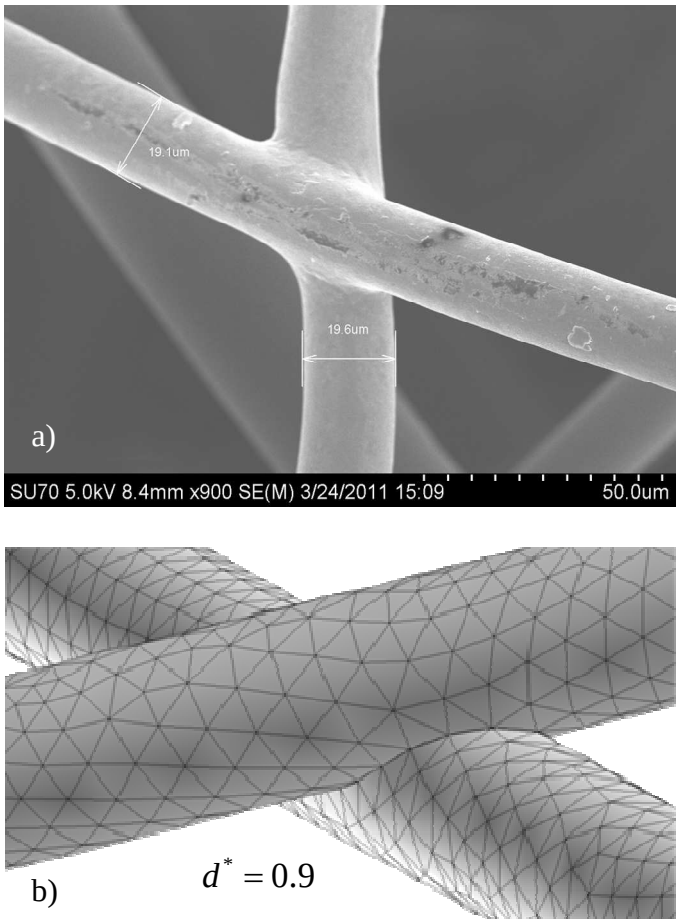

Figure 2.2: An example of a fiber-to-fiber contact in a real nonwoven fabric (a); (b) interpenetrating fibers considered to model an actual fiber-to-fiber contact. A of 0.9 is considered here.

To investigate if the allowable distance affects the structure generation process, a separate MATLAB code has been developed to compute the mean and the standard deviation of the fiber orientations for each generated structure. Once the fiber statistics are computed, histograms for fibers' in-plane and through-plane orientations are generated and compared with the input distributions (see Figure 2.3). The media considered in this figure have 3-D isotropic random structures with a constant SVF of

5%. It can be seen that the input and output fiber orientation distributions are in good agreements.

A d^* value in the range of $0.9 < d^* < 0.95$ has been used for the remainder of the simulations reported in this paper. Note that structures generated with a d^* values greater than 0.95 can be hard to mesh. Note also that as mentioned earlier, fiber-to-fiber contact area depends strongly on the material of the fibers and the manufacturing process by which they are produced. Therefore, to take full advantage of the simulation method developed in this work, one has to first calibrate the model with experiment to obtain the appropriate d^* for his/her specific media. Once the model is calibrated, it can be used to quantitatively study the effects of different microstructural parameters on the material's performance. Even in the absence of such calibration, the current results can still be used for design and development of new insulation media in a qualitatively manner.

It is worth mentioning that the total volume of the fibrous structures was obtained by numerically calculating the volume of the voids between the fibers and subtracting it from the simulation domain using the GAMBIT software (as opposed to adding up the volume of the individual fibers). Therefore, the overlapping volumes between the interpenetrating fibers will not be counted twice.

2.2.2Simulation Setup

Solution of Eq. (2.2) provides the temperature of the fibers and consequently, the total heat flux through the fibrous media. An example of such calculations is shown in Figure 2.4a. Before performing the parameter study, a series of computational

experiments were performed to ensure that the results of the calculations are not affected by the choice of REV or the density of the tetrahedral meshes.

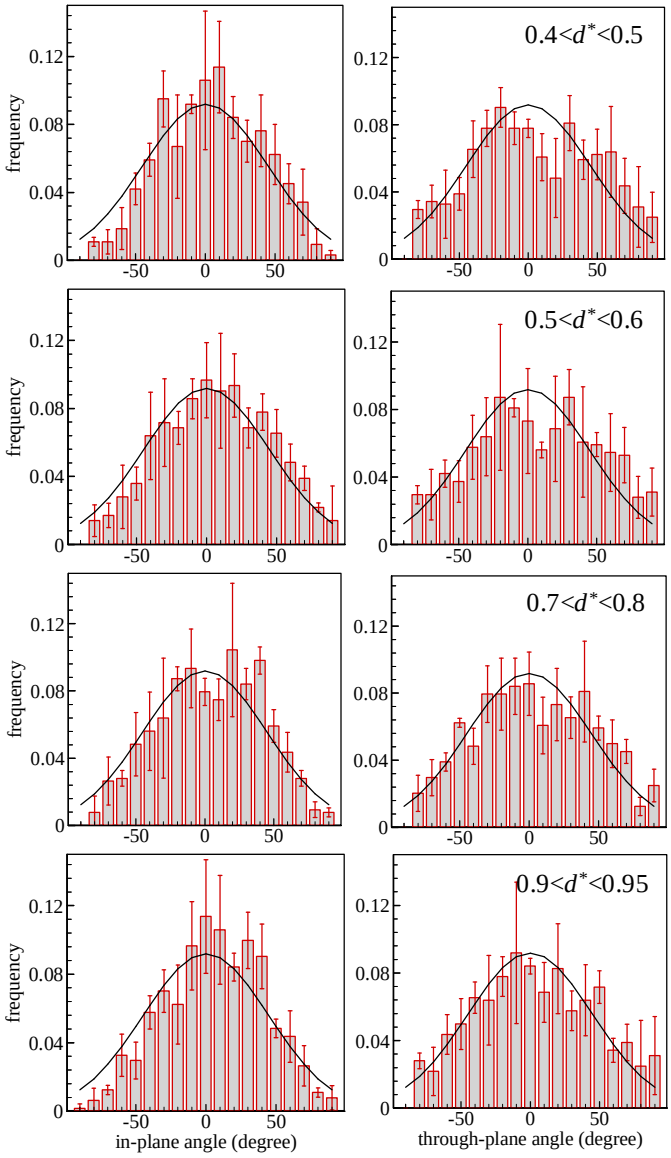

Figure 2.3: Comparison between the input and output in-plane and through-plane fiber orientation distributions for different values.

Therefore the solid phase thermal conductivity of 3-D isotropic fibrous structures was computed with given average microstructural parameters of $\alpha = 5\%$ and $d_f = 8\,\mu\text{m}$, but varied the x–z dimensions (the dimension normal to the heat flow) of the REV from $200 \times 200\,\mu\text{m}$ to $700 \times 700\,\mu\text{m}$. For this study, a thickness of $300\mu\text{m}$ for the computational domain and 30 grid points around the circular cross-section of each fiber was used. As can be seen in Figure 2.4b, statistical uncertainty of the simulation results becomes negligible for any x–z dimensions greater than about $300 \times 300\,\mu\text{m}$.

The virtual insulation media were meshed with tetrahedral elements with uniform mesh texture all over the computational domain. The effect of mesh density on the effective thermal conductivity was studied by varying the grid interval size in such a way to obtain 10, 13, 18 and 27 grid points around the circular cross-section of the fibers (see Figure 2.4 c). These results indicate that 13 grid points around each fiber (the value used in the remainder of this paper) is sufficient to obtain mesh-independent results. Note that with coarser mesh sizes, one may have difficulty meshing the structures.

In addition to monitoring the residual values associated with the energy equation during the iterative solution procedure, the heat flux values at both the hot and cold plates was also monitored. The simulations are considered to be converged when the heat flux values at these plates perfectly match with one another (conservation of energy) and also they no longer change upon additional iterations.

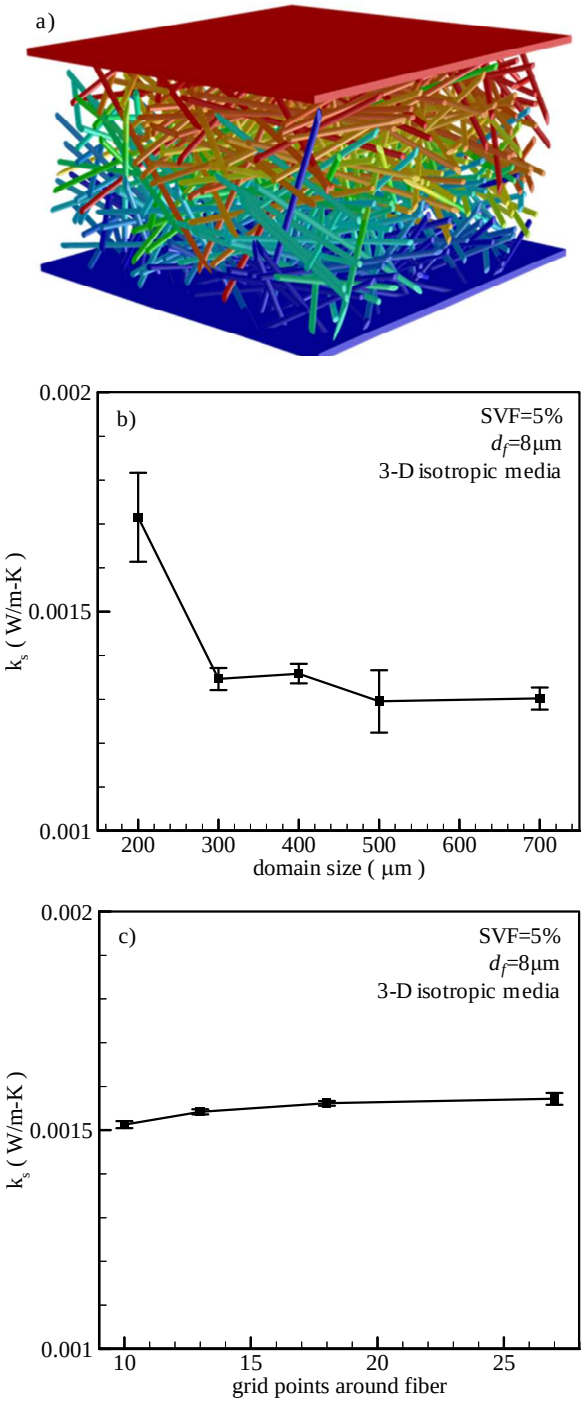

Figure 2.4: An example of fiber temperature calculations with red to blue representing hot to cold is shown in (a). Influence of domain size and mesh density on thermal conductivity prediction for a typical fibrous structure is shown in (b) and (c), respectively.

In Figure 2.5, a comparison is given between the results of the current simulations and those of Vassal *et al.*, 2008, in which the fiber-to-fiber contacts were treated with a convective boundary condition. To better isolate the effects of SVF, the conductivity values obtained for solid fibrous structures k_s are normalized by that obtained for media with an SVF of 10%. The media considered for this comparison have 3-D isotropic fiber orientations. Good qualitative agreement with the two approaches is evident.

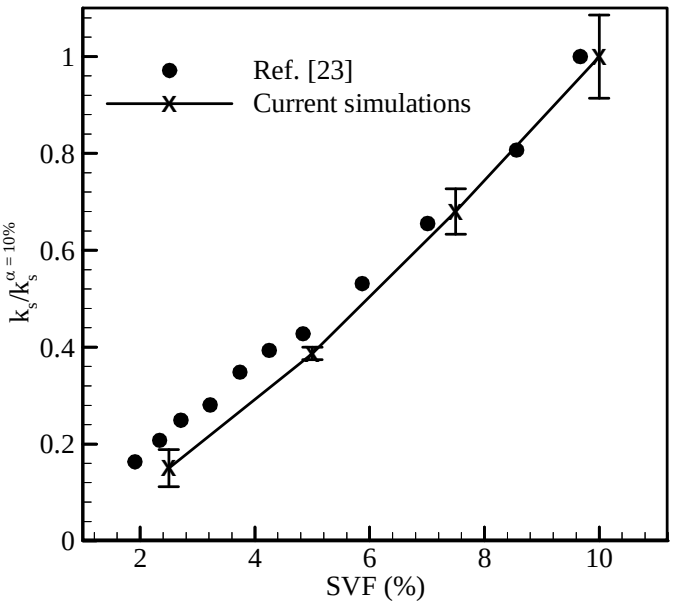

Figure 2.5: A comparison between normalized conductivity values obtained from the current numerical simulations and those of Vassal et al., 2008. The k_s for each SVF has been normalized with the value of k_s for SVF=10% ($k_s^{\alpha=10\%}$). The media considered for this comparison have 3-D isotropic fiber orientation.

2.3 Results and Discussions

The results presented in this section are obtained using a fiber diameter of 8μm in simulation domains with a thickness of 300μm and in-plane dimensions of $500 \times 500\,\mu m$, unless otherwise stated. To study the influence of fibers' through-plane orientation, a series of fibrous structures with identical parameters but different through-plane fiber orientations were generated. The in-plane fiber orientation distribution considered for these structures has a 45-degree standard deviation about a zero mean value (i.e., random in-plane fiber orientations). Figure 2.6a shows the effective thermal conductivity of the media with varying through-plane fiber orientations. It can be seen that increasing the through-plane orientation of the fibers increases the effective thermal conductivity of the solid structure. This is because increasing fibers' through-plane orientation increases the probability that heat flows along the length of the fibers as opposed to travelling in the transverse directions and so needing to go through the narrow fiber-to-fiber contact areas. For completeness of the presentation, the input and output fiber orientation distributions for each case have been reported.

Simulations of media with different in-plane fiber orientations are shown in Figure 2.6b. The media considered for these simulations have through-plane fiber orientation distributions with a zero mean value and a 15-degree standard deviation (i.e., almost layered structures). It can be seen that in-plane orientation of the fibers has no noticeable influence on the effective thermal conductivity of the structure. It is also interesting to note that although there are more number of fiber-to-fiber contacts in media with random in-plane fiber orientations (i.e., the media with a standard deviation of 45

degrees for the fibers in-plane orientation distribution) in comparison to those with aligned fibers (i.e., media with standard deviations much less than 45 degrees for the fibers in-plane orientation distribution), the average fiber-to-fiber contact area is larger when the fibers are aligned. The total number of fiber-to-fiber contacts in the domains was computed and it was found that as the standard deviation of the fibers' in-plane orientation distribution increases from 15 to 45 degrees, the number of fiber-fiber contacts increase by about 25%. However, the average overlap volume between any two fibers (proportional to the average contact area between two fibers) reduces by a factor of 3 to 5 leading to almost no influence on the materials thermal conductivity. For completeness of the presentation, the input and output fiber orientation distributions for each case have been reported.

The effect of varying fiber diameter on conductivity is studied in Figure 2.7a. It can be seen that fiber diameter considerably affects the performance of an insulation medium. This can be explained by considering the fact that increasing the fiber diameter, for a given SVF, reduces the number of fiber-to-fiber contacts thereby reducing the number of bottle necks on the heat flow paths from the hot plate to the cold plate, while increasing the area of each contact on average. Figure 2.7b shows the influence of varying solid volume fraction of the media. As expected, conductivity of the structure significantly increases by increasing the SVF. This conclusion was drawn based on the fact that the conductivity of the interstitial fluid is always less than that of the solid phase. Note however that, if the interstitial fluid happens to be more conducting than the solid phase, then the conductivity of the material decreases with increasing its SVF.

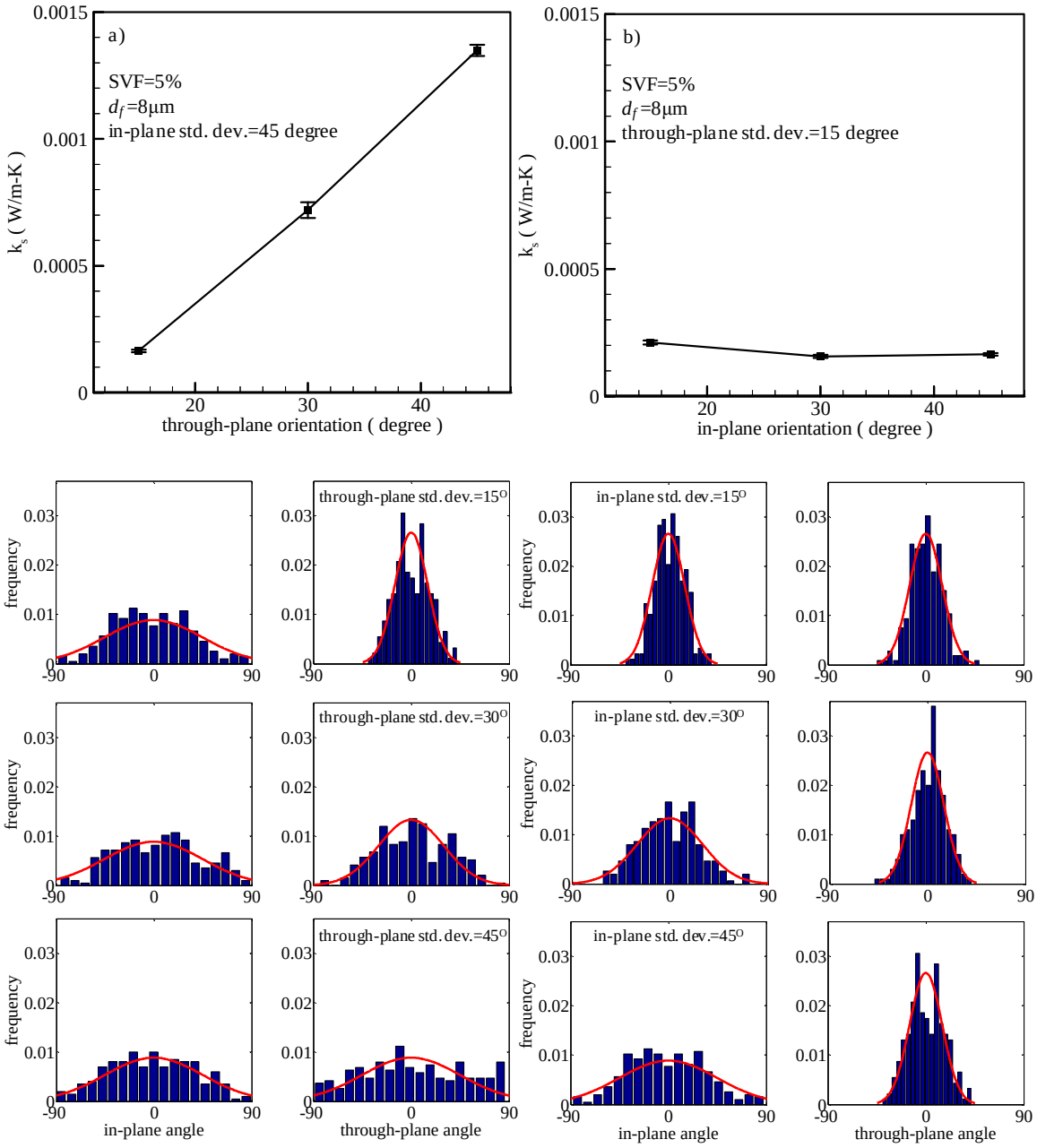

Figure 2.6: Effect of varying the through-plane (a) and in-plane (b) fiber orientations on conductivity of fibrous structures. Input and output fiber orientation distributions are shown below each plot for comparison.

Varying the SVF or fiber diameter did not show any influence on the in-plane or through-plane fiber orientation distributions (not shown for brevity). Similar trends are predicted by the analytical formulations given in Bankvall, 1973 and Bhattacharya, 1980.

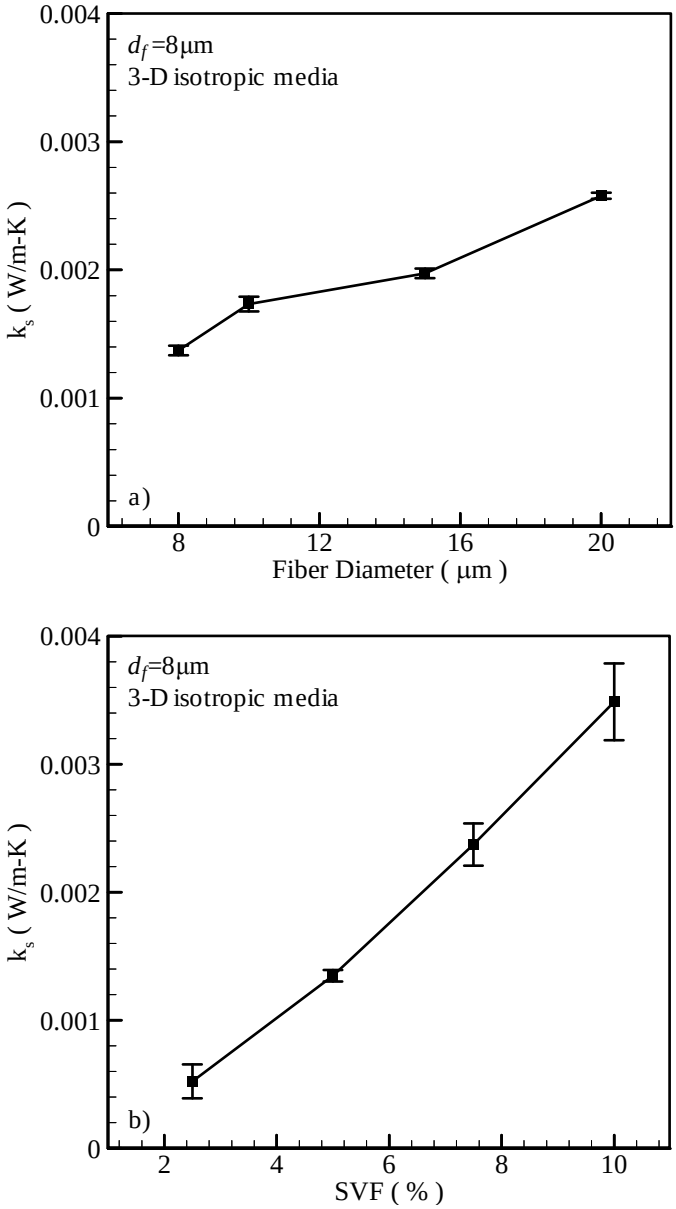

Figure 2.7: Effects of fiber diameter (a) and solid volume fraction (b) on thermal conductivity of fibrous structures for media with 3-D isotropic fiber orientations.

The solid structure conductivity values obtained from these simulations can easily be used to compute the effective thermal conductivity of the insulation material as a whole using Eq. (2.1). Figure 2.8 shows the effective thermal conductivity of insulation media made of different materials such as aluminum, stainless steel, glass, and polypropylene with air as the interstitial fluid, for the purpose of comparison. It can be seen that microstructural parameters of the fibrous structure have insignificant influence on the insulation performance of the material, if the conductivity of the solid material is close to that of air.

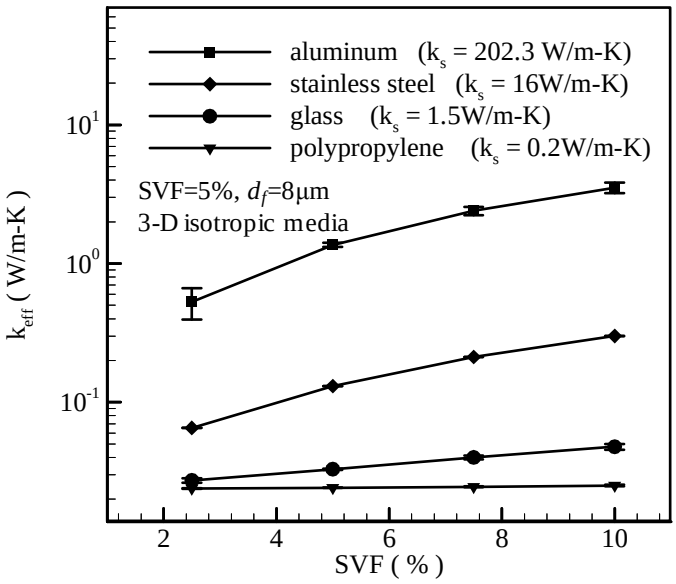

Figure 2.8: Effective thermal conductivity of fibrous insulation media made of different materials as a function of SVF. The intestinal fluid is air.

It is important to mention that there are some limitations to the simple simulation and design method presented here. First and foremost one should note that the simulation

strategy presented here is developed for when the conductive heat transfer is the dominant mode of heat transfer. When working with very high temperatures, radiation will also contribute to heat transfer across the media (Zhang *et al.*, 2008b). The major limitation of the current modeling approach is that the structure generation algorithm needs to be calibrated with experiment to obtain a suitable d^* value. However, once the tool is calibrated it can readily be used for designing new products. The other limitation of the model is the case where fibers barely touch one another at the crossovers. In this case, a d^* value very close to one should be used for generating the fibrous structures. Large d^* values results in structures which are hard to mesh. Moreover, narrowing the range of acceptable d^* values (say $0.95< d^* <0.97$) may affect the orientation distribution of the fibers (due to which the fiber orientation distribution was monitored for the case of $0.9< d^* <0.95$ throughout the paper). Although not a limitation of the simulation methodology, simulating thick media requires significant computational memory. The current simulation approach can also be modified to model media with crimped fibers or fiber made of more than one material, i.e., multi-component fibers.

2.4 Conclusions for Conduction Heat Transfer

An easy-to-implement simulation methodology is developed to study the role of microscale geometry of a fibrous material on its performance as an insulation medium. The simulation results presented here can be used qualitatively (or quantitatively after calibration) to better design and develop fibrous materials for insulating against conductive heat transfer. The results of the current numerical simulations indicate that

heat conduction through solid fibrous structures increases by increasing the solid volume fraction, fiber diameter, and fibers' through-plane orientations. The in-plane orientation of the fibers, on the other hand, did not seem to show any significant influence on the material's conductivity. It was also shown that the microstructural parameters of fibrous insulations have negligible influence on the material's performance if the conductivity of the solid phase is close to that of the interstitial fluid, as expected.

Chapter 3 Simulation of Radiative Heat Transfer via Monte Carlo Ray Tracing[2]

3.1 Introduction

The general procedure in MCRT is to emit a large number of energy bundles from randomly selected locations and directions from given surface, and then trace their propagation through the medium until they exit the domain, or are exhausted due to absorption. Parameters needed for MCRT in fibrous media include the basic microstructural parameters of the material such as fiber diameter, fiber optical properties, material porosity and thickness. MCRT can therefore be used in developing fundamental relationships between a material's thermal performance and its microstructural building blocks. The major restriction of the MCRT in fibrous media is that it requires the fiber diameter to be large compared to the wavelength of the incoming radiation, so that the rules of geometrical optics can be applied (Coquard and Baillis, 2005; Coquard and Baillis, 2006). When the principles of geometric optic are no longer applicable, as is the

[2] Contents of this section have been published in an article entitled "A Monte Carlo Simulation of Radiative Heat Through Fibrous Media: Effects of Boundary Conditions and Microstructural Parameters", by R. Arambakam, S.A. Hosseini, H.V. Tafreshi, and B. Pourdeyhimi, *International Journal of Thermal Sciences* **50,** 935 (2011); and part in "Analytical Monte Carlo Ray Tracing simulation of radiative heat transfer through bimodal fibrous insulations with translucent fibers", by R. Arambakam, H.V. Tafreshi, and B. Pourdeyhimi, *International Journal of Heat and Mass Transfer* **55,** 7234 (2012).

case for nanofiber media, Mie or Rayleigh scattering theory should be considered (Cunnington and Lee, 1996).

As the in-plane dimensions of the insulation materials are usually much larger compared to the thickness of the material, it is computationally expensive for simulating the entire insulation material. Therefore only a small portion of the insulation in the in-plane direction can be subjected to computational simulations. In order to do so it is necessary to impose boundary conditions that can effectively approximate the extended domain as a representative domain using periodic or symmetric boundary conditions. To the author's knowledge, treatment of the energy bundles' interaction with the periodic or symmetry boundary conditions for the MCRT method was not established.

In order to establish these boundary conditions, media consisting of specularly reflecting opaque fibers having unimodal/bimodal fiber diameter distributions were considered. The simulations were conducted in 2-D ordered geometries. Once the boundary conditions were established they were thoroughly tested using the 2-D geometries. After the validity of these boundary conditions were tested the MCRT method was then extended to simulate radiative transfer in 3-D disordered virtual fibrous media with unimodal and/or bimodal fiber diameter distributions consisting of fibers whose surfaces are specularly reflective, and are translucent to Infrared (IR) radiation. Scattering within the realm of geometric optics was incorporated into the current MCRT simulations using Snell's Law for ray refraction. Fibers' optical properties are obtained from Fresnel's law and Beer's law based on the refractive index of the material. Two

different treatments of “high” and “low” conductivities were considered for the fibers and their effects were studied.

3.2 Problem Setup and Boundary Conditions

The first step to simulating radiative heat transfer through fibrous materials is to construct a computational domain that resembles the media’s microstructure. Here, 2-D simulation domains were considered in which fibers are arranged in square arrays as shown in Figure 3.1.

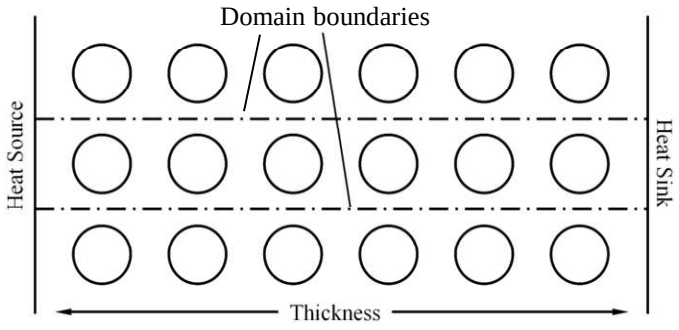

Figure 3.1: A schematic illustration showing the 2-D simulation domains considered in the current study.

To model fibrous materials with different properties, a MATLAB program was developed that generates 2-D simulation domains on the basis of the parameters of interest such as Solid Volume Fraction (SVF), fiber diameter, and media’s thickness. Because of the inherent symmetry present in the fiber arrangement, only one row of fibers is considered for the simulations (see Figure 3.1). Symmetric or periodic boundary conditions are considered for the upper and lower boundaries, and their corresponding

results are compared with one another. The source and sink boundaries are assumed to be perfect absorbers/emitters, and kept at constant temperatures of T_s=1200K and T_c=300K, respectively. Fibers are opaque with specular surface, and their diameters are considered to be greater than 30μm to permit neglecting diffraction effects in the simulations, as the wavelength of the IR radiation emitted from a high-temperature heat source (1200K here) is much smaller than 30μm (Argento and Bouvard, 1996). According to (Argento and Bouvard, 1996), for the geometrical optics to be accurate, wavelength of the thermal radiation and diameter of the fiber must satisfy the relationship $\pi d_f / \lambda < 10$. For instance, for a fiber diameter of 30μm, wavelength of the thermal energy should be smaller than 9.42μm for the geometric optics to be applicable. With such an upper limit and at a temperature of $T_s = 1200K$, almost 94% of the thermal radiation emitted from the source is in the band of $F_{0\to 9.42}$, according to Planck's law (Incropera *et al.*, 2006). This means that 94% of the energy emitted from the source can be correctly modeled using the algorithm presented here. It is also worth mentioning that, although the sink temperature is 300K and there are probably more errors associated with using geometric optics for rays emitted at such a temperature, the sink has practically no influence on the results since the radiative energy is proportional to the fourth power of the temperature. As it will be seen later that the minimum temperature attained by the fibers is around 700K indicating that at least 80% of the energy emitted by the fibers has a wavelength less than $9.42\mu m$. The above procedure is summarized in the flowchart shown in Figure 3.2.

For each ray emitted from a point source (either from a fiber or the heat source), the MATLAB code computes the trajectory of its path through the domain, as it penetrates into the medium and undergoes reflection across the surface of the fibers. This ray tracing algorithm is used for calculation of fiber-to-source, fiber-to-sink and fiber-to-fiber view factors, as well as energy transmittance through the media. Fiber-to-fiber view factor $F_{i,j}$ is the fraction of radiation energy emitted from fiber *i* that is intercepted by fiber *j*. Similarly, fiber-to-source view factor $F_{i,h}$ and fiber-to-sink view factor $F_{i,c}$ are fractions of radiation energy emitted from fiber *i* that are intercepted by source or sink plates, respectively. In view factor calculation, rays are emitted from the fibers, and no reflection or refraction event from the fibers, source, or sink is considered. Note that the fibrous media are modeled as "participating media" in the context of radiative heat transfer, and therefore for the transmittance calculations, the amount of radiation energy emitted by the source as well as that emitted by the fibers is computed. The rays are allowed to undergo subsequent scattering events as they travel through the media until they eventually reach the sink plate. Rays lose some energy every time they encounter a fiber. When the ray intersects with the fiber, it is reflected with the same incident angle (this is same in the case of symmetry boundaries as well). When the ray intersects with the sink or source, it ends path.

The ray tracing process is shown in Figure 3.3 with symmetric and periodic boundary conditions for better illustration. Note that the symmetry boundary condition treats the rays as a perfect reflector, i.e., the incident rays will get specularly reflected with the exact same intensity. The periodic boundary, on the other hand, translates the

incident ray to the alternate side of the domain while preserving the angle and intensity of the ray.

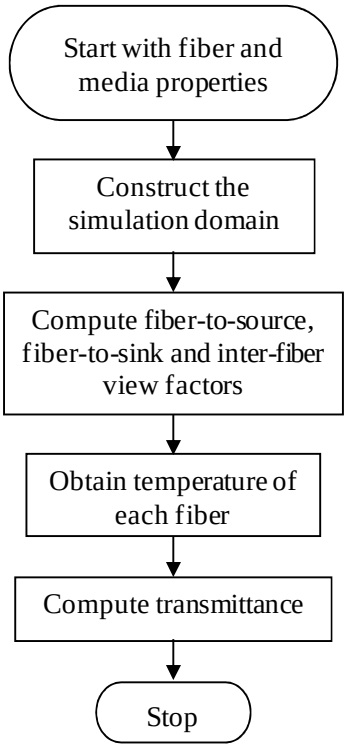

Figure 3.2: Flow chart summarizing the simulation steps.

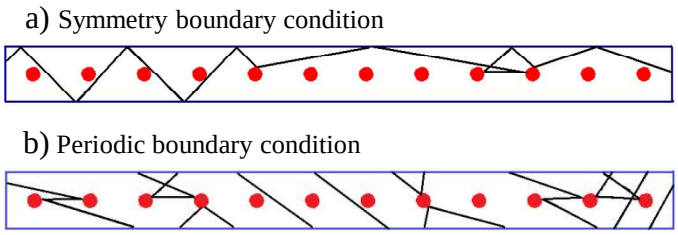

Figure 3.3: An example of rays traced through a simulation domain with symmetry (a) and periodic (b) boundary conditions.

After the view factors are calculated, steady-state fiber temperatures are obtained by solving the conservation of energy equation. For a given fiber one can write:

$$\sum_{j=1}^{n} F_{i,j}(T_i^4 - T_j^4) + F_{i,h}(T_i^4 - T_h^4) + F_{i,c}(T_i^4 - T_c^4) = 0 \qquad (3.1)$$

where T_h , T_c , and T_i represent temperature of the hot plate, cold plate, and the fibers, respectively. Writing the conservation of energy for each fiber in the domain, *n* equations for *n* unknowns (fiber temperatures) are obtained. These equations can be written in matrix form $A \times B = C$, where:

$$A = \begin{bmatrix} \sum_{j=1(i\neq j)}^{n} F_{1,j} + F_{1,h} + F_{1,c} & -F_{1,2} & \cdots\cdots\cdots & -F_{1,n} \\ -F_{2,1} & \sum_{j=1(i\neq j)}^{n} F_{2,j} + F_{2,h} + F_{2,c} & \cdots\cdots\cdots & -F_{2,n} \\ \cdot & \cdot & \cdots\cdots\cdots & \cdot \\ \cdot & \cdot & \cdots\cdots\cdots & \cdot \\ \cdot & \cdot & \cdots\cdots\cdots & \cdot \\ \cdot & \cdot & \cdots\cdots\cdots & \cdot \\ \cdot & \cdot & \cdots\cdots\cdots & \sum_{j=1(i\neq j)}^{n} F_{n,j} + F_{n,h} + F_{n,c} \end{bmatrix},$$

$$B = \begin{bmatrix} T_1^4 \\ T_2^4 \\ \cdot \\ \cdot \\ \cdot \\ T_n^4 \end{bmatrix},$$

and $C = \begin{bmatrix} F_{1,h}T_h^4 + F_{1,c}T_c^4 \\ F_{2,h}T_h^4 + F_{2,c}T_c^4 \\ . \\ . \\ . \\ F_{n,h}T_h^4 + F_{n,c}T_c^4 \end{bmatrix}$.

It must be noted that with periodic or symmetric boundary conditions, one has to exclude the view factor, $F_{i,i}$, corresponding to the rays that were emitted from a fiber and intercepted by the very same fiber, from the view factor summation (diagonal elements) in matrix A. This is especially important when the medium is made of fibers which are arranged in ordered configurations. In the case of randomly distributed fibers this effect may only affect the fibers close to the symmetry boundaries. With the periodic boundary conditions in disordered media, the effect is even less pronounced as the likelihood of a ray emitted from a fiber getting intercepted by itself after reentering the domain is quite small. The above equation is numerically solved in MATLAB. Now the total energy received by the sink is calculated and normalized by the total energy emitted.

3.2.1 Validation of the Method

To verify the accuracy of the view factor calculations, a simple case for which an analytical expression exists was simulated. View factor for the geometry shown in Figure 3.4a can be obtained using Eq. (3.2) (Incropera *et al.*, 2006):

$$F_{h,f} = (d/s)\cos^{-1}(d/s) + 1 - \sqrt{1-(d/s)}^2 \qquad (3.2)$$

A simulation domain was setup which was similar to the one shown in Figure 3.4a (one single fiber in a domain with symmetry or periodic boundary conditions), the fraction of radiation energy released from the source boundary and received by the fibers is calculated. With $d = 10$ $s = 20$, a view factor of $F_{h,f} \cong 0.64$ was obtained, which is in excellent agreement with Eq. (3.2). Note that, according to this equation, view factor $F_{h,f}$ (and therefore $F_{f,h}$) is independent of the distance between the fibers and the source, which has also been observed from the simulation results.

For further validation of the algorithm, a row of fibers placed between a hot and cold plate as shown in Figure 3.4b was considered. Temperature of the fibers at steady-state can be calculated by writing the conservation of radiative energy for the fibers. Here, the energy received by the fibers from the hot plate should be balanced by that emitted to the cold plate:

$$A_f F_{f,h}(T_h^4 - T_f^4) = A_f F_{f,c}(T_f^4 - T_c^4) \qquad (3.3)$$

where $F_{f,h}$ is the view factor for rays emitted from the fibers and received by the hot plate, and A_f is the surface area of a given fiber (note that $A_f F_{f,h} = A_h F_{h,f}$). Because of the existing geometrical symmetry, $F_{f,h} = F_{f,c}$. Eq. (3.3) therefore results in $T_f^4 = (T_h^4 + T_c^4)/2$.

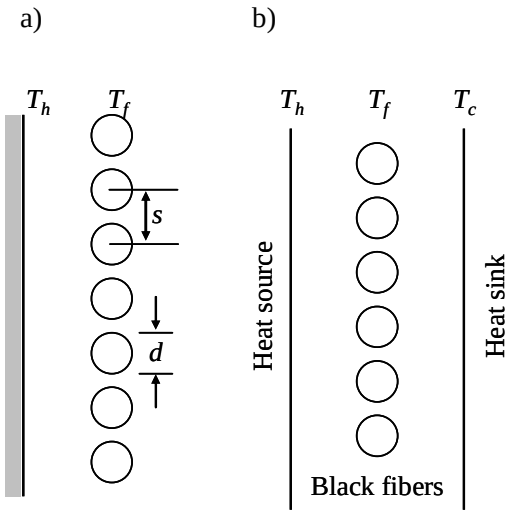

Figure 3.4: Schematic of the cases considered here for validation of a) view factor calculation, and b) steady-state temperature calculation.

Radiative heat transfer in the above geometry was computed and a fiber temperature of $T_f = 1010K$ with the plate temperatures of $T_h = 1200K$ and $T_c = 300K$ was obtained, which is the same as what one obtains using Eq. (3.3), indicating excellent agreement between the simulations and analytical calculations. It is worth mentioning that if the view factor $F_{i,i}$ is not excluded from the summation given in matrix A, with symmetry or periodic boundary conditions, a wrong temperature prediction will be obtained from the simulations. It is also interesting to note that, according to Eq. (3.3), temperature of the fibers is independent of the numerical value of the view factor between the fibers and the heat source (sink). This has also been observed in the simulation results.

To further assess if periodic and symmetry boundary conditions can correctly represent an extended domain, the temperature profiles obtained from a one-row

simulation domain are compared to the ones having periodic or symmetric boundary conditions (Figure 3.3 a, b), with that of an extended twelve-row domain as shown in Figure 3.5. The medium considered in these simulations has a SVF of 5% and a thickness of 1.36 mm, with fibers having a diameter of 30μm. Similarly, $F_{i,i}$ view factors are excluded from the calculations, even though they are mostly zero for fibers far from the boundaries. Temperature predictions obtained from these calculations are shown in Figure 3.5b. Temperature of each row in the extended model matches perfectly with those obtained from the abovementioned one-row simulation domains with either periodic or symmetric boundary conditions (Figure 3.3 a, b). Also note that periodic and symmetry boundary conditions result in identical temperature profiles in the simulations considered here.

3.2.2 Testing of the Model

For the sake of simplicity, an averaged diameter representing each fiber diameter distribution was assumed. Unless otherwise stated, fibers with an emissivity of 0.3 considered and a minimum diameter of 30μm was used. The source and sink temperatures are considered to be 1200K and 300K, respectively.

In Figure 3.6, temperature profiles in three different media with a fiber diameter of 30μm but different SVFs of 5, 10, and 15% was compared. It can be seen that temperature decreases across the thickness. It is interesting to note that although distance between the fibers and the source increases by decreasing SVF, their temperatures change only very slightly (note that the media's thickness increases by decreasing the SVF when the fiber

diameter and their count are kept constant). This can be explained by considering the fact that radiation is the only mode of heat transfer in the calculations (no conduction through the air), and the rays intensity is preserved no matter how far they travel through the media until they encounter with a fiber.

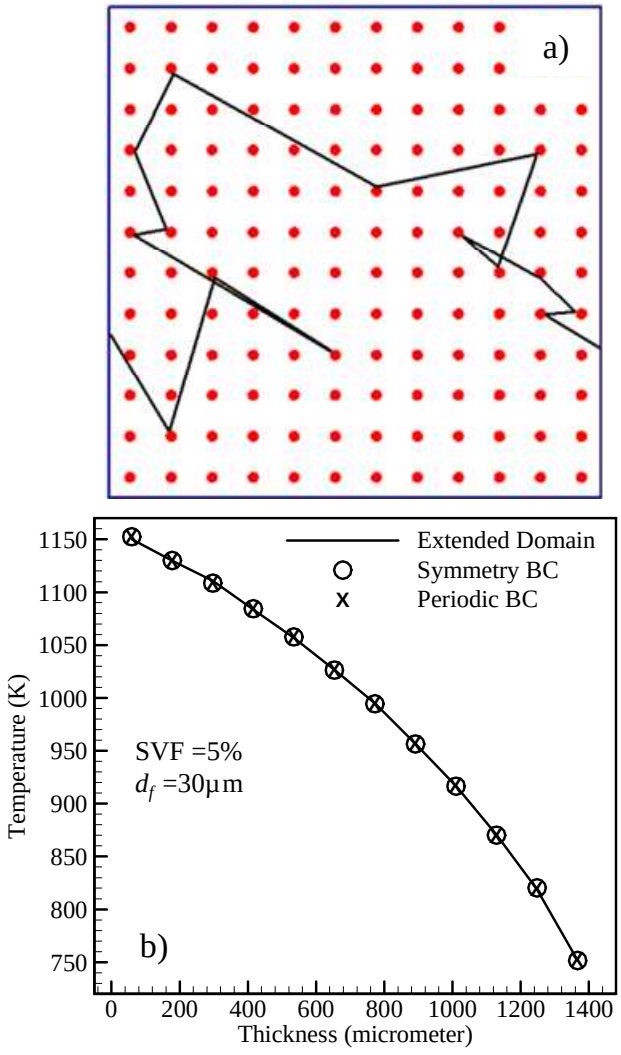

Figure 3.5: An example of the extended simulation domains (a) and its fiber temperature profile (b). Temperature profiles obtained from simulations with one-row domains shown in Figure 3 are also added for comparison.

To study the effects of material's thickness on the backside temperature of the insulation media, six different media with different thicknesses were simulated. Figure 3.7, shows the backside temperature (temperature of the last row of the fibers) of different fibrous insulators with different thicknesses, but identical SVFs and fiber diameters of 5% and 30μm, respectively. It can be seen that the back temperature decreases by increasing the material's thickness, as expected.

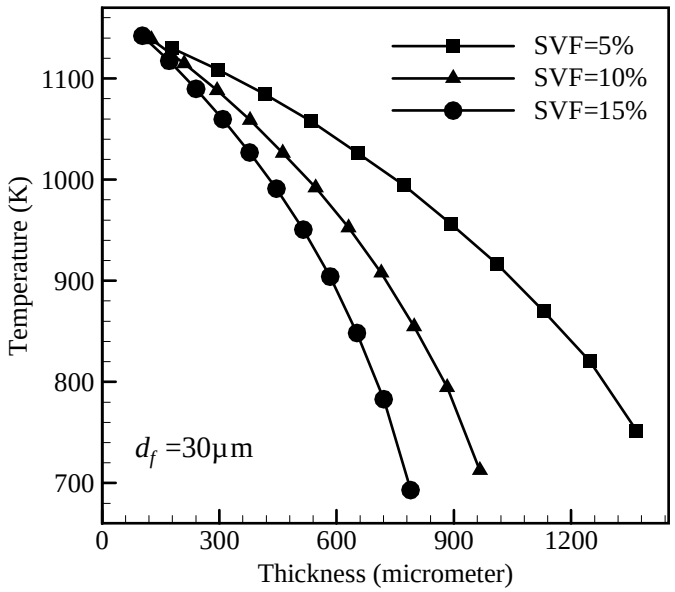

Figure 3.6: Temperatures of individual fibers across thickness of three different media with respective SVFs of 5%, 10%, and 15%, but identical fiber diameters.

Figure 3.8 compares the steady-state energy transmittance through fibrous insulation materials with different thicknesses and SVFs, for fibers with different absorptivity values. It can be seen that transmittance decreases with increasing thickness,

SVF, and absorptivity. This is because increasing the thickness or SVF of the media increases the number of times a ray may encounter a fiber before exiting the domain.

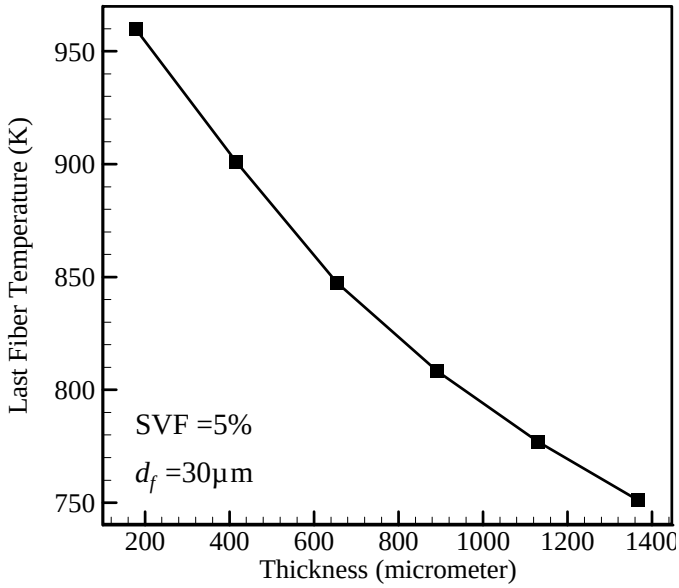

Figure 3.7: Effect of thickness of insulation media on the material's back (last fiber row) temperatures.

The decrease in energy transmittance due to absorptivity increase is interpreted as follows. The energy received by the sink is a combination of the energy emitted from the source (having a temperature of 1200K) and that emitted from the fibers (having different temperatures ranging from, say 1150 to 700K). Fibers with low absorptivity (i.e., low emissivity but high reflectivity), can efficiently transmit (reflect) the high-energy rays emitted from the high-temperature source through the media, but they cannot efficiently emitting rays themselves. On the contrary, fibers with high absorptivity (i.e., high emissivity but low reflectivity), can efficiently emit at their own temperature (less than the source temperature), but they do not allow the high-energy rays from the source to get

through the media. As a ray's energy is proportional to the fourth power of its temperature, it can be expected that the contribution of the energy emitted from the source be greater than that from the fibers, and therefore, fibers that reflect better lead to higher transmittance.

Figure 3.9 shows the effect of fiber diameter on the steady-state radiation transmittance versus SVF. Twelve fibers per row were used for the simulations reported in this figure. It can be seen that transmittance is independent of fiber diameter when number of fibers and SVF are kept constant. This is because by increasing the fiber diameter in this condition, the simulation domain increases with the same scaling factor, and so the resulting transmittance remains unchanged. This effect could be attributed to the nature of 2-D ordered simulation domains. When the thickness and SVF are kept constant, decreasing the fiber diameter leads to an increase in the number of fibers, which in turn, leads to an increase in the specific surface area of the medium. In the 2-D simulations reported here, number of fibers is kept constant, while the thickness where allowed to change.

Bimodal fibrous media where two different fiber diameters are used to represent each fiber species were also studied. Figure 3.10a shows a schematic illustration of the fiber arrangement considered in the simulations. For the sake of brevity, only the case where the fine (n_f) and coarse (n_c) number fractions are identical, and are equal to 0.5 is considered. We vary, however, the coarse-to-fine fiber diameter ratios, R_{cf} , from 1 to 12. Figure 3.10b, shows temperature profiles obtained for media having but different R_{cf} but identical SVF, fine fiber diameter, and number of fibers per layer.

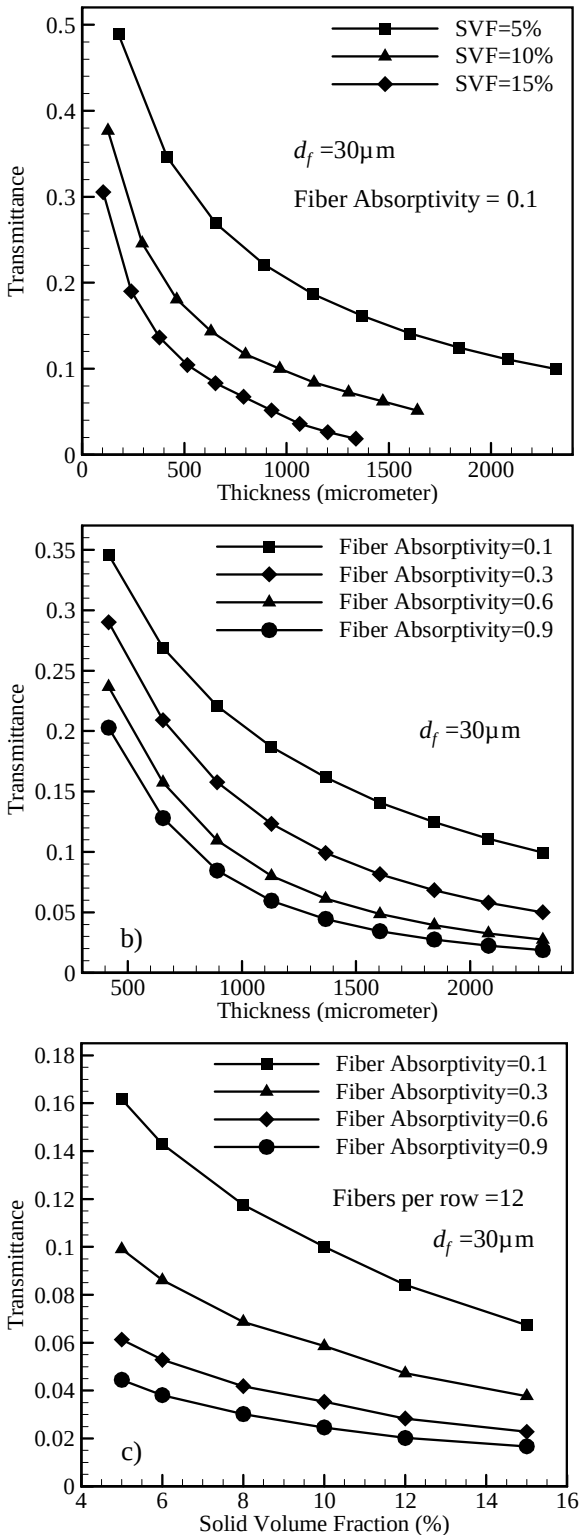

Figure 3.8: Influence of thickness (a), fiber absorptivity (b), and SVF (c) on energy transmittance.

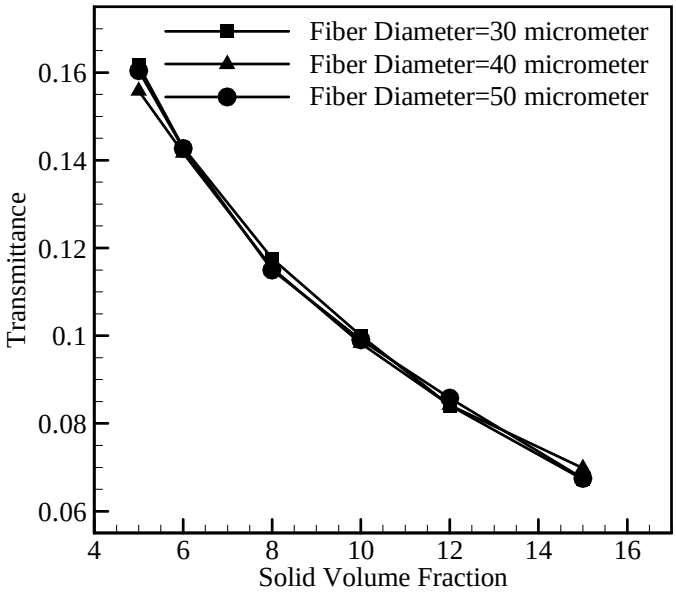

Figure 3.9: Effect of fiber diameter on transmittance as a function of SVF. Note that the number of fibers is kept constant, but the thickness of the media is allowed to vary.

As can be seen, media thickness increases by increasing R_{cf} . The fibers' temperature, however, stays almost the same regardless of the media's SVF.

Figure 3.11 compares the steady-state radiation transmittance through fibrous insulation materials with different R_{cf} . Note that total number of fibers are kept constant and is equal to 12 per row. It can be seen that by increasing R_{cf} from 2 to 12, transmittance increases by about 25%. This indicates that transmittance is weakly dependent on the coarse-to-fine fiber diameter ratios. Note again that here the total number of fibers are fixed. It was speculated that R_{cf} will have a much strong influence of transmittance, if the number of fibers where allowed to decease as a result of increasing R_{cf} when SVF and thickness are kept constant. After through validation and testing of the

MCRT technique it was extended to simulate radiative heat transfer through fibrous insulation materials.

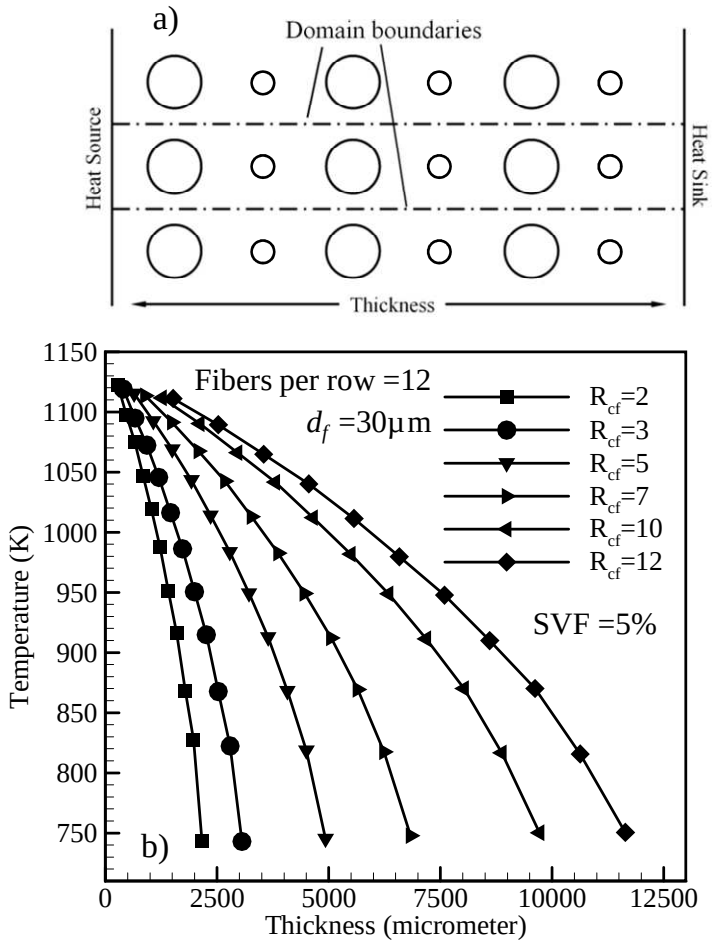

Figure 3.10: a) a schematic illustration of bimodal fibrous media considered in the current study. b) Temperature profiles obtained from simulating bimodal fibrous media with different coarse-to-fine fiber diameter ratios.

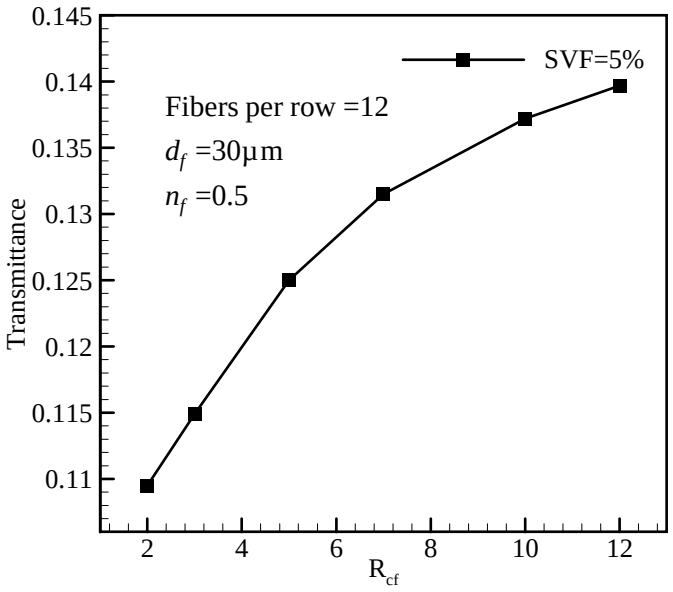

Figure 3.11: Influence of coarse-to-fine fiber diameter ratio on energy transmittance through media with a fixed SVF, number of fibers, and a fine fiber number fraction.

3.3 MCRT simulation of Radiative heat in 3-D Fibrous media made of translucent fibers

To perform microscale simulation of radiative heat transfer through fibrous materials (i.e., simulations in the absence of a continuum phase and at scales comparable to fiber dimensions), one needs to construct a computational domain that resembles the media's microstructure described in Section 1.3. To model fibrous materials with different properties, a MATHEMATICA program was developed to generate 3-D simulation domains on the basis of the parameters of interest, such as solid volume fraction (SVF), fiber diameter, the media's thickness, porosity, and in-plane and/or through-plane orientation (see Figure 1.3).

Periodic boundary conditions are considered for the treatment of rays encountering the boundaries. The in-plane size of the simulation domain is considered to be much larger than the length scale of the system, fiber diameter, to minimize statistical errors associated with the simulation domain size. The source and sink boundaries are assumed to be perfect absorbers/emitters, and are kept at constant temperatures of T_s=850 K and T_c=308 K, respectively. A MATLAB program which uses the virtual fibrous structures and computes the trajectory of the rays through the media was developed. The fibers' refractive index used in the current study (glass fibers) is obtained from the work of (Larkin, 1957; Larkin and Churchill, 1959). Diameter of the fibers is considered to be greater than 20 μm for the geometric optics assumption to be valid (Argento and Bouvard, 1996). The sink plate's temperature is 308 K, and there are probably some minor errors associated with using geometric optics for modeling the interactions between the fibers and rays emitted at such a temperature. However, in comparison to the source plate, the contribution of the sink plate in the final heat flux or fiber temperature values is quite insignificant. This is because the intensity of radiative energy is proportional to the fourth power of temperature, and so the rate of heat transfer is more sensitive to the source plate's temperature.

For each ray emitted from a point source (either from a fiber or the heat source), the MATLAB code computes the trajectory of its path through the domain as it penetrates the medium and undergoes reflection across the surface of the fibers, as is shown in Figure 3.12. In this figure, the red lines show the trajectory of an IR ray traveling through the medium, whereas the blue and gray cylinders represent coarse and fine fibers. To

better visualize how the periodic boundary conditions are implemented, the ray is shown with a black line every time it exits from a periodic boundary and reenters from the opposite side of the box.

A ray undergoes a series of reflection or transmittance events until its energy reaches a negligible value, or till the ray encounters the source or sink boundaries. Once the intersection of a ray with a fiber is known, the angle between the incoming ray and the normal to the cylinder at that intersection point, i.e., angle of incidence θ_i, is computed. Using Snell's law (Eq. (3.4)), the angle of refraction θ_t can then be easily obtained (see Figure 3.13a) as:

$$\theta_t = \sin^{-1}\left[\frac{n_1 \sin\theta_i}{n_2}\right] \tag{3.4}$$

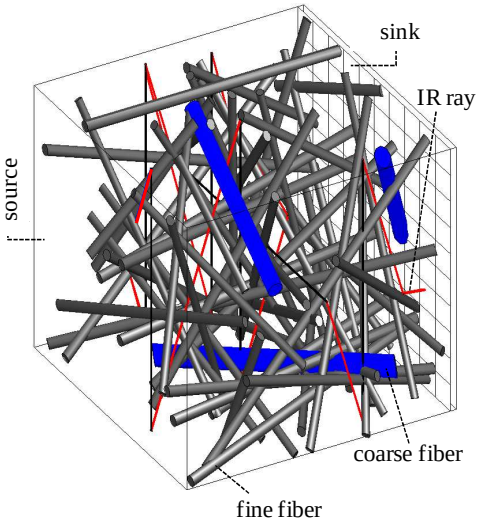

Figure 3.12: Visualization of the trajectory of a ray traced through a bimodal fibrous medium for illustration. The ray is shown in red color. Black lines show the ray changing position when periodic boundaries are encountered. Coarse and fine fibers are shown with blue and gray colors, respectively.

With these angles available, the absorptive or reflective nature of the fiber to the IR ray is computed using Fresnel's Eq. (3.5) to Eq. (3.8). The reflectivity and transmissivity of the interface to the parallel and perpendicular components of an IR ray are given by Eq. (3.5) , Eq. (3.6), Eq.(3.7), and Eq.(3.8), respectively (Bohren and Huffman, 1983).

$$\rho_{\parallel} = \frac{\tan(\theta_i - \theta_t)}{\tan(\theta_i + \theta_t)} \tag{3.5}$$

$$\rho_{\perp} = \frac{\sin(\theta_i - \theta_t)}{\sin(\theta_i + \theta_t)} \tag{3.6}$$

$$t_{\parallel} = \frac{2\sin\theta_t \cos\theta_i}{\sin(\theta_i + \theta_t)\cos(\theta_i - \theta_t)} \tag{3.7}$$

$$t_{\perp} = \frac{2\sin\theta_t \cos\theta_i}{\sin(\theta_i + \theta_t)} \tag{3.8}$$

With the above components computed, the effective reflectivity and transmissivity of the interface can be calculated to be the mean values of the squares of parallel and perpendicular components $\rho_{avg} = (\rho_{\parallel}^2 + \rho_{\perp}^2)/2$ and $t_{avg} = (t_{\parallel}^2 + t_{\perp}^2)/2$. Note that these mean values should satisfy the relation $\rho_{avg}^2 + t_{avg}^2 (n_2 / n_1)(\cos\theta_t / \cos\theta_i) = 1$. If a ray undergoes a transmittance event, the intensity of the transmitted light is computed using Beer's law, which is given as (Zappe, 2010):

$$I = I_0 e^{-\alpha d_t} \tag{3.9}$$

Here, the value $\alpha = 4\pi k / \lambda$ is given by the imaginary part of the complex refractive index, and d_t is the distance travelled by the energy bundle inside the fiber before it exits it from the other side (see Figure 3.13a). Once the direction of the refracted ray inside the

fiber is determined, the point where the ray exits the fiber can be obtained, and the normal to the fiber at that point can be computed. With this information, one can use Snell's law to determine the angle of the outgoing ray.

In the MCRT method, a random point of emission $O(x_0, y_0, z_0)$ and the normal direction vector $[a,b,c]$ at that point are generated on the surface in consideration (fiber or source/sink plate). Note that IR rays can originate from the fibers' surface as well as fiber interior. For the sake of simplicity, only the case where the IR rays to originate from the surface of the fibers was considered. Also for simplicity, it was assumed that the rays travel outwards to avoid complicated calculations dealing with internal reflections within a fiber. Also, when IR radiation encounters the tip of a fiber with a certain angle of incidence angle, it undergoes total internal reflections. Such situations are not expected to occur too often and so are ignored. With the origin and direction of the ray known, one can obtain the equation of the line that describes the ray, as (see Figure 3.13b):

$$(x_0 - x)/a = (y - y_0)/b = (z - z_0)/c = t \tag{3.10}$$

Let C be any circular fiber having a radius of r_f, with any arbitrary location and orientation. Let $A(x_A, y_A, z_A)$ and $B(x_B, y_B, z_B)$ be the centers of the circular ends of the fibers, and $P(x_P, y_P, z_P)$ be any point on the surface of the cylinder. These points form a triangle ABP. Assume d_1, d_2, and d_3 be the distances between A and B, P and A, and P and B, respectively, i.e.:

$$d_1 = \sqrt{(x_B - x_A)^2 + (y_B - y_A)^2 + (z_B - z_A)^2} \tag{3.11}$$

$$d_2 = \sqrt{(x_P - x_A)^2 + (y_P - y_A)^2 + (z_P - z_A)^2} \tag{3.12}$$

$$d_3 = \sqrt{(x_B - x_P)^2 + (y_B - y_P)^2 + (z_B - z_P)^2} \tag{3.13}$$

The area of the triangle ABP is given as:

$$A_r = r_f d_1 / 2 \tag{3.14}$$

Let $p = (d_1 + d_2 + d_3)/2$ be one half of the triangle's perimeter. Using Heron's formula, the area of the triangle can also be found as:

$$A_h = \sqrt{p(p - d_1)(p - d_2)(p - d_3)} \tag{3.15}$$

With Eq. (3.14) and Eq. (3.15) one can obtain an expression for the coordinates of any arbitrary point P which lies on the infinitely long cylinder shown in Figure 3.13b, as:

$$A_r^2 - A_h^2 = 0 \tag{3.16}$$

The distance from the middle point of the fiber axis to any point on the cylinder must be finite for the point to lie within the simulation box. Assume for a moment that the point P is at one end of the cylinder, then the distance between points M and P can be considered as:

$$q = \sqrt{r^2 + (x_A - x_M)^2 + (y_A - y_M)^2 + (z_A - z_M)^2} \tag{3.17}$$

Now, if point P is considered to be the intersection point between the cylinder and a ray originated from $O(x_0, y_0, z_0)$ with a normalized direction vector $[a,b,c]$, one can describe point P in parametric form as:

$$(x_0 - x)/a = (y - y_0)/b = (z - z_0)/c = t_p \tag{3.18}$$

With Eq. (3.16) and Eq. (3.18), one can obtain two values for t_p each representing coordinates of an intersection point between the ray and the cylinder. The distance between M and any point P must be less than or equal to q for a particular point $D(x_D, y_D, z_D)$ to be the point of intersection of the ray and the fiber within the simulation domain. After the two intersections of a ray and a cylindrical surface $D(x_D, y_D, z_D)$ and $D'(x_{D'}, y_{D'}, z_{D'})$ are computed, (see Figure 3.13d), the actual intersection point (the one on the side facing the ray's origin) is obtained by picking the intersection point $D(x_D, y_D, z_D)$ which is located at the shortest distance from the origin of the ray. The point $D'(x_{D'}, y_{D'}, z_{D'})$ which is located further away from the origin should not be considered as the intersection point. This is because a ray entering the fiber undergoes a refraction process, thereby changing its direction towards point $O'(x_{0'}, y_{0'}, z_{0'})$ (see Figure 3.13d).

The direction vector of the reflected ray is computed by first obtaining the coordinates of point $Q\left(x_Q, y_Q, z_Q\right)$ which is the projection of the intersection point onto the fiber axis (the coordinates of point $Q\left(x_Q, y_Q, z_Q\right)$ can be obtained by projecting the vector $\overrightarrow{AD}$ onto the fiber axis $\overrightarrow{AB}$). The normal vector to the fiber surface at the point of intersection $[n_x, n_y, n_z]$ is then obtained using points Q and D. The direction of the reflected ray can then be calculated using the reflection matrix given by Eq. (3.19).

$$\begin{bmatrix} -n_x^2 + n_z^2 + n_y^2 & -2n_x n_y & -2n_x n_z \\ -2n_x n_y & -n_y^2 + n_x^2 + n_z^2 & -2n_y n_z \\ -2n_x n_z & -2n_y n_z & -n_z^2 + n_y^2 + n_x^2 \end{bmatrix} \tag{3.19}$$

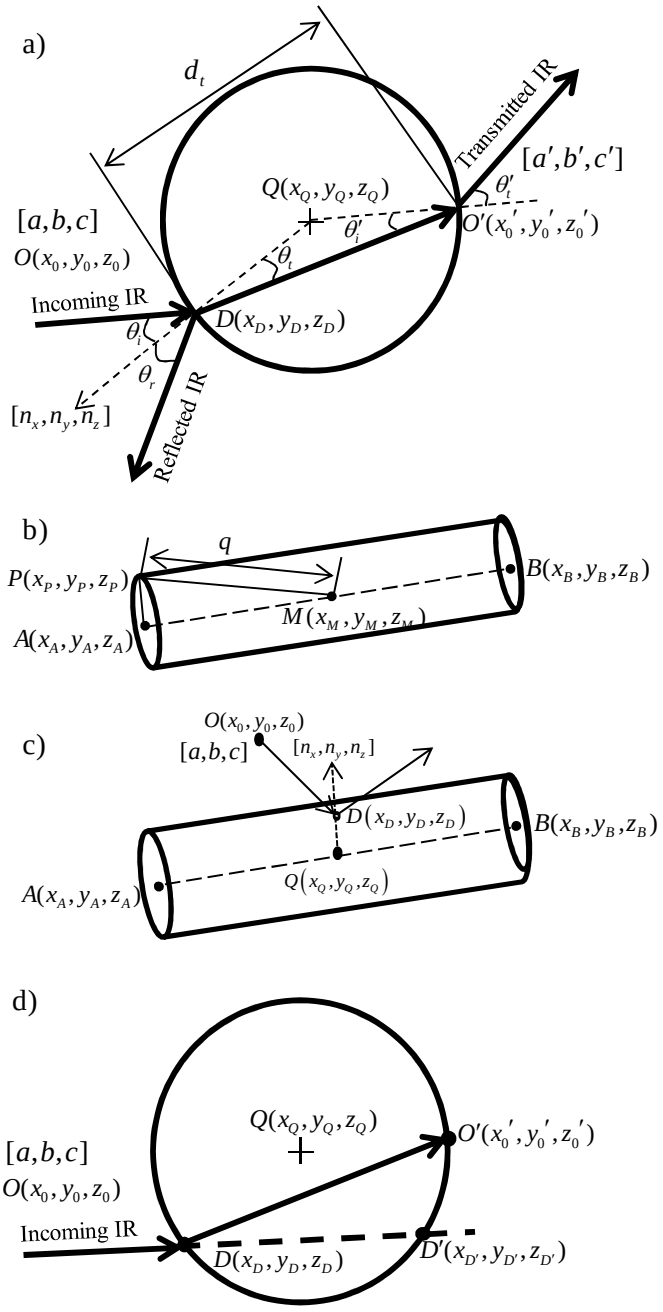

Figure 3.13: Schematic of a ray through a fiber (a); fiber end points (b); ray reflection from a fiber (c); and intersections of a ray with the fiber surface (d).

When a ray does not intersect with the fibers, it either encounters a periodic boundary or reaches the sink (or source) plate. If a ray encounters a periodic boundary, it exits the domain at that particular point but reenters from the opposite side of the simulation box with the same direction vector. This process is repeated until the ray's energy reaches a negligible value, or it encounters the source/sink boundaries.

When the intersection of a ray and a fiber is found, a random number R_t is generated in the closed interval of 0 to 1. If the value of R_t is less than the interface transmissivity (obtained from Fresnel's equations), then the ray is transmitted through the fiber and emitted with an intensity calculated using the fiber absorptivity from Beer's law. The intensity of the transmitted ray depends on the distance that the ray travels inside the fiber d_t, as well as the value of the imaginary part of the refractive index. The origin and direction of the emitted ray is determined using Snell's Law. On the other hand, if the value of the random number R_t is greater than the fiber transmissivity, the ray is assumed to be reflected specularly. The reminder of the ray tracing procedure is described in Section 3.2.

Two different treatments for the variations of the temperature of a fiber along its length were considered. To model a high-conductivity fiber, a single temperature for the entire length of the fiber is calculated according to Eq. (3.1). For fibers which are not highly conductive, however, a new modeling strategy was developed. In this case, each fiber was divided into some number of segments and each segment was treated as an individual fiber with a uniform temperature. This increases the number of fibers in the domain, and consequently slows down the simulations. However, it allows the fibers to

attain a semi-continuous temperature gradient along their lengths. For these calculations, rather than dividing the fibers into segments along their axes—the most obvious but yet computationally least efficient method—they were sliced in the direction of the imposed temperature gradient (i.e., the *x*-direction). This means that fibers with a greater through-plane orientation will be divided into a larger number of segments. Obviously, fibers with no through-plane orientations, like the fibers in layered media, will not be divided into fiber segments (see Figure 3.14). This segmentation algorithm has been motivated based on the fact that fibers with a greater through-plane orientation attain a greater temperature gradient along their lengths, and so must be divided into a larger number of segments for accurate temperature calculations in comparison with fibers with a smaller through-plane orientation. In the calculation with such fibers, as a better accuracy is needed, 250 rays from each fiber segment were emitted (as opposed to 2500 from the entire fiber).

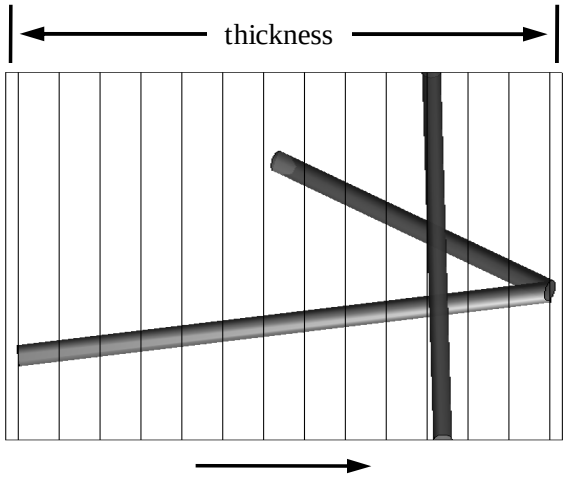

Figure 3.14: A schematic drawing showing the fibers divided into different number of segments depending on their position and through-plane orientations.

3.3.1 Validation of the Method

Apart from the validation studies performed for the case of 2-D fibrous media, additional validation was performed to ensure the accuracy and reliability of the MCRT procedure.In order to validate the view factor calculations in 3-D, a simple 3-D geometry of two perpendicular cylinders with a given separation at the centers, as shown in Figure 3.15 was simulated. An analytical expression exists for this case (Incropera et al., 2006), and is shown in the following equations:

$$F_{1-2} = 0.178(X/2.59)^{-0.95}(L/X)^{-0.16}\exp(-0.537\left|\ln(L/X)\right|^{1.61}) \quad if\ (L/X<1) \qquad (3.20)$$

and

$$F_{1-2} = 0.178(X/2.59)^{-0.95}(L/X)^{-2.32}\exp(2.024\left|\ln(L/X)\right|^{0.889}) \quad if\ (L/X>1) \qquad (3.21)$$

where $L = l/r$, $C = c/r$, and $X = 2.42C - 2.24$. With l =200 µm, c = 75 µm, and r =15 µm. The simulations predict a value of 0.049, which is in perfect agreement with the value (0.049) obtained from the above analytical expressions. Note that the periodic boundary conditions used in the simulations were turned off when this validation study was performed, since the cylinders in this context have a finite length, and the periodic boundaries represent infinitely long fibers.

A series of trial simulations were also conducted to ensure that the results of the computations are independent of the number of rays emitted from the source plate or fibers. An example of such calculations is shown in Figure 3.16. For these calculations, a fibrous structure with a domain size of 500×500×832 µm, an SVF of 5%, and a fiber diameter of 20 µm was used.

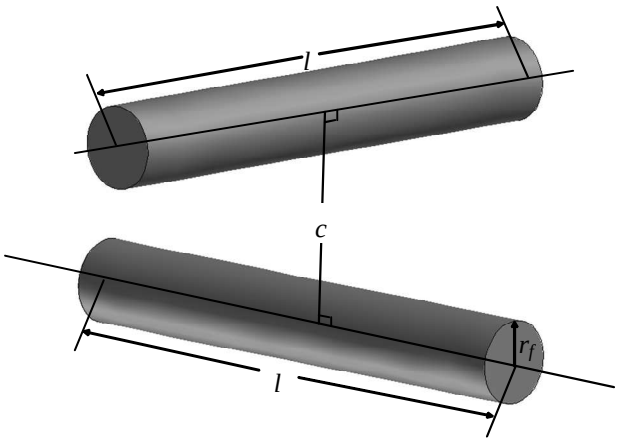

Figure 3.15: A simple configuration considered for validation of view factor calculation in 3-D.

The number of rays emitted from each fiber was varied from 50 up to 2500 and the temperature of the fibers was monitored (for a total of 65 fibers in the domain). The fiber temperatures obtained by emitting a different number of rays from each fiber are compared with those obtained by emitting the maximum number of rays (2500 rays per fiber), and shown in Figure 3.16. It can be seen that for any number of rays per fiber greater than 250, the calculation error is less than about 2%. Hence 250 rays per fiber were used as a default value for the remainder of the simulations presented here. Similar studies were conducted for the transmittance values as well (not shown for the sake of brevity). They all indicated that emitting 250 rays from the fibers or the source plate leads to acceptable results.

In order to verify the accuracy of the implementation of the physics of geometric optics in the code the following analysis was conducted. It is a well-known phenomenon that extinction of IR occurs due to the shape of the scattering objects and of course due to the material (Bohren and Huffman, 1983). Therefore it is expected that as the SVF of the

material increases, the transmittance of the material reaches to a minimum value and then starts to increase.

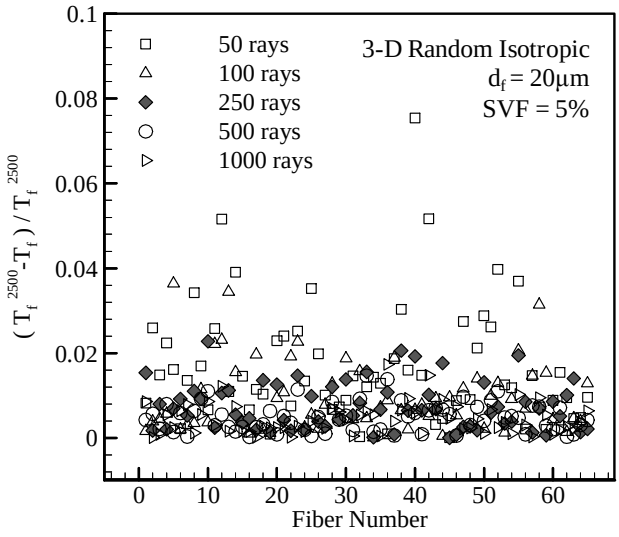

Figure 3.16: Effects of number of rays emitted from a high-conductivity fiber on its predicted steady-state temperature.

To study this effect of SVF on radiation transmittance of the medium, a modified form of the 2-D ray tracing code was used. The 2-D ray tracing code was modified to incorporate scattering in the geometric optics limit (as seen in Figure 3.13). The study started with choosing 2-D simulation domains of $250\mu m \times 250\mu m$. Fibers were randomly generated in the domain to resemble the case of fibers with zero in-plane and through-plane angles (see Figure 3.17). Different simulation domains ware studied starting with a minimum SVF of 2.5%. The value of SVF was increased to a SVF of 55% (see Figure 3.17b) and to further increase the SVF beyond 55% it was assumed that fibers in the center of the simulation domain merge to form a bigger fiber see Figure 3.17c. The

diameter of the fiber situated at the center was increased until the SVF of the domain reached 85%. A hot plate temperature of 800 K and a cold plate temperature of 300 K were used. The fibers were assumed to be made of glass and the refractive index was obtained from the work of Larkin, 1957. A fiber diameter of 20 μm was used.

From Figure 3.18 it can be seen that as SVF of the medium increases from 2.5% to 100% the transmittance of the medium first decreases and then increases. This can be explained based on the fact that after an SVF of 55%, the number of scatters in the medium decrease as the SVF increases. The transmittance of the medium at 100% is calculated using Beer's law (Eq. (3.9)) after compensating for the reflection losses of the IR due to interaction with the glass surface. The loss of energy due to reflection of light from two surfaces of the glass slab is calculated by computing the reflectivity (ρ_g) of the glass using the following equation:

$$\rho_g = \frac{(n_1 - n_2)^2}{(n_1 + n_2)^2} \tag{3.22}$$

Here n_1 is the refractive index of the medium from which the IR originates and n_2 is the refractive index of the medium into which the IR enters.

To better examine the accuracy of the simulations, the results were compared with those obtained from the two-flux model (see Appendix A). The two-flux model treats the radiative heat transfer through a participating medium as a 1-D problem in the direction of the thickness.

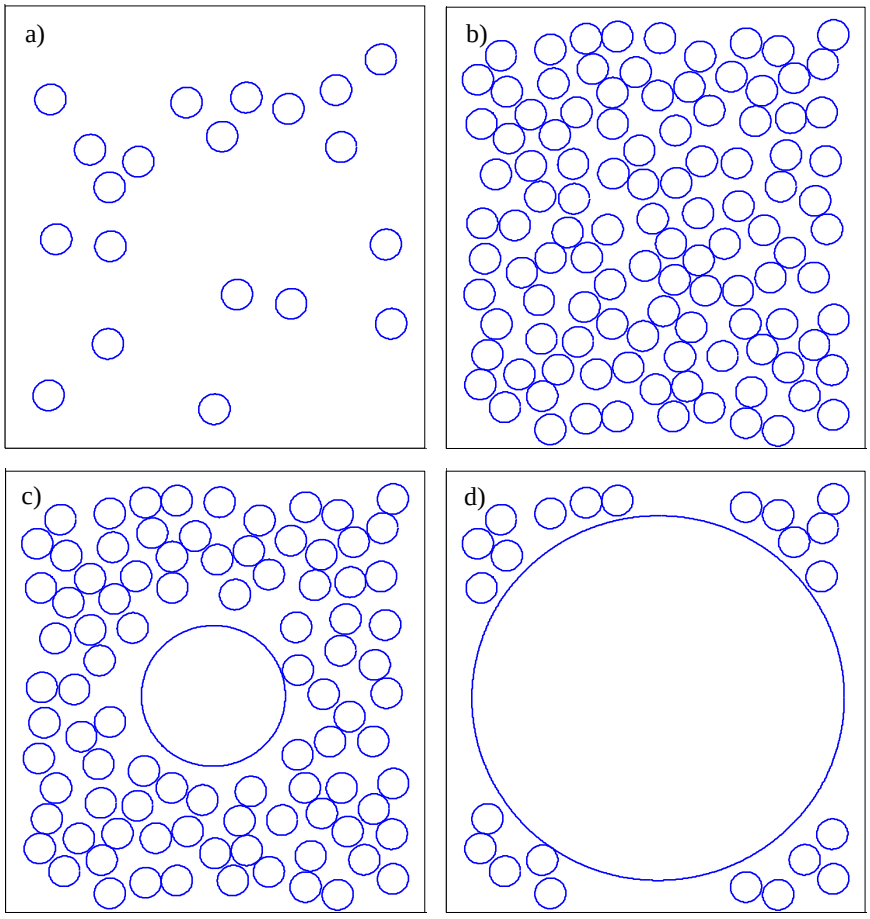

Figure 3.17: Simulation domains containing 2-D translucent glass fibers with SVFs of (a) 10%, (b) 55%, (c) 65% and (d) 85%.

Radiative heat transfer through fibrous insulation materials was investigated theoretically and experimentally by (Larkin, 1957). Transmission measurements were conducted with source temperatures varying from 370 to 700 K, while the sink plate was held at the room temperature.

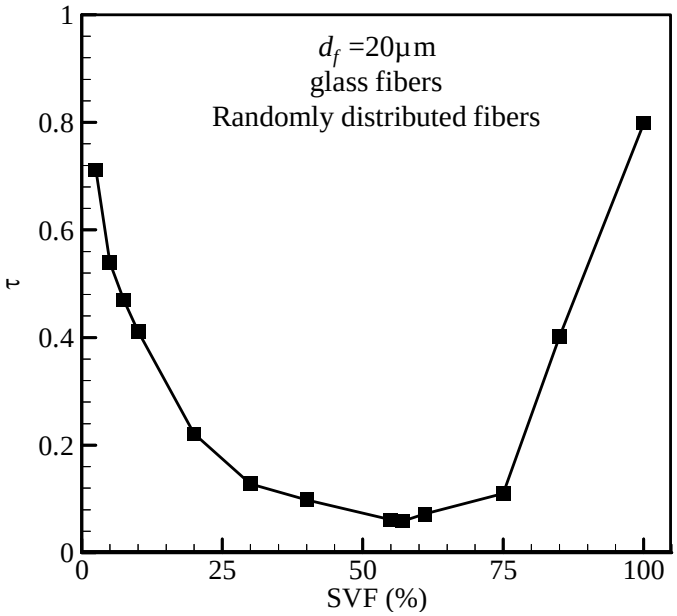

Figure 3.18: Effect of SVF on the transmittance of the fibrous media made of glass fibers.

The collected data were interpreted in terms of the two-flux approximation method for solving the RTE. The materials were assumed to be isotropic and homogenous with radiative heat propagating in the forward and backward directions only, as described in the two-flux approximation method. Heat flux transmitted through the fibrous materials (provided by Owens-Corning Fiberglass Corporation) was measured by (Larkin, 1957) and utilized to compute the scattering and absorption cross-sections. The materials used in the study included fiberglass types A and B as well as and unbounded glass fibers with different diameters such as 2.5, 5, 10, 20 and 35 µm. It is worth mentioning that although Larkin (Larkin, 1957) did not investigate the effects of impurities on the radiative properties of his media, he observed traces of carbon impurities in the glass fibers used in his experiment. Using the two flux model, (Larkin, 1957) developed an equation for radiative heat flux through fibrous media.

$$q_1(0) = \frac{2\sqrt{M^2 - N^2}}{\sqrt{M^2 - N^2} + M} e^{-l\sqrt{M^2 - N^2}} \sum_{n=0}^{\infty} (-1)^n \left[\frac{\sqrt{M^2 - N^2} - M}{\sqrt{M^2 - N^2} + M} \right]^n e^{-2nl\sqrt{M^2 - N^2}} \quad (3.23)$$

Numerical values for M and P are experimentally obtained by (Larkin, 1957) for glass fibers with a diameter of 20 μm at a temperature of at 700 K. The value of *N* is computed from Eq. A-5 of Appendix A. Results of this equation, normalized with the total flux values emitted by the source plate, are added to Figure 3.19 for comparison. As can be seen in this figure, the MCRT method and the two-flux method show similar trends for the variations of the radiation transmittance with SVF. More importantly, considering the very different nature of the two methods, and the fact that both methods are based on series of simplifying assumptions, one can argue that the general agreement between the two methods is acceptable.

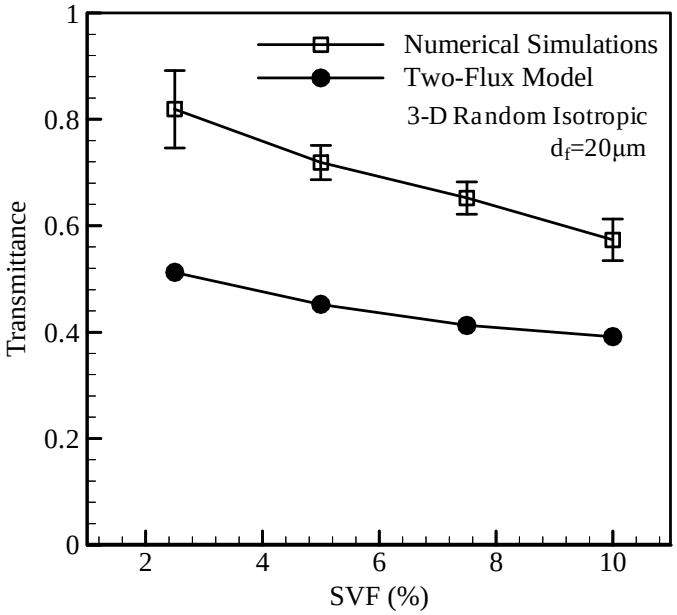

Figure 3.19: A comparison between transmittance values obtained from current numerical simulations with low-conductivity fibers and the two-flux model. The media have a SVF of 5% with 3-D isotropic fiber orientations.

3.4 Results and Discussion

Unless otherwise stated, fibers with a diameter of 20 μm were considered (fine fiber diameter in the case of bimodal media). The simulations are conducted in domains with a thickness of 832 μm and in-plane dimensions of 500×500 μm. The source and sink temperatures are considered to be 850 K and 308 K, respectively. The absorptivity, reflectivity, and transmissivity values for each fiber are calculated using Fresnel's Law and Beer's Law for each fiber–ray interaction. Due to the random media generation process, each simulation is repeated at least three times to reduce statistical uncertainties in the results presented.

To study the influence of in-plane and through-plane orientation of the fibers on the insulation performance of fibrous materials, a series of fibrous structures with identical parameters but different fiber orientations were generated (Figure 1.3). Figure 3.20a shows the temperature profile across media with different degrees of through-plane fiber orientation (structures shown in Figure 1.3a–d). These fibers are assumed to have a low conductivity, and therefore, develop a non-uniform temperature profile along their lengths. It can be seen that through-plane orientation of the fibers has no significant influence on the temperature profile across the thickness of the fibrous structure. Increasing the through-plane orientation of the fibers, however, increases the IR transmittance through the materials as can be seen in Figure 3.20b. This conclusion is in agreement with the work of (Lee, 1989) who used electromagnetic wave theory to predict performance of fibrous insulation materials. Note that in calculating the temperature profile across the thickness, the domain is divided into a number of slices and the

temperature of each slice is obtained by mass-weighted averaging of the temperatures of the fiber segments within the slice. For the case of layered media (media with no through-plane fiber orientation), the layer temperature was taken as the slice temperature.

The simulation results for media having layered structures (structures shown in Figure 1.3) with different in-plane fiber orientations are shown in Figure 3.20c–d. It can be seen that the fibers' in-plane orientation has no influence on the temperature profile across the thickness of the media. The transmittance results also show no dependence of the in-plane orientation of the fibers. This is also in agreement with the previous results by (Lee, 1989). Note that, since fibers in layered structures have no through-plane orientations, they attain uniform temperatures along their lengths independent of their conductivity values. Interestingly, increasing the fiber conductivity for media with non-zero through-plane fiber orientations tends to flatten the temperature profile across the material's thickness, leading to a more uniform temperature distribution across the thickness (see Figure 3.20e). This effect is negligible when the fibers' through-plane orientation of the fibers is quite small (say, a standard deviation of 15 degrees or less), but becomes noticeable through-plane orientation increases. This effect somewhat resembles the problem of heat conduction through a solid wall where increasing the conductivity of the wall reduces the temperature gradient across the thickness. Figure 3.20f shows the IR transmittance results for the case of highly conductive fibers with different through-plane fiber orientations. Comparing these results with those shown in Figure 3.20b, one can conclude that the effect of fiber conductivity on IR transmittance is negligibly small. Slightly higher transmittance values (less than 3% higher) from

simulations conducted without the high fiber conductivity assumption may be attributed to the fact that maximum fiber temperature is slightly higher for this case, and the intensity of the heat flux emitted from the fibers (being proportional to the fourth power of fiber temperature) is slightly higher. Note again that in the transmittance calculations, the energy received by the sink includes the energy emitted from both the fibers and the source plate (Boulet *et al.*, 1993).

To better compare and discuss the differences observed in the results shown in Figure 3.20a and 3.20e, the temperature of three arbitrary fibers from within the structure were compared (shown with different colors in the inset of Figure 3.21a). The comparison is between the fiber temperatures obtained with and without the high-conductivity assumption for the fibers. For a better illustration, one of the fibers is randomly taken from the left side of the domain (near the source plate), one from the right side of the domain (near the sink plate), and the third is chosen such that in spans across the thickness. It can obviously be seen that with the high-conductivity assumption, the fibers have uniform temperatures along their lengths, while the in the absence of such an assumption, some temperature gradients are established along the fibers. More interestingly, it can be seen that higher maximum temperatures (on the left side of the domain) and lower minimum temperatures (on the right side of the domain) are obtained when fibers are less conductive, which is in agreement with the results obtained for the whole media. For convenience, the temperature profiles shown in Figure 3.20a and 3.20e for media with a through-plane standard deviation of 45 degrees were isolated and compared them with one another in Figure 3.21b.

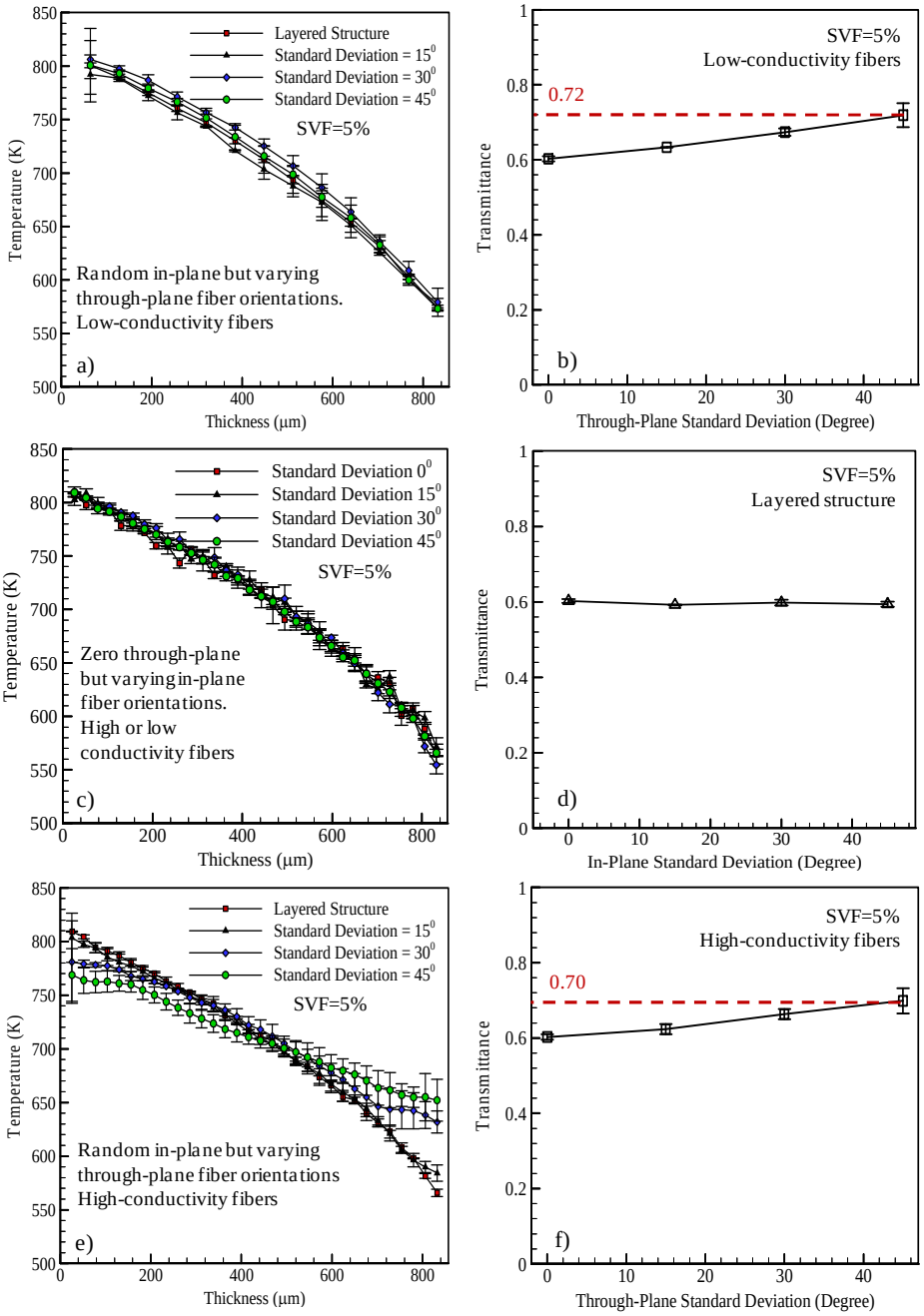

Figure 3.20: Temperature profiles and transmittance values for media with random in-plane but varying through-plane fiber orientations and low fiber conductivity (a and b); zero through-plane but varying in-plane fiber orientations and arbitrary fiber conductivity (c and d); random in-plane but varying through-plane fiber orientations and high fiber conductivity (e and f). All structures have an SVF of 5% and a fiber diameter of 20 μm.

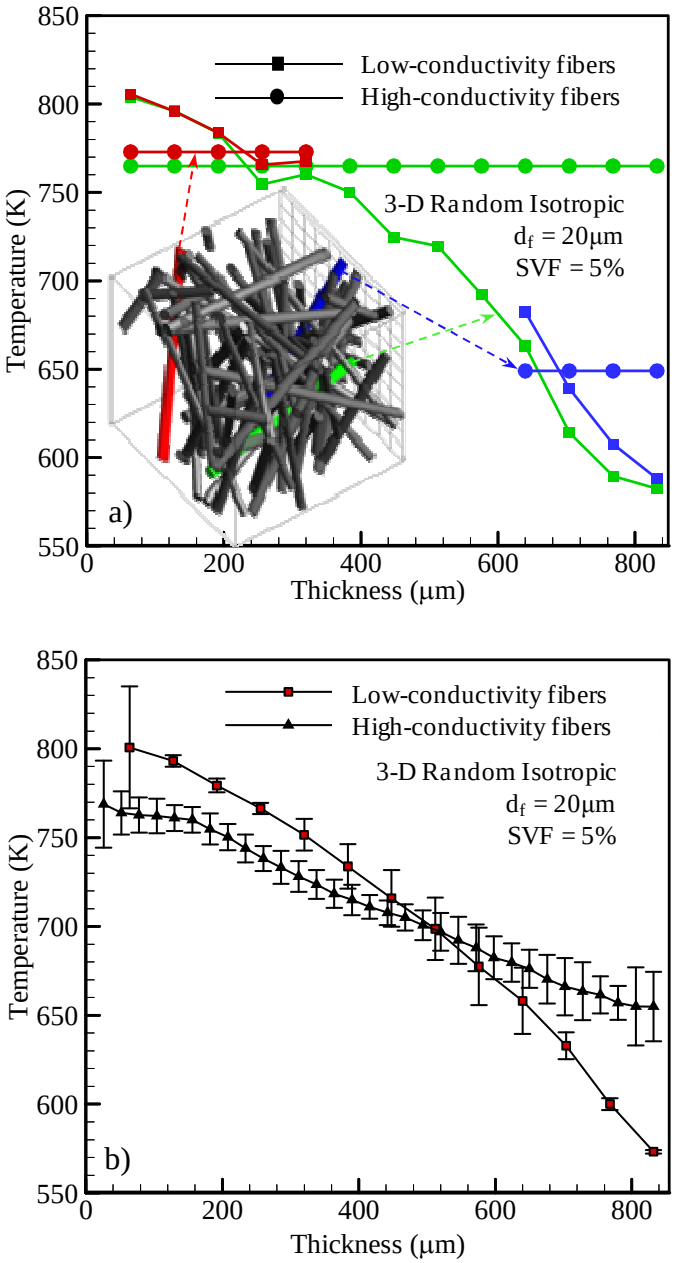

Figure 3.21: a) A comparison between temperature of three fibers shown in red, blue, and green for two different fiber conductivity treatments of "low" and "high". b) Temperature profiles across the thickness of media with identical microstructural parameters but different fiber conductivities of "low" and "high". The media shown in this figure have an SVF of 5%, a fiber diameter of 20μm with 3-D isotropic fiber orientations.

It can be seen that average temperature of the whole media remains almost constant, independent of the fiber conductivity, although temperature distribution is more flat with high-conductivity fibers. It is worth noting that heat and fluid flow in fibrous structures similar to that shown in Figure 1.3e can be studied using 2-D disordered domains, as there are no temperature gradients in the direction of the fiber axes. With the heat transfer performance of an insulation material being independent of the in-plane orientation of the fibers (Figure 3.20c and 3.20d), one can conclude that simulations devised in 2-D disordered domains can reliably provide predictions with accuracy equal to those of 3-D simulations conducted for layered media, but with easier math and faster CPU times. Similar simulations can also be conducted using 2-D ordered geometries. However, in the ordered geometries, the thickness of the media has to be a multiple of the thickness of the unit cell (see (Arambakam *et al.*, 2011) for more information).

To study the influence of SVF on heat transmittance and fibers' temperature, a series of media with different SVFs were simulated. Only layered media (shown in Figure 1.3h) and media with 3-D isotropic random fiber orientations (shown in Figure 1.3d), with both high-conductivity and low-conductivity fibers were studied. As expected, temperature decreases across the thickness. However, it is interesting to note that, as SVF increases, temperature of the fibers closer to the source increases, while that of the fibers farther away from the source decreases (see Figure 3.22). The underlying physics behind this effect seems to be the fact that, at higher SVFs, fibers closer to the source better block the IR rays, thereby shielding the remainder of the fibers. This causes these fibers to attain higher temperatures, and those closer to the sink to remain colder.

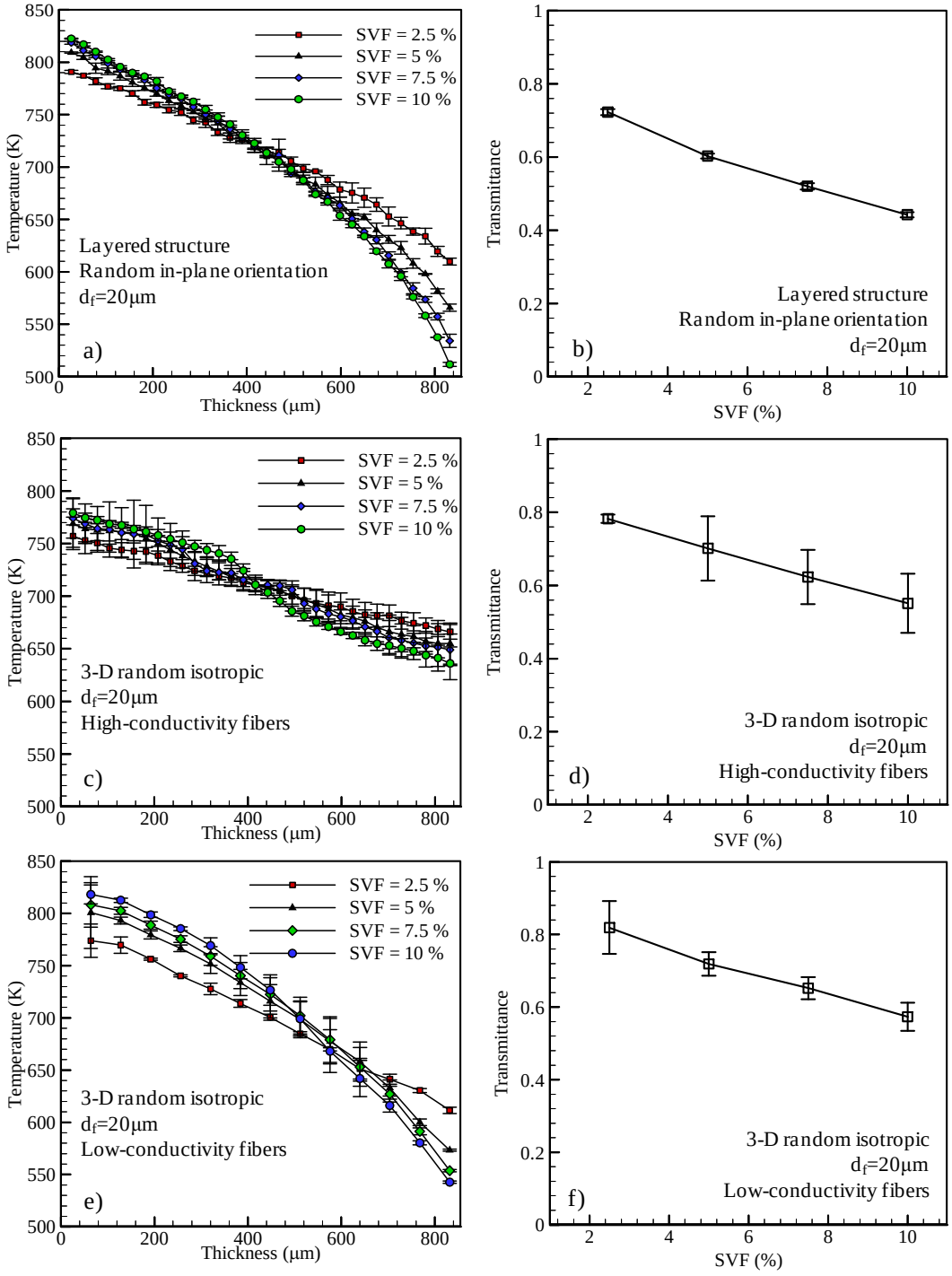

Figure 3.22: Temperature profile and transmittance values for media with varying SVFs for layered structures and arbitrary fiber conductivity (a and b); 3-D isotropic structures and high-conductivity fibers (c and d); and 3-D isotropic structures and low-conductivity fibers (e and f).

From heat transmittance calculations (Figure 3.22b, 3.22d and 3.22f), it can be concluded that increasing the SVF results in a decrease in the heat transmittance through the media, as there will be more fibers blocking a direct path from the source to the sink. As mentioned earlier, a slight increase in transmittance is observed when a low conductivity is assumed for the fibers. Note also that the layered media can better block the IR transmittance, indicating again that decreasing the through-plane orientation of the fibers results in better heat insulation.

Fibrous materials with bimodal fiber diameter distributions were also studied. For the sake of simplicity, fibers are assumed to be either fine or coarse (no actual diameter distribution), as shown in Figure 3.12. Additional parameters that must be introduced to the simulations are the mass fraction of the fine (or coarse) fibers, and the coarse-to-fine fiber-diameter ratio R_{cf}. The fine fiber diameter in all the bimodal simulations is kept constant at $d_f = 20\,\mu\text{m}$. Figure 3.23a shows temperature profiles obtained for media having a coarse mass fraction of 0.5 but different R_{cf}. The SVF of the media is kept constant at 7.5%, and the fibers have orientations with in-plane and through-plane standard deviations of 45 and 15 degrees, respectively (i.e., the structures are almost layered). The media are assumed to be made up low-conductivity fibers. As can be seen in Figure 3.21a, increasing R_{cf} results in an effect similar to that caused by reducing the SVF in Figure 3.22—reduction of the temperature gradient across the thickness. However, the effect of R_{cf} on the temperature profile seems to be less pronounced than that of SVF. This effect can be explained by considering the fact that increasing R_{cf},

when all other microstructural parameters (e.g., SVF) are kept constant, results in fibrous geometries with fewer fibers shielding the sink plate. Similar calculations conducted for media made up of high-conductivity fibers resulted in less noticeable differences between the two cases studied. The transmittance values for the two cases of R_{cf} equal to 2 and 3 are found to be 0.610 and 0.625, respectively, indicating a slight increase in transmittance with increasing R_{cf}. Increasing the mass fraction of coarse fibers, when the coarse-to-fine fiber-diameter ratio is kept constant, results in a flatter temperature profile across the thickness (see Figure 3.23b). A slight increase in the IR transmittance is also observed when increasing m_c from 0 to 0.5, with the corresponding values of 0.620 and 0.625, respectively. The transmittance values for the case of high-conductivity fibers were found to be almost 3% lower than the above values for low-conductivity fibers.

3.5 Conclusions for Radiation heat transfer using MCRT

Most of the studies reported on radiative heat transfer through a fibrous material treat the medium as a continuum, with the effects of its microstructural parameters (fiber diameter, fiber emissivity, material's porosity…) lumped together in the form of a series of macroscale material coefficients such as an extinction coefficient. The objective of the current work was to develop an analytical, and so computationally feasible, simulation method to isolate each individual microstructural parameter of a fibrous material, and study its influence on the insulation performance of the medium. The current simulations were conducted in 3-D disordered fibrous media with unimodal and/or bimodal fiber diameter distributions.

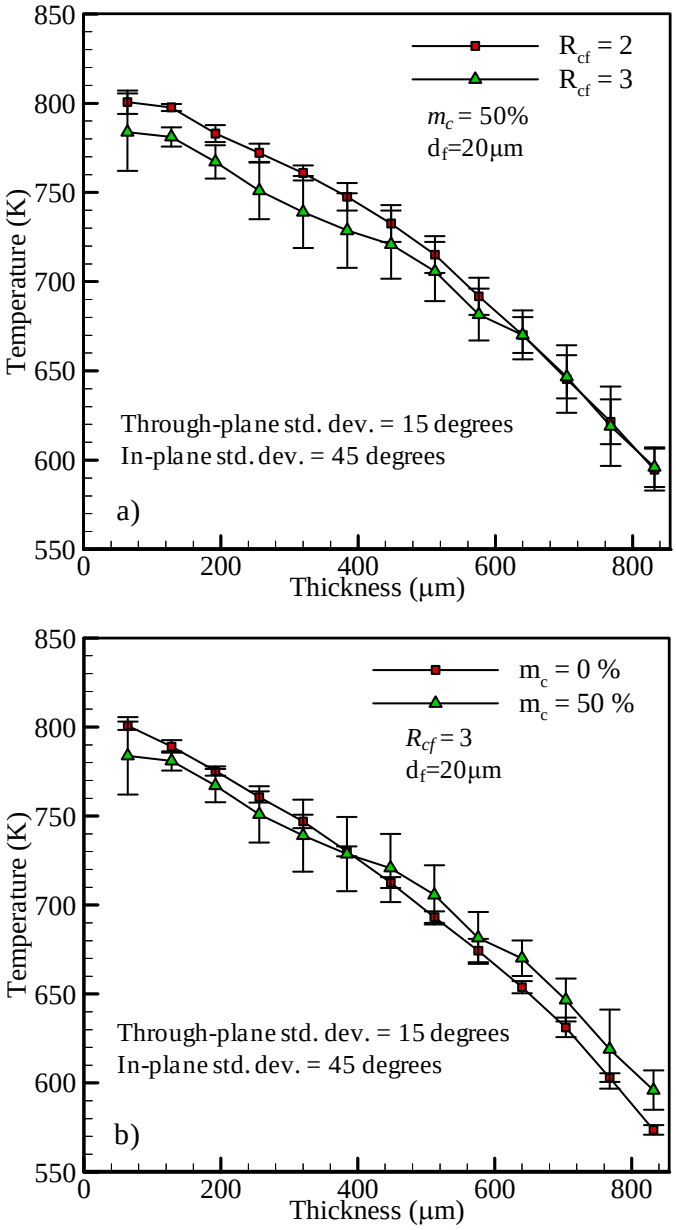

Figure 3.23: Temperature profile across thickness of bimodal fibrous structures with a m_c of 50% but different coarse-to-fine fiber diameter ratios (a); media with an identical R_{cf} of 3 but different coarse fiber mass fractions (b). The media simulated here have zero-mean in-plane and through-plane fiber orientations with standard deviations of 45 and 15 degrees for the in-plane and through-plane fiber orientation distributions, respectively.

The effects of the fiber conductivity are included in the current radiation modeling by considering two different scenarios of high-conductivity or low-conductivity fibers.It was found that for media with non-zero through-plane fiber orientations, increasing conductivity of the fibers lowers the temperature difference across the media's thickness. The current results indicate that heat flux through a fibrous medium decreases with increasing solid volume fraction of the fibers. It was also observed that IR transmittance increases with increasing through-plane orientation of the fibers, but is independent of their in-plane orientations. The fibers in-plane or though-plane orientations were found to have negligible effect on the temperature profile across the media's thickness unless the fibers are highly conductive. The results obtained from simulating bimodal fibrous structures indicate that increasing the fiber-diameter dissimilarity, or the mass fraction of the coarse fibers, slightly increases the radiation transmittance through the media, and accordingly reduces the temperature gradient across the thickness. The simulation results are compared with those from the two-flux model and other studies in the literature, and good agreement is observed.

Chapter 4 A Dual-Scale 3-D Approach for Modeling Radiative Heat Transfer in Fibrous Insulations[3]

4.1 Introduction

In this chapter, a dual-scale computationally-feasible 3-D method is developed to simulate the transfer of radiative heat through fibrous media comprised of fibers with different diameters and orientations. The simulations start by generating a virtual fibrous material with specified microstructural properties and then compute the radiative properties of each fiber (i.e., effective phase function, as well as scattering and absorption coefficients) in the structure using the Mie Scattering theory. Considering independent scattering formulations for the fibrous media (media with high porosities), the radiative properties of the insulation material are computed by summing up the radiative properties of each individual fiber, after transforming the phase function values from the fiber's local 3-D coordinates system to a fixed global coordinates system. The radiative properties of the media are then used in the Radiative Transfer Equation (RTE) equation, an integro-differential equation obtained for computing the attenuation and augmentation

[3] Contents of this section have been published in an article entitled "Dual-Scale 3-D Approach for Modeling Radiative Heat Transfer In Fibrous Insulations", by R. Arambakam, H.V. Tafreshi, and B. Pourdeyhimi, *International Journal of Heat and Mass Transfer* **64**, 1109 (2013).

of an InfraRed ray's energy as it travels through a fibrous medium. Using the Discrete Ordinate Method (DOM), the RTE is then discretized into a system of twenty-four coupled partial differential equations and solved numerically using the FlexPDE program to obtain the amount of heat transfer through the entire thickness of the media.

4.2 Macroscale Formulations

In order to compute the radiative properties of insulation media, a virtual geometry of the media's microstructure is first generated using an in-house MATLAB code. The MATLAB code was developed to generate 3-D simulation domains on the basis of the parameters of interest, such as solid volume fraction (SVF), fiber diameter, the media's thickness, in-plane and/or through-plane orientation (Figure 1.3). When generating the virtual fibrous structures, careful attention was paid to assure that the fibers are located at a certain specified distance from each other, and the distance is determined by the clearance parameter (Lee, 1994). The radiative properties of such structures can be computed using electromagnetic theory and the radiative heat transfer through the material can be predicted using the Radiative Transfer Equation.

The RTE (Eq. (1.3)), being an integro-differential equation, is hard to solve numerically or analytically. However, the Discrete Ordinates Method (DOM) can be utilized to simplify and solve the equation numerically. In the DOM method, the integral term in the RTE (which is the term describing incident radiation from all the directions) is approximated by a weighted sum of intensities scattered in different directions. In the current work, DOM equations were considered in three scattering directions in each

quadrant (known as the S4 approximation) and are solved using the FlexPDE finite element program from FlexPDE Inc. Using the S4 approximation Eq. (1.3) simplifies to a system of 24 coupled partial differential equations (3 equations for intensity in each quadrant of the simulation domain, see Figure 4.1). The integral term in Eq. (1.3) is replaced by a summation term with weight factor w by using the quadrature formulation of Chandrasekhar, 1960. The RTE in DOM can be written as:

$$\frac{dx}{dS}\frac{dI_p}{dx}+\frac{dy}{dS}\frac{dI_p}{dy}+\frac{dz}{dS}\frac{dI_p}{dz}=\vec{A}_p\frac{dI_p}{dx}+\vec{B}_p\frac{dI_p}{dy}+\vec{C}_p\frac{dI_p}{dz}=-\beta I_p+\kappa I_b+\frac{\sigma}{4\pi}\sum_{p=1}^{24}w_p I_p\Phi_p \tag{4.1}$$

Here $\vec{A}_p$, $\vec{B}_p$ and $\vec{C}_p$ are the direction cosines of the incident radiation. The subscript p represents the number of angles considered in the DOM. The quadrature weight and direction cosines are obtained based on the predetermined directions in the S4 approximation, for which the intensity field ($\vec{I}_p$) is to be calculated.

Eq. (4.1) can numerically be solved using a generic partial differential equation solver, subject to the boundary conditions at the source and sink given as:

$$I_p(x=0)=\varepsilon I_{b,S} \tag{4.2}$$

$$I_p(x=t)=\varepsilon I_{b,C} \tag{4.3}$$

where $x=0$ and $x=t$ are the locations of the source and sink plates, respectively with a value of $\varepsilon=1$. The boundary conditions on the lateral sides of the simulation domain are symmetry boundary conditions. Note that the choice of symmetry or periodic boundary

condition makes no difference for the geometries considered in the study—insulation material placed between two infinitely large parallel walls (see Figure 4.2).

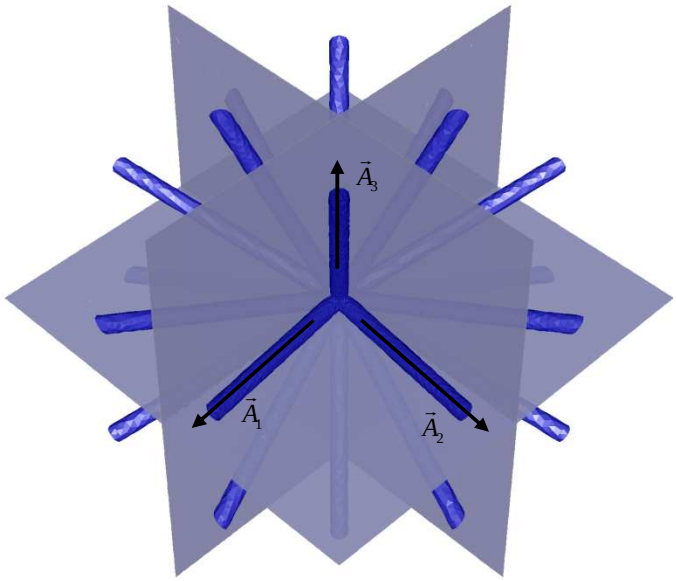

Figure 4.1: Scattering directions in 3-D for DOM. Radiation is scattered in 24 directions in 3-D space.

This is because temperature gradient is only in the thickness direction making the heat flow in lateral directions insignificant. For the same reason, one could also expect that the macroscale calculations in 2-D and 3-D results in identical solutions (phase function calculations must be in 3-D). Nevertheless, to better emphasize on the generality and completeness of the simulation approach all calculation presented in this paper are conducted in 3-D domains (see Figure 4.3).

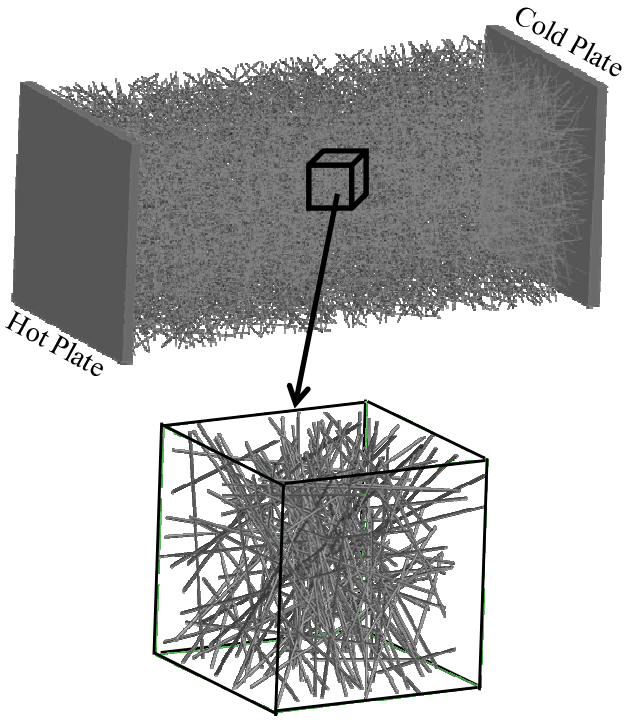

Figure 4.2: An example of fibrous media considered in this work. The in-plane and through-plane orientation of the fibers are random.

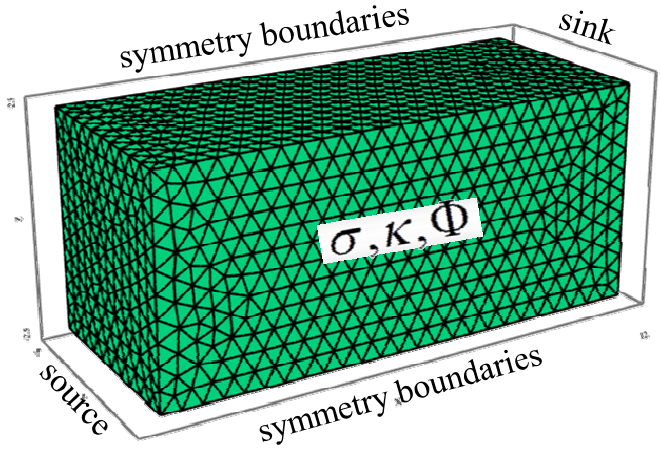

Figure 4.3: The simulation domain and its boundary conditions.

4.3 Microscale Formulations

Numerical values for σ, κ, β and Φ can be obtained by computing the extinction cross-section C_{ext}, and scattering cross-sections C_{scat}, which are the effective fiber cross-sectional areas that encounter a beam of incident radiation and have the unit of area. Φ is the scattering phase function of each individual fiber inside the media, and it gives the probability of light incident on the fiber being scattered into any arbitrary direction in 3-D space (Howell *et al.*, 2011).

$$\sigma = \frac{1}{V}\sum_{f=1}^{N} C_{sca,f} \tag{4.4}$$

$$\kappa = \frac{1}{V}\sum_{f=1}^{N} C_{abs,f} \tag{4.5}$$

$$\beta = \frac{1}{V}\sum_{f=1}^{N} C_{ext,f} \tag{4.6}$$

$$\Phi = \frac{1}{\sigma}\sum_{f=1}^{N} \frac{dC_{sca,f}}{d\Omega} \tag{4.7}$$

These parameters are influenced by the fibers' through-plane orientation angle, diameter, complex refractive index, wavelength of the incident IR, and the refractive index of material surrounding the fibers (i.e., air).

4.3.1 Radiative Properties of a Single Fiber

The equations for the interaction of an IR ray with a fiber are developed in a coordinate system with reference to the fiber (Bohren and Huffman, 1983). Therefore, the angle with which the IR is incident on the fiber and the direction of the scattered radiation

are defined with respect to the fiber (see Figure 4.4a) (Bohren and Huffman, 1983). Since different fibers have different orientations, the orientations of the fiber, incident IR and scattered IR must be defined in a global coordinate system (see Figure 4.4b) to estimate the radiative properties of the insulation medium as a whole. To transform the angles from a fixed coordinate system to the material coordinate system Lee has derived a set of trigonometric relations (Bohren and Huffman, 1983). The angles defined in terms of the fibers' coordinate system (local coordinate system) can be related to the material's coordinate system (global coordinate system) as (see Figure 4.4 for angle descriptions):

$$\cos\phi_C = \sin\phi = \vec{R}_i \cdot \vec{R}_f = \vec{R}_s \cdot \vec{R}_f \tag{4.8}$$

$$\cos\eta = \vec{R}_i \cdot \vec{R}_s \tag{4.9}$$

$$\cos\theta = \frac{\cos\eta - \cos^2\phi_C}{\sin^2\phi_C} \tag{4.10}$$

The radiation scattered by a fiber propagates along the surface of a cone, and the scattering angle (η) has a maximum possible value for a specified fiber orientation (ξ_f) and this maximum scattering angle ($\eta_{\max}$) is given by the following relation.

$$\cos\eta_{\max} = \min\left(2\cos^2\phi_C - 1, 2\left(\cos\xi\cos\xi_f\right) - 1\right) \tag{4.11}$$

For the complete derivation of the above equations the readers are referred to Lee, 1994. After the coordinate transformations have been made the radiative parameters of the fibrous media are now expressed in terms of angles η and ϕ_C (in the global coordinates system) rather than in terms of ϕ and θ (in the local coordinates system). However the angle η is determined by the directions of the S4 approximation.

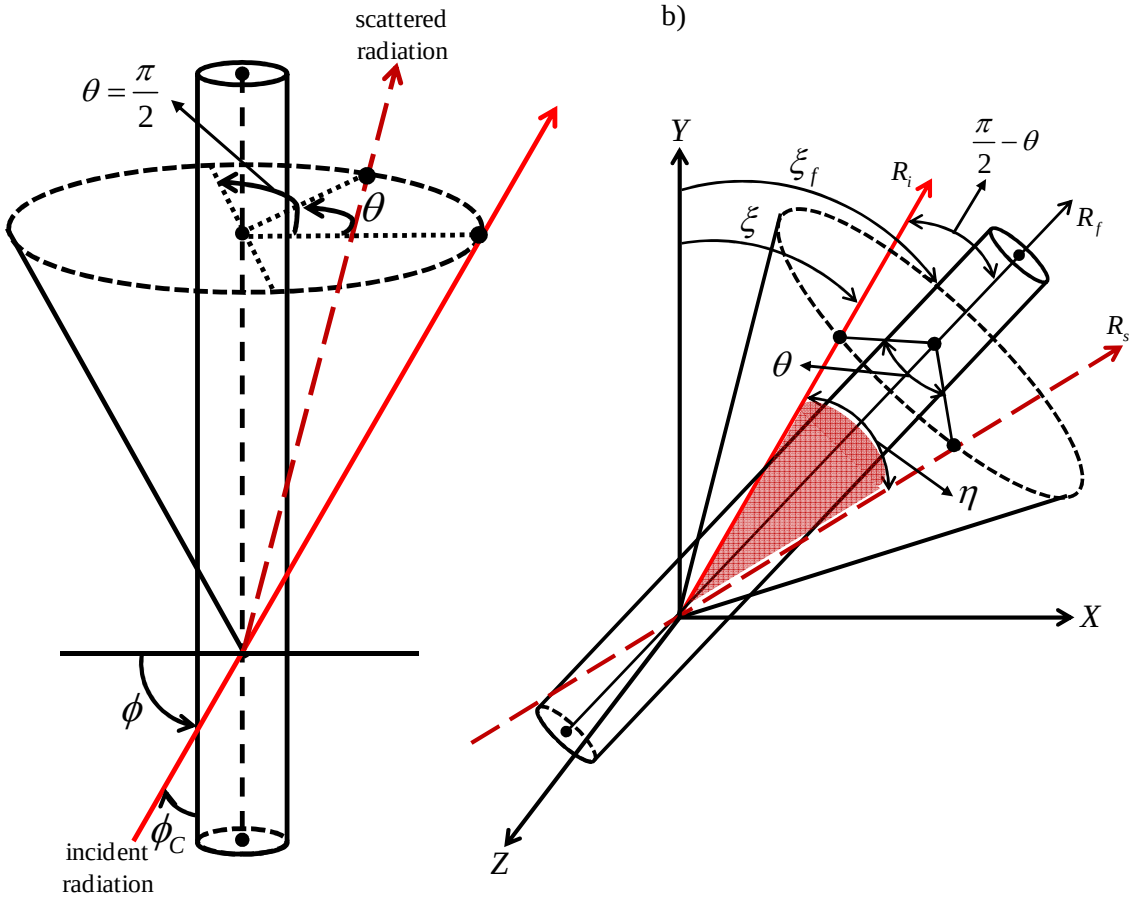

Figure 4.4: Schematic of a fiber oriented in its local coordinate system (a) and the material's coordinate system (b).

After the virtual fibrous structures are produced, a MATLAB code was developed to compute the orientation of the fibers in the domain. As the orientation of each individual fiber inside the domain is determined, the corresponding ϕ_C is computed based on the incident IR direction. With this angle computed, all possible directions in which an IR ray can be scattered by the fiber can be determined. After these directions are obtained, the algorithm checks if any of these possible scattering directions coincide with

the pre-defined DOM directions. If it is determined that a fiber with a random orientation can scatter in any of the 24 possible DOM directions, then the corresponding phase function (Φ) value is computed using the angle η (calculated using the above transformations). After the value of η is calculated the corresponding θ is computed and used for calculating the radiative properties of the fiber. This procedure is repeated for all the fibers in the virtual microstructure.

The scattering cross-section of a fiber for parallel and perpendicularly polarized electric components of incident IR is given as:

$$C_{sca,\mathrm{I}} = \frac{2d_f}{x}\left[\left|b_{0\mathrm{I}}\right|^2 + 2\sum_{n=1}^{n_{\max}}\left(\left|b_{n\mathrm{I}}\right|^2 + \left|a_{n\mathrm{I}}\right|^2\right)\right] \tag{4.12}$$

$$C_{sca,\mathrm{II}} = \frac{2d_f}{x}\left[\left|a_{0\mathrm{II}}\right|^2 + 2\sum_{n=1}^{n_{\max}}\left(\left|a_{n\mathrm{II}}\right|^2 + \left|b_{n\mathrm{II}}\right|^2\right)\right] \tag{4.13}$$

Similarly the extinction cross-section of a fiber for parallel and perpendicularly polarized electric components of incident IR is given as:

$$C_{ext,\mathrm{I}} = \frac{2d_f}{x}\mathrm{Re}\left\{\left|b_{0\mathrm{I}}\right|^2 + 2\sum_{n=1}^{n_{\max}} b_{n\mathrm{I}}\right\} \tag{4.14}$$

$$C_{ext,\mathrm{II}} = \frac{2d_f}{x}\mathrm{Re}\left\{\left|a_{0\mathrm{II}}\right|^2 + 2\sum_{n=1}^{n_{\max}} a_{n\mathrm{II}}\right\} \tag{4.15}$$

After the scattering and absorption cross-sections are known an absorption cross-section can be computed using the following equations:

$$C_{abs,\mathrm{I}} = C_{ext,\mathrm{I}} - C_{sca,\mathrm{I}} \tag{4.16}$$

$$C_{abs,\mathrm{II}} = C_{ext,\mathrm{II}} - C_{sca,\mathrm{II}} \tag{4.17}$$

The differential scattering cross-section ($dC_{sca}/d\Omega$), which is used for computing the phase function, is obtained from the following equations:

$$\frac{dC_{sca,I}}{d\Omega} = \frac{4\lambda}{\pi^2 \sin\theta \sin^2\phi_C}\left|T_1^2\right| \tag{4.18}$$

$$\frac{dC_{sca,II}}{d\Omega} = \frac{4\lambda}{\pi^2 \sin\theta \sin^2\phi_C}\left|T_2^2\right| \tag{4.19}$$

$$\frac{dC_{sca}}{d\Omega} = \frac{1}{2}\left(\frac{dC_{sca,I}}{d\Omega} + \frac{dC_{sca,II}}{d\Omega}\right) \tag{4.20}$$

The differential scattering cross-section is the energy scattered per unit time into a unit solid angle along a direction Ω, which is specified by the angles θ and $\eta_{\max}$ for unit incident irradiance (Bohren and Huffman, 1983). After the values of scattering, extinction and absorption cross-sections of each fiber for the two incident IR polarizations are computed, the average values of each of the cross-sections are calculated. These average values are used in the calculations shown in Eq. (4.4) – Eq. (4.7). The values for a_{I}, b_{I}, a_{II}, b_{II}, T_1 and T_2 are computed using the electromagnetic wave theory (see the Appendix for the formulations and Figure 4.4b for complete description of the angles θ, η and ϕ_C). It is important to note that the upper limit for the summations (n_{max}) in the above equations (Eq. (4.12) – Eq.(4.15)) are determined by the diameter of the fibers and the wavelength of the IR ray which are related by Eq. (4.21) (Bohren and Huffman, 1983).

$$n_{\max} = x + 4x^{\frac{1}{3}} + 2 \tag{4.21}$$

Note that the length of the summation is directly proportional to the fiber diameter and inversely proportional to the wavelength of the IR ray.

After the microscale radiative properties of the fibrous media are obtained, the RTE (macroscale) is solved numerically using the FlexPDE software. Solution of the RTE yields the distribution of intensity in each direction of the utilized DOM approximation (S4 in the present study). A sample contour plot of the intensity distribution in an insulation medium with a fiber diameter of 7μm, 3-D isotropic fiber orientation, SVF of 0.5%, and a thickness of 1.2 cm is shown in Figure 4.5.

4.3.2 Validation

For the finite element calculations (solution of the RTE), the simulation domains were meshed using 16,000–25,000 tetrahedron cells (see Figure 4.3). A series of trial simulations were conducted prior to collecting simulation data to ensure that results are not affected by the choice of mesh size.

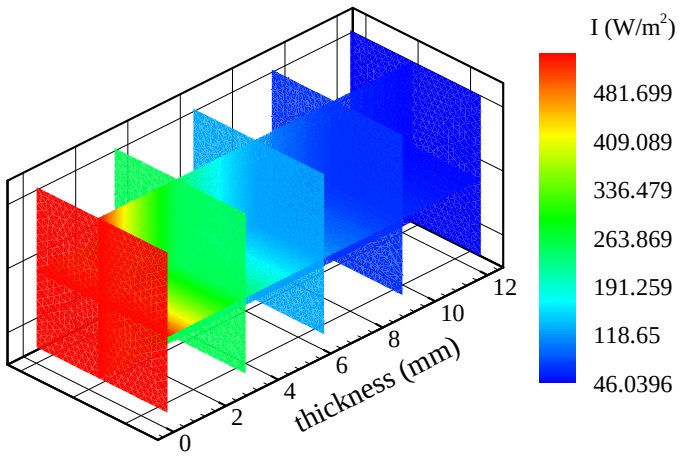

Figure 4.5: An example of the intensity contour plots obtained from the macroscale simulations.

To verify the accuracy of the analytical results, the phase function values obtained from current calculations for a medium with a fiber diameter of 1 µm, a through-plane and in-plane fiber orientations of 5 and 45 degrees, respectively, are compared with those reported in (Lee, 1994) (note that the phase function is independent of SVF and thickness of the insulation material) (Lee, 1990). Good general agreement between the two works is evident (Figure 4.6a), which allows one to extend the current method to compute the radiative properties of media with different microstructural parameters.

In Figure 4.6b the transmittance results from the current simulations are compared to the semi-empirical transmittance values obtained by Houston and Korpela for fiberglass insulations with an SVF of 0.33%, a mean fiber diameter of 7.45 µm, and a thickness of 3.8 cm (Houston and Korpela, 1982). In their work, the authors analytically calculated the flux of conductive heat through their media. The heat flux through their media was also measured experimentally, which includes the contribution of both the conduction and radiation. The heat flux results of Houston and Korpela are shown in Appendix B for reference. Subtracting the theoretically calculated conduction heat flux from their experimental data, an estimate of the transmitted radiative heat flux values were obtained and normalized by the incident radiation heat flux values to obtain the values of τ for comparison with the current simulation results (Figure 4.6b). To generate these simulation results, virtual fibrous structures as close as possible to the actual fiberglass media used in the experiments reported in (Houston and Korpela, 1982) were produced (the through-plane and in-plane fiber orientations were estimated to be about 15 and 45 degrees, respectively, for the lack more accurate information). The refractive

index data for the temperature range used in the currents simulations was obtained from the work of Hsieh and Su, 1979 (see Appendix C for the values). From Figure 4.6b it can be seen that the current simulations produce results with reasonable agreement with the results reported in (Houston and Korpela, 1982).

4.4 Results and Discussion

A thorough parameter study is conducted in this work to study the influence of different microstructural parameters on heat insulation performance of a fibrous material. Unless otherwise stated, fibers with a diameter of 7 μm were used throughout this study. The simulations are conducted in domains with a thickness of 12 mm and in-plane dimensions of 5×5 mm. The source and sink temperatures are considered to be 479 K and 300K, respectively. The absorption coefficient, scattering coefficient and the phase function for the media are computed using the Mie scattering theory.

To study the influence of fiber diameter on insulation performance of fibrous materials, a series of fibrous structures with identical parameters but different fiber diameters were generated. Fibers in these structures are allowed to have 3-D isotropic orientations. It can be seen in Figure 4.7a that as fiber diameter increases from 0.75 μm to 20 μm the heat transmittance first decreases and then starts to increase. Similar conclusions were made in the work of Larkin and Churchill (1959). However, the optimal fiber diameter at which best radiation insulation can be achieved depends on the application temperature, and has not been quantified previously. It can be seen from

Figure 4.7b that as the operating temperature increases from about 410 K to about 725 K, the optimal fiber diameter decreases from about 10μm to about 3μm.

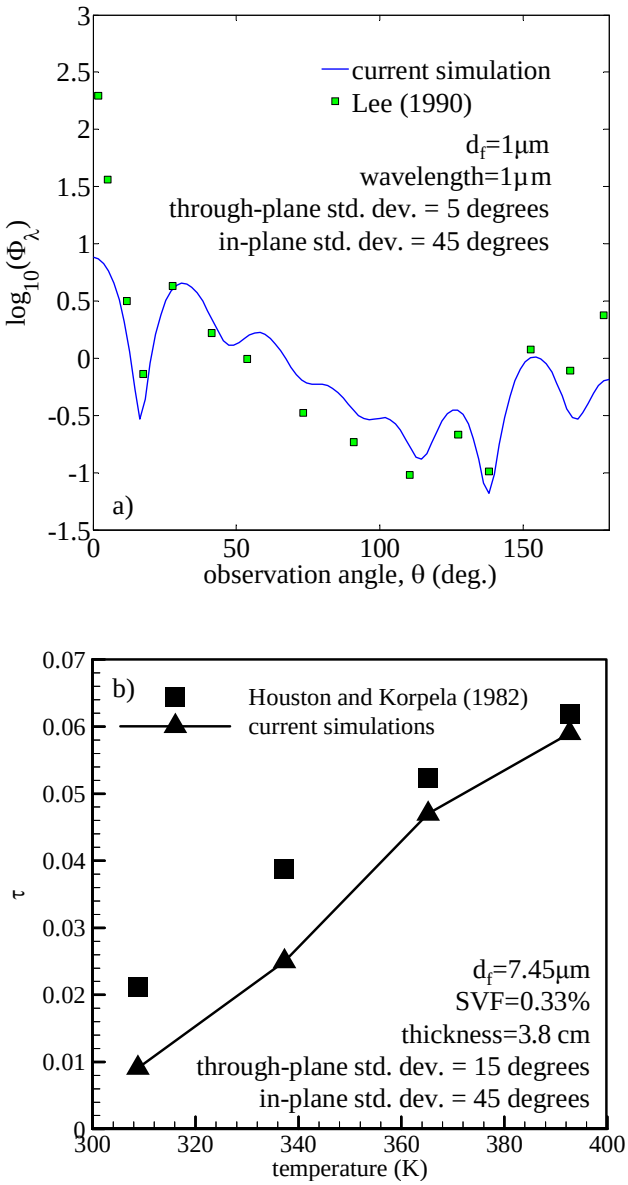

Figure 4.6: a) Comparison between the current phase function ($\Phi_{\lambda,m}$) calculations and those of Lee, 1989 for a single fiber. b) comparison between transmittance values obtained from current simulations and those reported in Houston and Korpela, 1982.

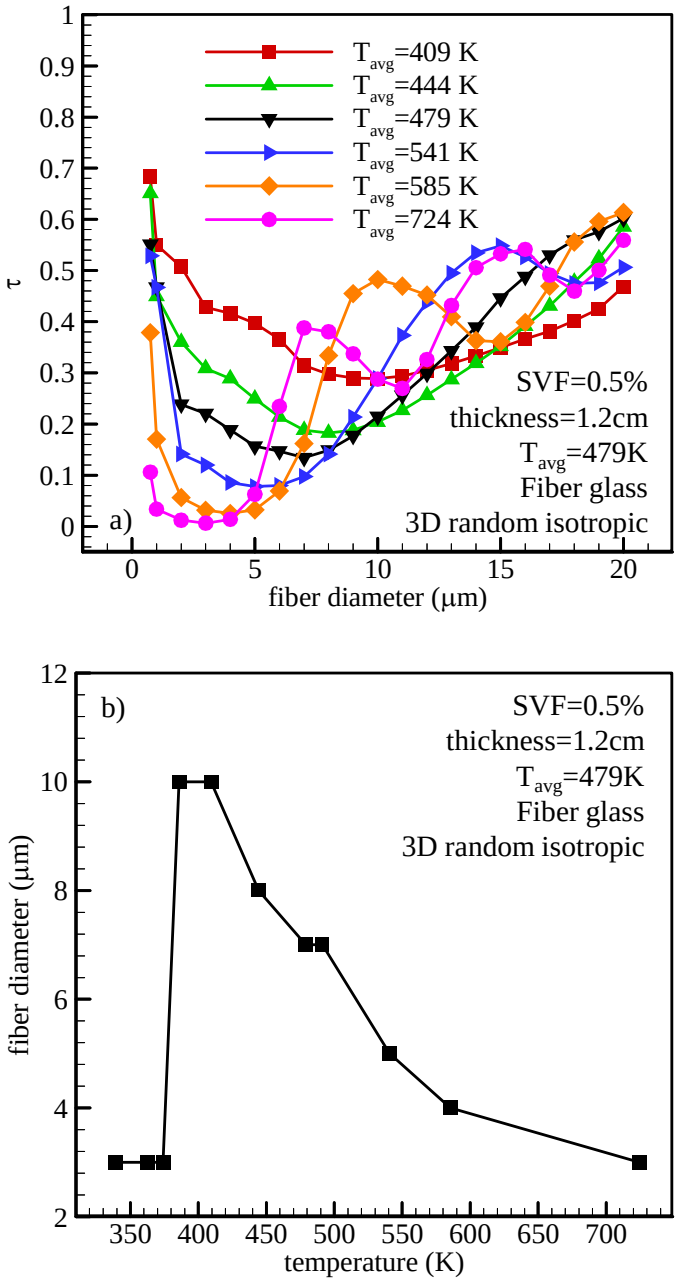

Figure 4.7: a) Transmittance values for media with different fiber diameters at different operating temperatures, b) optimal fiber diameter as a function of temperature. The structures are 3-D isotropic with an SVF of 0.5% and a thickness of 1.2 cm.

To study the influence of fibers' through-plane orientation on the performance of insulation media, a series of fibrous structures with identical parameters but different fiber orientations were generated, and their performance at a temperature of 479 K (chosen arbitrarily) was computed. In these structures, fibers were allowed to have random in-plane orientations, but their through-plane orientations are controlled. These fibers have a zero mean through-plane orientation, but the standard deviation about this mean value varies from 0 to 45 degrees. Note that a standard deviation of 45 degrees represents a random through-plane orientation. Structures with random in-plane and through-plane orientations are referred to as three-dimensionally isotropic.

Figure 4.8a shows the transmittance through the media with different through-plane fiber orientations. It can be seen that as through-plane orientation of the fibers increases from 0 to 45 degree, the transmittance through the material increases by about 40%. Therefore, one can conclude that media with small through-plane fiber orientations are better insulators. This conclusion is also in agreement with the predictions of the MCRT simulations conducted for media made of micron-sized fibers as well as the results of Lee and coworkers (Lee, 1989 and 1990).

To further investigate if the optimal fiber diameter reported in Figure 4.7 is affected by the orientation of the fibers, a series of simulations for materials with different fiber diameters and orientations at a fixed temperature of 479 K were conducted (see Figure 4.8b). It can be seen that the optimal fiber diameter at a given temperature is not affected by the fiber orientation. The best radiation insulation is obtained when the through-plane fiber orientation is zero.

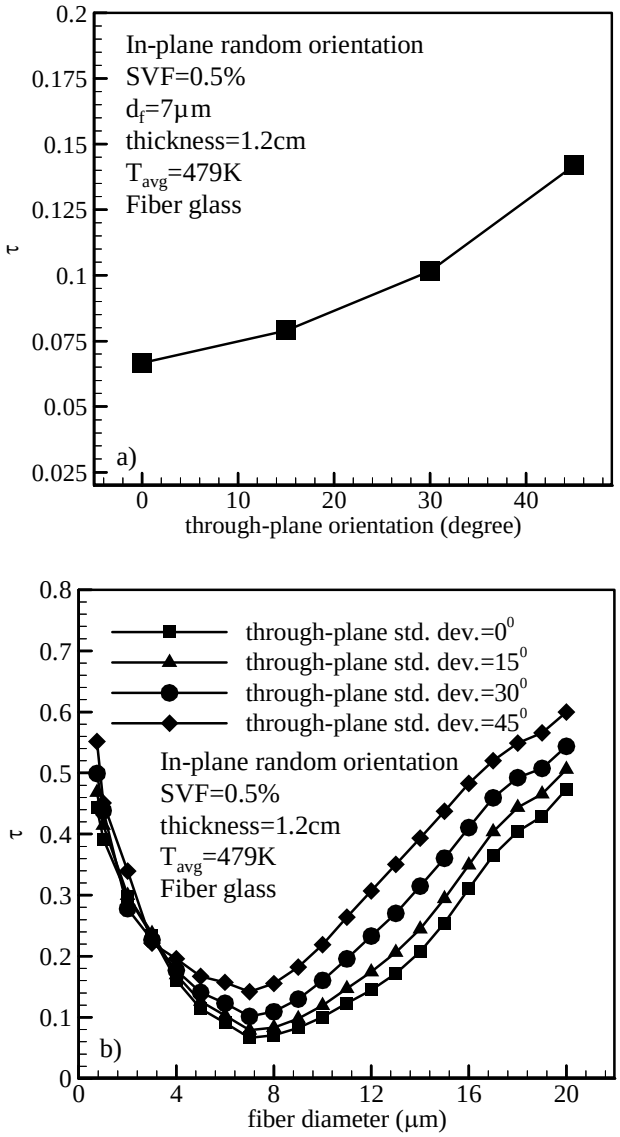

Figure 4.8: a) Effect of varying through-plane fiber orientations on IR transmittance, b) effects of fiber orientation on transmittance for fibers with different diameters. The media simulated here have random in-plane fiber orientations but varied through-plane orientations. A fiber diameter of 7 μm, an SVF of 0.5%, and a thickness of 1.2 cm were considered.

To study the influence of SVF on the radiation insulation performance, a series of fibrous structures with identical parameters but different SVFs were generated. Fibers in

the structures were allowed to have random isotropic orientations. It can be seen from Figure 4.9 that as SVF increases the heat transmittance decreases. This is due to the fact that value of the extinction coefficient of the media increases with SVF. In Figure 4.9 the investigation of the effect of thickness on heat insulation can be seen. For these results, SVF, fiber diameter and fiber orientation were held constant and the thickness of the material was varied from 1 mm to 12 mm. It can be seen that radiation transmittance decreases as thickness increases. Note that SVF and thickness will not influence the optimal fiber diameter (Figure 4.7) due to the fact that the equations used for computing the radiative properties of the fibers (Eq. (4.4)– Eq. (4.20)) do not depend on SVF or thickness.

4.5 Comparison of transmittance values obtained from MCRT and RTE methods

To compare the dual-scale modeling approach for calculating radiation heat transfer with the MCRT method, the fibrous structures used for MCRT calculations in Figure 3.19 and Figure 3.20f were considered. The dual-scale approach was used to compute the radiation transmittance through these structures. The same value of refractive index which was used for the MCRT study was used here. Figure 4.10 shows a comparison of transmittance values obtained using MCRT and the dual-scale approach. In Figure 4.10a variation of transmittance with SVF is presented and can be seen that the two approaches show a very good agreement. For the sake of completeness, in Figure 4.10b the variation of transmittance with through-plane orientation is presented and a

good agreement can be observed. However it can be noted in both these comparisons the values of transmittance computed using the dual-scale approach are higher.

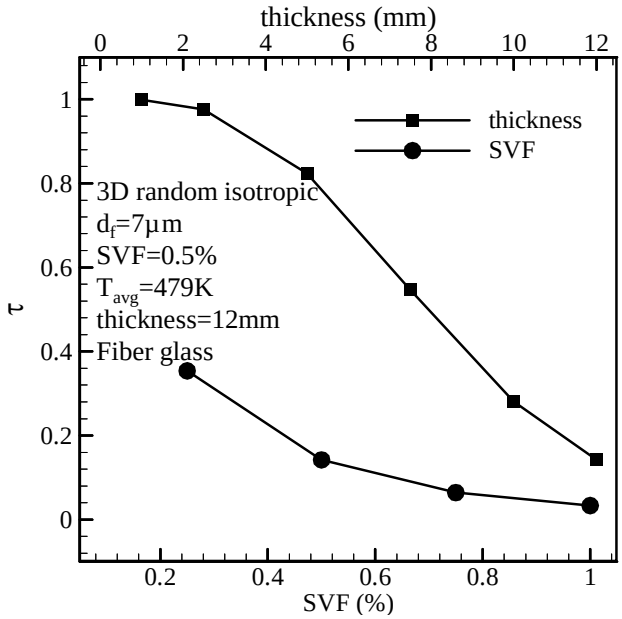

Figure 4.9: Transmittance values for media with varying SVF and thickness having 3-D isotropic structures. The fiber diameter is 7 μm.

Comparing the MCRT and the RTE methods of predicting radiation heat transfer in fibrous insulation materials, advantages and shortcoming of both the methods are outlined. The advantages of MCRT method are the radiative transfer through the insulation material can be computed directly without the need for solving an integro-differential equation (the Radiative Transfer Equation), which is needed for the alternative approach. Refractive index of the fibers is the only radiative properties needed for the calculations.

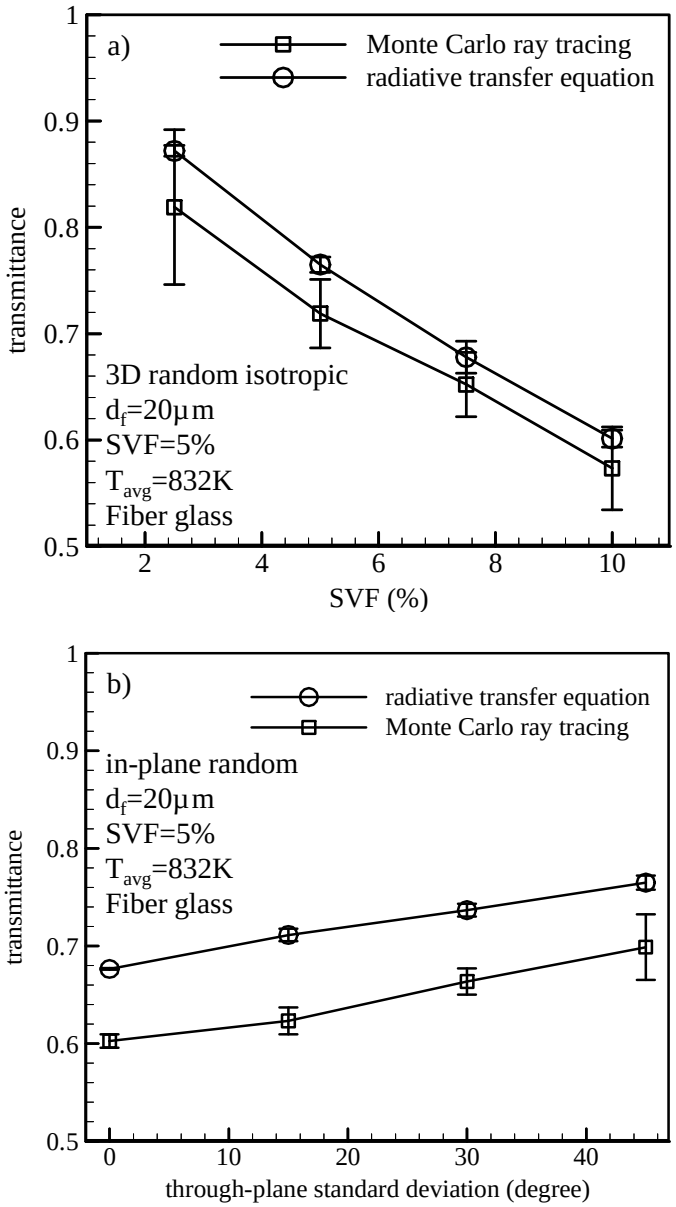

Figure 4.10: Comparison of transmittance values calculated using MCRT and dual-scale approach for media with varying (a) SVF and (b) through-plane orientations.

Different fiber geometries like elliptical, trilobal, cylindrical etc. can be simulated. Few of the shortcomings of MCRT are that it is computationally expensive compared to RTE method. Allowable fiber diameter range is limited by the operating temperature. MCRT

becomes inaccurate for fibers comparable in size to the wavelength of the IR radiation. The advantages of the electromagnetic wave theory it is computationally less expensive compared to MCRT. Wide range of fiber diameters can be simulated as the temperature does not limit the lowest possible fiber diameter. However this method has its shortcomings too. It requires solving the RTE–an integro-differential equation. Complicated math is involved in the calculation of the radiative properties. The accuracy of the method depends on the numerical procedure used to discretize and solve the RTE. Fiber geometry is limited to cylindrical or maybe at most elliptical fibers and the scattering directions need to be approximated for solving the RTE.

4.6 Conclusions for Dual-Scale Modeling Approach

A dual-scale approach is developed in this work to predict how different fibrous structures perform as insulation media in a quantitative manner. The dual-scale nature of the method presented here allows one to devise computationally-feasible simulations for media made up of thousands of fibers (i.e., the actual thickness of the material). This methodology can be adopted for design and development of insulation materials for different applications.

The parameter study revealed that for media with different microstructural properties, increasing SVF, thickness, or fibers' through-plane orientation, increases the amount of radiation heat transfer through insulation. Moreover, it was found, and quantified, that there exists a fiber diameter for which heat transfer through a fibrous

media is minimal. For glass fibers in a temperature range of about 340 to 750 K, best insulation performance was with fibers having a diameter of about 3 to 10 µm.

Chapter 5 Heat Transfer in Multi-Component Fibrous Insulations[4]

5.1 Introduction

Heat generally transfers across a medium via a combination of conduction, convection, and radiation. As mentioned earlier in Chapter 1, heat transfer via convection is often negligible in a typical fibrous insulation. Unlike convection, conduction is an important contributor in the total heat transfer across a fibrous insulation, and has been extensively studied in the past decades. Numerous analytical (e.g., Bankvall, 1973; Bhattacharya, 1980; Furmanski, 1991) and experimental (e.g., Cunnington and Lee, 1996 and Zhang *et al.*, 2008) studies have been conducted to define a thermal conductivity for the combined solid and the fluid (interstitial phase) conductivities in a fibrous insulation. Fortunately, for high-porosity insulation media with air as the interstitial fluid, the analysis is quite simple, as the contribution of the solid phase in the overall heat conduction is often non-existent. However, if the thermal conductivity of the fibers' material is high in comparison to that of air (e.g., steel or aluminum fibers in air), or if the porosity of the media is not high enough, then the properties of the solid fibrous structure

[4] Contents of this section have been submitted to a journal for publication as an article titled "Modeling Performance of Multi-Component Fibrous Insulations against Conductive and Radiative Heat Transfer", by R. Arambakam, H.V. Tafreshi, and B. Pourdeyhimi, *International Journal of Heat and Mass Transfer*.

(e.g., fiber diameter, fibers in-plane or through-plane orientations etc.) should be considered in the analysis. See Chapter 2 for the complete description of the technique.

In contrast to conduction and convection, estimating the contribution of radiative heat transfer in heat transfer through a fibrous insulation is not straightforward. This is because radiative properties of a fibrous medium (e.g., scattering phase function, absorption cross section, or scattering cross section) strongly depend on both the geometry and the material of the fibers. These properties are nonlinear functions of temperature and are very different for fibers of identical geometry but made of different parent materials, for instance. Figure 5.1 shows a comparison between refractive index values for copper (Brewster, 1992), glass (Hsieh and Su, 1979), and mineral wool (Ljungdhal *et al.*, 1991) as a function of temperature.

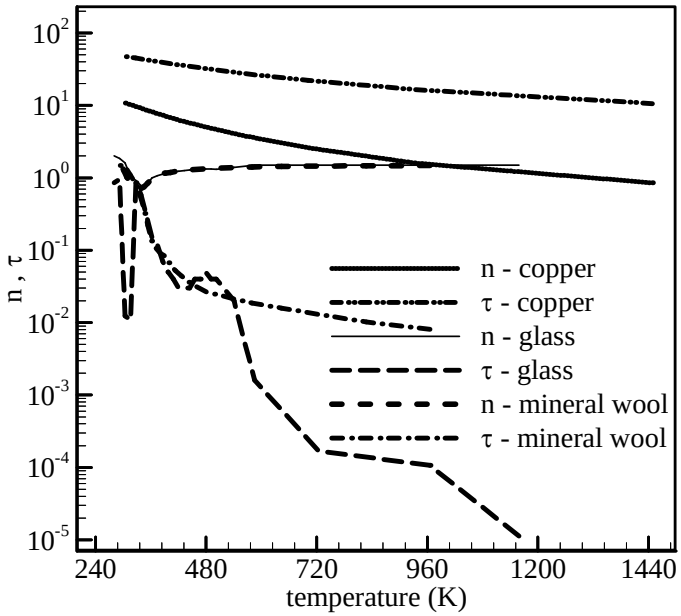

Figure 5.1: Refractive indices of copper, glass and mineral wool at different temperatures.

The most traditional method to predict performance of a fibrous insulation treats radiation heat transfer in a porous medium as a diffusion process. In this method, a radiation thermal conductivity using the Rosseland approximation is defined and used in conjunction with the thermal conductivity of the material to estimate its insulation performance (Tong and Tien, 1980). On a parallel track, radiative heat transfer in a fibrous medium has also been studied using the Radiative Transfer Equation (RTE) (Eq. (4.1)), which is a mathematical representation of the conservation of energy written for an IR beam that travels in a given direction. RTE tallies the change in the beam's energy due to absorption and scattering in different directions along its path. Obviously, the radiative properties of the media must be known before the RTE can be solved. Extensive research has been carried out to calculate these radiative properties using the theory of electromagnetic waves (see e.g., Bohren and Huffman, 1983; Lee, 1989, 1990 and 1994). As the RTE is a complicated integro-differential equation, it can only be solved via approximate methods. The Discrete Ordinates Method (DOM), for instance, has been widely used to replace the integral term in the RTE with a summation. The DOM converts the RTE to a set of coupled differential equations which can be solved numerically (Chandrasekhar, 1960).

In this regard, a simulation technique was developed where an accurate RTE solution via the DOM's S4 approximation has been obtained for insulation media as thick as several centimeters or more, without excessive computational requirements (see Chapter 4). The flexibility of this computational method allows us to investigate insulation performance of media made up of fibers with materials and diameters, as will

be seen later. A special attribute of the simulation method developed in this work, is that it can easily be utilized to predict the insulation performance of media made up of fibers from different materials, orientations and diameters. It can also be used to simulate the effect of blending dissimilar fibers or layering them over each other, among many others. Such a capability can be of great interest for design and development of new insulation products where a combination of fibers with different dimensions or material are used to perhaps improve the mechanical strength of the fibrous structure, among many other properties.

5.2 Combining Conduction and Radiation

Once the conduction (Chapter 2) and radiation components (Chapter 4) of the heat fluxes across an insulation is obtained (see previous sections), one can obtain a total conduction–radiation thermal conductivity to be used in for the media assuming that media's resistance to conduction and radiation act like resistors in a parallel configuration (see Figure 5.2). Therefore, the total resistance to heat flow can be obtained as:

$$R_{total} = A\left[\frac{1}{R_{cond}} + \frac{1}{R_{rad}}\right]^{-1} \tag{5.1}$$

where $R_{cond} = \frac{L}{k_{eff} A}$ and $R_{rad} = \frac{T_h - T_c}{q''_{rad} A}$ are thermal resistance to conductive and radiative heat flows, respectively. The radiation flux values are obtained from the simulation technique outlined in Chapter 4. The total heat flux can be computed using Fourier's law of heat transfer that is rewritten in terms of the above total thermal resistances as:

$$q''_{cond+rad} = \frac{\Delta T}{R_{total}} \tag{5.2}$$

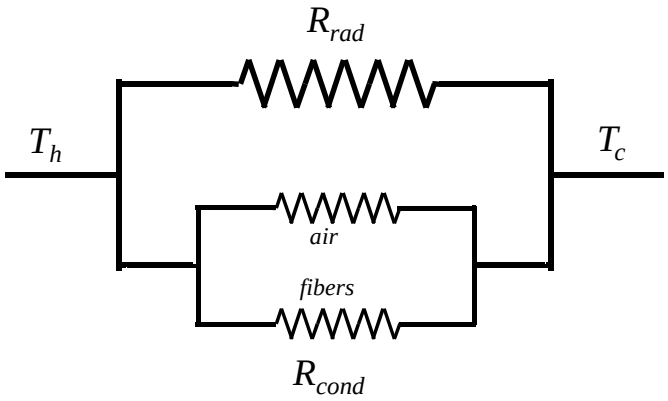

Figure 5.2: Schematic of the thermal resistance model considered here.

5.3 Results and Discussion

Before we further discuss our simulations of multi-component insulations, a validation study is presented to better examine the accuracy of our calculations. Figure 5.3 shows a comparison between the experimental data of Houston and Korpela obtained for fiberglass insulations and our simulation of the same media. These authors reported their fiberglass media to have an SVF of 0.33%, a mean fiber diameter of 7.45 μm, a thickness of 3.8 cm. Their experiments were conducted for heat transfer between two parallel plates with a fixed sink temperature of 285 K but a adjustable source temperature. To produce our simulation data, we generated virtual fibrous structures that resemble the actual fiberglass media of Houston and Korpela, 1982 as closely as possible, based on the information provide in the paper by these authors. In the absence of detailed

information about the fiber in-plane/through-plane orientations, we assumed that the media tested by Houston and Korpela had perhaps relatively planar structures with random in-plane fiber orientation distribution. We therefore used standard deviations of 45 and 15 degrees about zero mean values for the in-plane and through-plane orientations of the fibers. The refractive index data for the temperature range shown in Figure 5.3 was obtained from the work of Hsieh and Su, 1979. For the simulation results shown in Figure 5.3, we considered air conductivity values at an average temperature of the source and sink (i.e., for a sink temperature of 285 K and source temperatures of 309 K, 337 K, 365 K, and 393 K we used air conductivity values of 0.0262, 0.0273, 0.0282, and 0.0292 W/m-K, respectively) (Incropera *et al.*, 2006). For glass fibers a conductivity value of 1.5 W/m-K was used. We combined the contributions of conduction and radiation (obtained from our simulations) as discussed in Section 5.2. Good agreement can be observed between our numerical results and the experimental data of Houston and Korpela, 1982.

5.3.1 Fiber Material versus Fiber Diameter

As discussed earlier (see Figure 5.1), radiative properties of a fiber are greatly influenced by its material. In this sub-section, we compare insulation performance of media made of either mineral wool or glass with different fiber diameters. For this comparison, we generated a series of single-component fibrous structures with identical parameters but made different fiber diameters. Fibers in these structures have 3-D isotropic orientations. A thickness of 12 mm is considered for the insulations. The in-

plane dimensions of the simulation domain are considered to be 5×5 mm. The source and sink temperatures are considered to be 479 K and 300K, respectively.

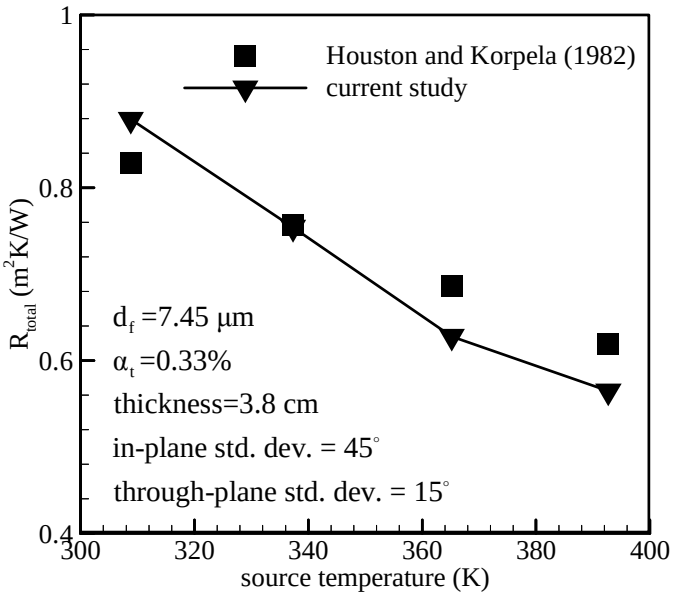

Figure 5.3: Comparison between the experimental thermal resistance values of Houston and Korpela, 1982 and our simulations.

As can be seen in Figure 5.4, total thermal resistance increases with fiber diameter from 0.75 µm to about 5–7µm, but starts to decrease afterwards. Similar observation was reported in the papers by Larkin and Churchill, 1959; McKay and Timusk, 1984; and Gibson *et al.*, 2007. The optimal fiber diameter for best heat insulation is about 5µm for mineral wool fibers and 7µm for glass fibers (see Figure 5.4a). In the remainder of the calculations, we used air (0.032 W/m-K) and fibers (1.5 W/m-K for both glass and mineral wool) conductivity values obtained at an average temperature of 390 K. For the radiative properties, however, we used the fibers refractive index (from Hsieh and Su for

glass and Ljungdahl *et al.* for mineral wool) at the source temperature (479 K), because of the 4th power dependence of radiative transfer on temperature (i.e., hot surfaces making a stronger contribution to the total radiative heat).

In Figure 5.4b, the radiation (R_{rad}) and conduction (R_{cond}) thermal resistance values for the cases shown in Figure 5a are presented separately for better comparison. It can be seen from this figure that resistance to radiative heat is higher than that against conductive heat when the media is made of small fibers, especially for mineral wool. Resistance to conduction and radiation are almost equal for media with a fiber diameter of about 10μm (for the structural and thermal conditions considered here). Media with larger fiber diameters tend to block radiative heat much less effectively as can be seen in Figure 5.4b.

5.3.2 Insulations with Dissimilar Fibers

In this section, the influence of fiber dissimilarity, both in terms of diameter and material, on insulation performance of composite fibrous media is studied. A total thickness of 12 mm is considered for the virtual insulation media (spacing between the source and sink walls). A total SVF of $\alpha_t = 1\%$ for the whole media was also assumed. Similarly, in-plane dimensions of 5×5 mm are as well as source and sink temperatures of 479 K and 300 K, respectively, are considered for the simulations.

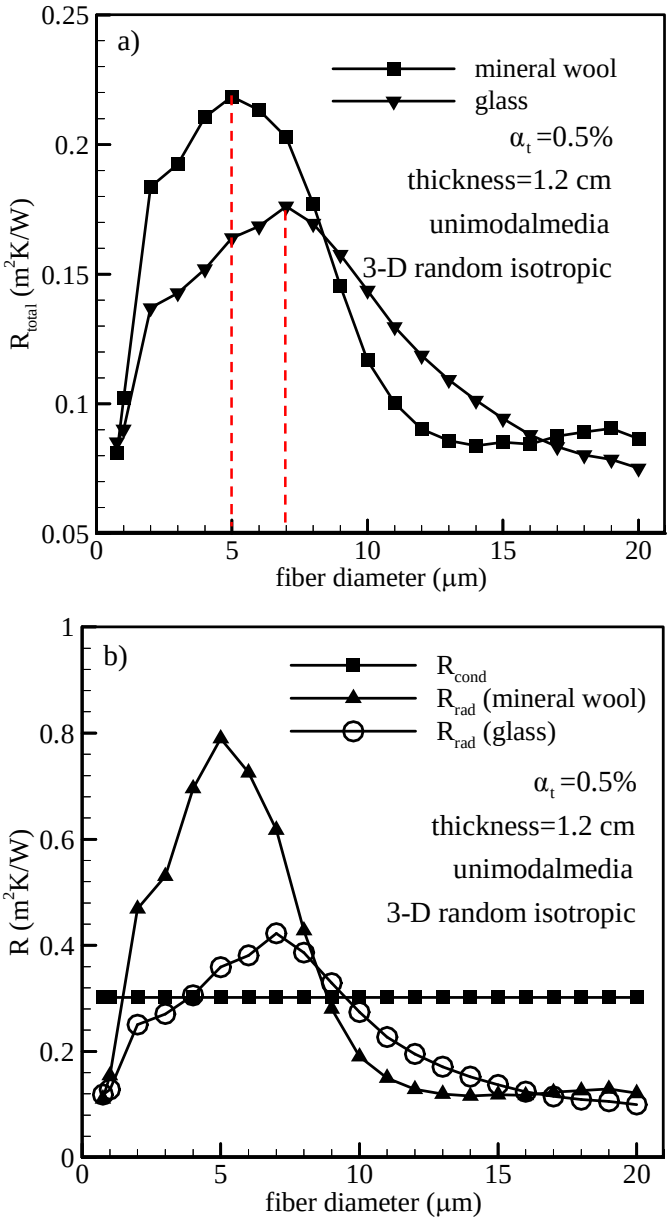

Figure 5.4: Thermal resistance values for media with different fiber diameters and materials for source and sink temperatures of 479 and 300 K, respectively (a) and their individual radiation and conduction components (b).

5.3.2.1 Media with Bimodal Diameter Distributions of Same Material

In simulating blended media with bimodal fiber diameter distribution (see Figure 5.5) made of same material, we considered the fine fibers with a diameter of 5 and 7 µm for media made of mineral wool and glass fibers, respectively. Figure 5.6 shows the effect of R_{cf} on the total thermal resistance of the bimodal fibrous media. A blend configuration for media with two different through-plane fiber orientations (zero-mean through-plane orientations with standard deviations of 15 and 45 degrees) is simulated.

In constructing the virtual fibrous insulations, we considered a coarse-fiber mass fraction value of 75% and total SVF of $\alpha_t = 1\%$. It can be seen in Figure 5.6a that increasing R_{cf} while keeping all other parameters constant, decreases the total thermal resistance of the media. This effect can be explained by considering the information shown in Figure 5.4: when the total SVF is held constant, media with higher R_{cf} have less number of 5 µm fibers (fibers which are very efficient in blocking radiative heat). Although not shown in Figure 5.6a for the sake of brevity, we in fact simulated multi-component media having coarse fibers as thick as 50 µm (R_{cf} =10), to mimic insulation media for which mechanical stability of the fibrous structure is important. A thermal resistance value of R_{total} = 0.18 was obtained from the simulations with fibers having a through-plane standard deviation of 15 degrees, indicating again that the insulation performance of a medium is mostly determined by the number of most efficient fibers (i.e., the 5 µm fibers here) in the media.

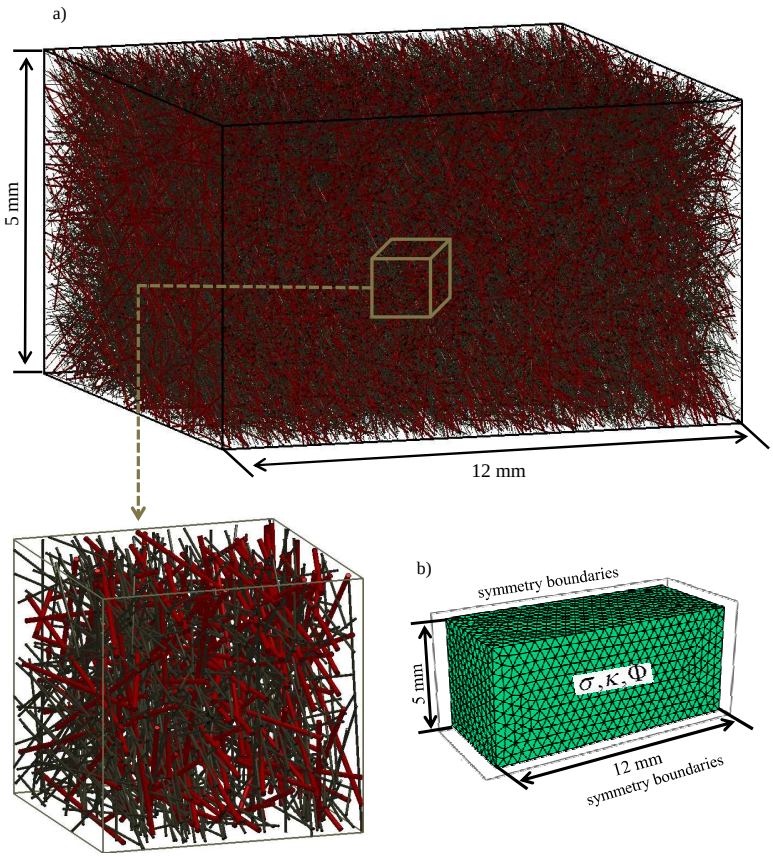

Figure 5.5: An example of the virtual fibrous structures produced in this study (a) and its finite element simulation domain (b). The medium shown here has a zero mean through-plane orientation with a 15-degree standard deviation.

Note also that the small hump in R_{total} values near $R_{cf} = 4$ can also be explained using the information in Figure 5.4, where a slight increase in the thermal resistance is observed for fiber diameters near 20 µm.

The above conclusions are obtained for when the fine fibers are chosen to be the most efficient fibers (5µm for mineral wool fibers). To demonstrate such cases where fine fiber diameter is smaller than the optimal fiber diameter, we used a fine fiber

diameter of 2 μm and varied R_{cf} in Figure 5.6b. It can be seen that thermal resistance slowly increase until $R_{cf} \cong 3$ and then starts to decrease. This trend is again attributed to the optimal fiber diameter for mineral wool being 5μm (see Figure 5.4). Here, we have also considered media with different through-plane fiber orientations to investigate if the fiber orientation affects the above conclusions. As can be seen in Figure 5.6, fibrous structures with smaller through-plane orientation are better at insulating heat transfer. However, the above conclusions are not affected by the in-plane orientation of the fibers.

For the completeness of the study, we have also compared the effects of separating fibers of different diameters into layers stacked on top of each other instead of homogenously blending them across the thickness. Figure 5.7shows the fibrous medium and finite element simulation domain considered for our layered-media simulations (compare with that in Figure 5.5). For modeling layered insulations, we solve the RTE for each separate layer, and use their layer-specific radiative properties (κ, σ, β and Φ). Boundary conditions similar to those specified in Equations (5.3) and (5.4) are used at the source and sink boundaries. At the interface between the two layers, the radiation intensity and its derivatives are considered to be identical for both layers:

$$I_p\left(\sigma_c, \kappa_c, \beta_c, \Phi_c\right)\Big|_{\text{intf}} = I_p\left(\sigma_f, \kappa_f, \beta_f, \Phi_f\right)\Big|_{\text{intf}} \tag{5.3}$$

$$\left.\frac{dI_p\left(\sigma_c, \kappa_c, \beta_c, \Phi_c\right)}{d\varphi}\right|_{\text{intf}} = \left.\frac{dI_p\left(\sigma_f, \kappa_f, \beta_f, \Phi_f\right)}{d\varphi}\right|_{\text{intf}} \tag{5.4}$$

where φ here represents any of the three Cartesian coordinate system directions.

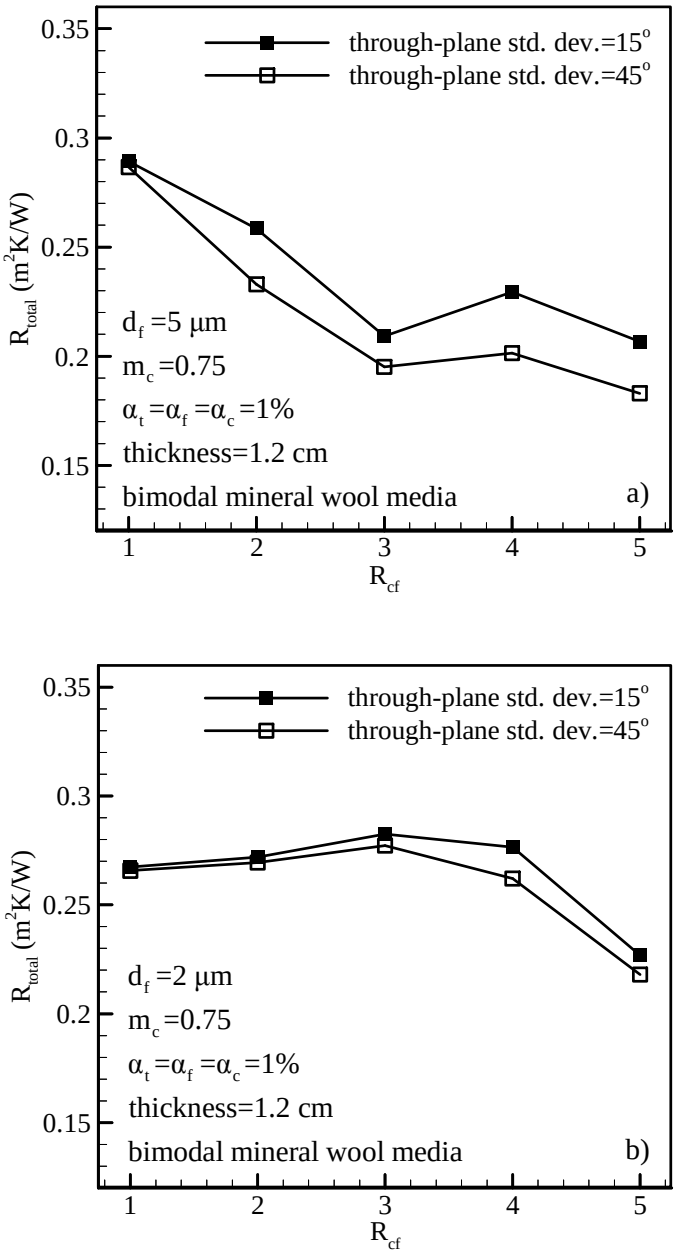

Figure 5.6: Thermal resistance values for media made of mineral wool fibers of different diameters with a constant mc of 0.75 in the blended configuration with a fine fiber diameter of 5 µm (a) and 2 µm (b).

Here we also study the effects of varying m_c on insulation performance of bimodal media. In this case, we started by generating layered bimodal media with fine and coarse

fiber layer thicknesses of 3 mm and 9 mm respectively, but different SVFs for the coarse-fiber layer leading to different coarse-fiber mass fractions. Note that in this case the total SVF of the media will not remain constant. We held the coarse-to-fine fiber diameter constant at $R_{cf} = 3$ with a fine fiber diameter of 5 μm. The media considered here have 3-D isotropic fiber orientations. It can be seen from Figure 5.8 that total thermal resistance of the media increases as SVF of the coarse-fiber layer increases from $\alpha_c = 0.25\%$ to $\alpha_c = 1\%$. This is simply because increasing α_c increases the total SVF α_t of the media.

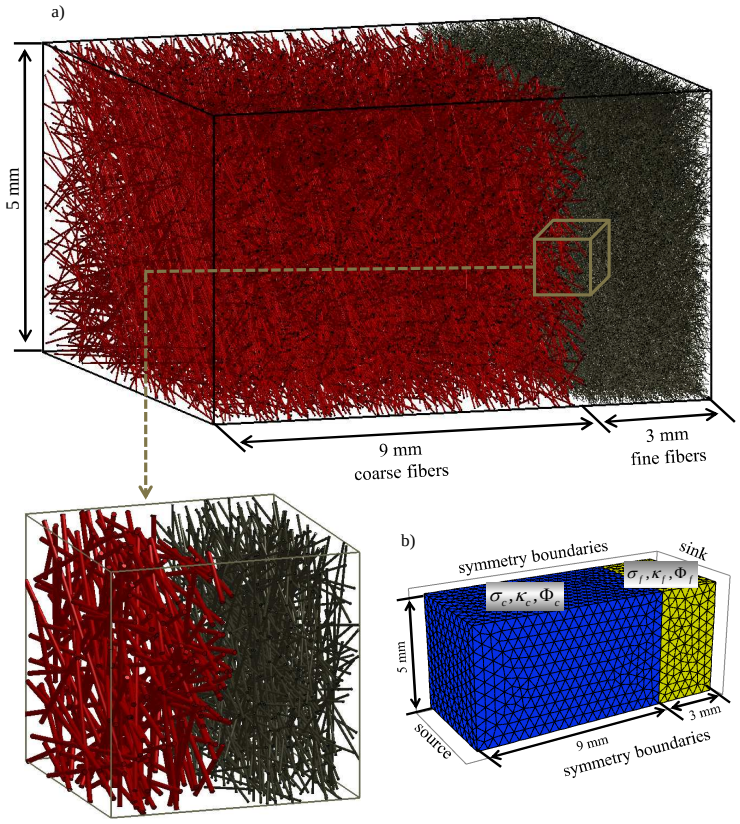

Figure 5.7: An example of the layered fibrous structures produced in this study (a) and its finite element simulation domain (b). The medium shown here has a zero mean through-plane orientation with a 15-degree standard deviation.

To further explore the effects of increasing the mass fraction of the coarse fibers (for instance), we blended the coarse and fine fibers in the above layered media (Figure 5.7a) and repeated the simulations, while maintaining all other parameters the same. These results are also added to Figure 5.8 for comparison. From this figure it can be seen that blended or layered configurations of fibers exhibit almost identical heat insulation performance. This can be explained by the fact that the equations used for the calculation of the radiative properties of the media are not a function of fiber position (Bohren and Huffman, 1983). We also reversed the position of the fine and coarse fiber layers with respect to the heat source and observed similar thermal resistance values indicating that the order by which the layers of different properties are stacked next to one another does not influence the steady state performance of the media. This result is in agreement with the work of Tian *et al.*, 2012.

5.3.2.2 Media with Bimodal Diameter Distributions from Different Materials

In this section, we consider bimodal media made up of blends of fibers from different materials (glass and mineral wool). As mentioned earlier thermal resistance of glass and mineral wool fibers are very different at an operating temperature of about 479 K (see Figure 5.4). Here we consider bimodal media with the fine fibers made of mineral wool with a diameter of 5µm and the coarse fibers made of glass. In Figure 5.9, we vary the coarse-to-fine fiber diameter R_{cf} from 1 to 5 while keeping m_c at 50%. From this figure, it can be seen that as the R_{cf} increases the thermal resistance of the material decreases.

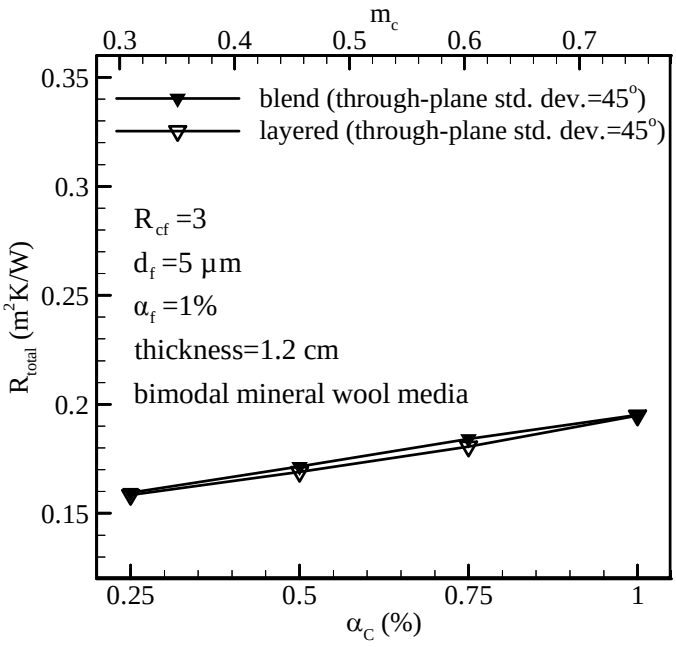

Figure 5.8: Thermal resistance values for media made of mineral wool fibers with different coarse-fiber mass fractions but a constant Rcf of 3 in the blended and layered configurations with a fine fiber diameter of 5 µm. The coarse-fiber solid volume fraction α_c changes with changing m_c .

Again, referring to Figure 5.4, it can be seen that mineral wool fibers with a diameter of 5µm are better insulators compared to glass fibers of any other diameter ranging from 5 to 25µm.

5.4 Conclusions for modeling heat transfer in multi-component fibrous insulations

The study presented here demonstrates the possibility of developing 3-D geometries resembling the microstructure of a fibrous insulation to be used in simulating the performance of such media when composed of different combinations of fibers in terms of both the materials and dimensions. Such a capability is believed to be of great

value to manufacturers of fibrous insulations in reducing the cost of design and optimization of new insulation materials. Our simulation method is designed for high-porosity insulation media with air as the interstitial fluid conduction where conduction through the solid structure is minimal.

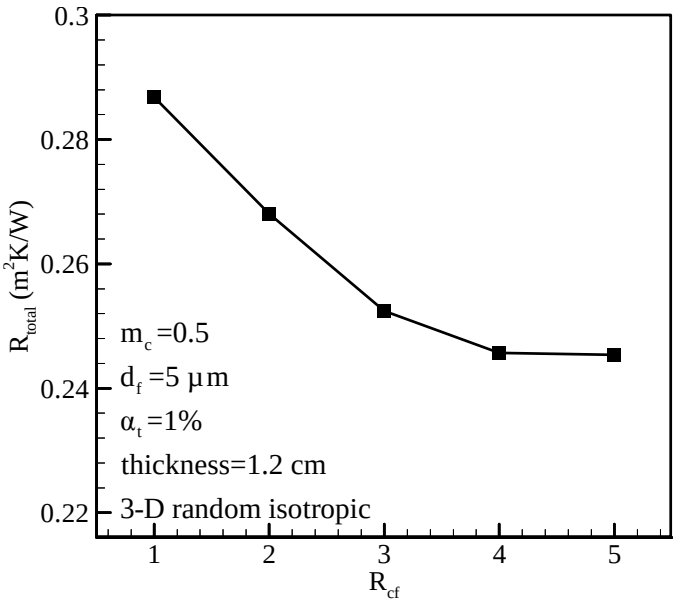

Figure 5.9: Thermal resistance values of bimodal blend media with a fine fiber diameter of 5µm, a coarse-fiber mass fraction of 0.5, and different R_{cf} values. The fine and coarse fibers are mineral wool and glass fibers, respectively.

Considering media made of different mass fractions of glass and mineral wool fibers with different diameters, we showed that virtual 3-D fibrous structures (incorporating fiber-level information) can be used to obtain radiative properties of such media (e.g., scattering phase function, scattering coefficient, and absorption coefficient) via the Mie scattering theory, and thereby predict the radiative component of heat flux through

insulation media by solving the RTE–DOM equations. The novelty of the simulation method presented here is that it is well suited for custom-design of insulation media for different applications.

From the parameter study conducted here, it was concluded that materials with glass or mineral wool fibers offer maximum thermal resistance when comprised of fibers with a diameter of about 5–7μm (for a source temperature of 479 K). It was also found that layered and blended fibrous multi-component insulations exhibit similar performance. It was also found that the stacking sequence does not affect the thermal resistance of layered media, in agreement with previous studies (Tien *et al.* 2012).

Chapter 6 Overall Conclusions and Future Work

In this work, the effect of materials' microstructure on the performance of fibrous heat insulation was investigated. Heat transfer via conduction was investigated using a computational technique developed by us which enables one to drastically reduce the computational size of the simulation domain (Chapter 2). Radiation heat transfer, on the other hand, was investigated using the Monte Carlo Ray Tracing technique and also via solution of the Radiative Transfer Equation (Chapters 3 and 4). In Chapter 5, the simulation techniques developed in Chapters 2–4 were combined to predict the thermal resistance of multi-component fibrous insulation materials. The simulation techniques developed in this dissertation allow one to computationally predict the insulation performance of materials made up of different combinations of fibers with different materials or dimensions. Such a capability can be of great interest for design and optimization of new insulation products.

The following conclusions can be drawn from the study conducted here:

- Heat conduction through the solid fibrous structures increases by increasing the material's solid volume fraction, fiber diameter, and fibers' through-plane

orientations. The in-plane orientation of the fibers, on the other hand, did not show any significant influence on the material's conductivity.

- It was also observed that the microstructural parameters of fibrous insulations have negligible influence on the material's performance if the conductivity of the solid phase is close to that of the interstitial fluid.
- From the radiation heat transfer simulations it was observed that IR transmittance through the media increases with increasing through-plane orientation of the fibers, but is independent of their in-plane orientations.
- With regard to the role of fiber diameter, it was found that there exists a fiber diameter for which heat transfer through a fibrous media is minimal, ranging between 3 to 10 µm for glass fibers operating in a temperature range of about 400–750 K. For mineral wool fibers, this optimal fiber diameter at a temperature of 479 K was observed to be 5 µm.
- Increasing the fiber diameter dissimilarity affects the thermal insulation capability of a material. It is obvious from the above conclusion that if the material consists of a greater number of fibers with the optimal fiber diameter, the material is a good insulator.
- The contribution of conduction and radiation heat transfer to the total heat transfer through the insulation material depends on its fiber diameter, through-plane orientation, SVF and thickness.

From the parameter study conducted here, the following are recommendations for designing optimal heat insulation:

Table 6.1: Recommendations for optimal insulation design

increasing	radiation	conduction	design recommendation
solid volume fraction	decrease	increase	find the optimum
fiber diameter	has a unique optimal value	increases	find the optimum
in-plane orientation	no effect	no effect	does not matter
through-plane orientation	increase	increase	reduce the through-plane orientation
fiber dissimilarity	fiber diameter dependent	increases	find optimum blend
fiber-to-fiber contact	no effect	increases	reduce fiber-to-fiber contact

There are several topics of research arising from this work which could be pursued:

- This work can directly be extended to study effects of different fiber cross-sectional shapes on the heat insulation performance of the materials.
- In this study refractive index of the fiber material is obtained at the source temperature. However a more accurate prediction of radiation heat transfer can be made if the fiber refractive index is obtained for the fiber temperature and hence should be explored.

- The interstitial fluid in the current simulations is assumed to be vacuum or air. This method can also be extended to cases where a binder is used as the interstitial phase.
- Another assumption made in this work was the independent scattering assumption. An approach relaxing this assumption is based on including the effects of dependent scattering. This work can be extended to predicting insulation performance of denser fibrous insulations when dependent scattering effects are included.
- This work can also be extended to conduct a transient study on heat transfer in insulation materials. The time dependent effects of conduction and radiation on the heat insulation can be studied. This is especially important for problems like shuttle re-entry.
- The current simulation approach can also be modified to model media with crimped fibers

List of References

List of References

Arambakam R., Hosseini S.A., Tafreshi H.V., and Pourdeyhimi B., A Monte Carlo Simulation of Radiative Heat through Fibrous Media: Effects of Boundary Conditions and Microstructural Parameters, International Journal of Thermal Sciences **50**, 941 (2011).

Arambakam R., Tafreshi H.V., and Pourdeyhimi B., A Simple Simulation Method for Designing Fibrous Insulation Materials, Materials and Design **44**, 99 (2013a).

Arambakam R., Tafreshi H.V., and Pourdeyhimi B., Analytical Monte Carlo Ray Tracing Simulation of Radiative Heat Transfer through Bimodal Fibrous Insulations with Translucent Fibers, International Journal of Heat and Mass Transfer **55**, 7234 (2012).

Arambakam R., Tafreshi H.V., and Pourdeyhimi B., Dual-Scale 3-D Approach for Modeling Radiative Heat Transfer in Fibrous Insulations, International Journal of Heat and Mass Transfer **64**, 1109 (2013b).

Argento C., Bouvard D., A Ray Tracing Method for Evaluating the Radiative Heat Transfer in Porous Media, International Journal of Heat and Mass Transfer **39** (15), 3175 (1996).

Baillis D., Sacadura J.F., Thermal Radiation Properties of Dispersed Media: Theoretical Prediction and Experimental Characterization, Journal of Quantitative Spectroscopy and Radiative Transfer **67** (5)**,** 327 (2000).

Bankvall C., Heat Transfer in Fibrous Materials, J Test Eval **1** (3), 235 (1973).

Bhattacharya R.K., Heat-transfer Model for Fibrous Insulations, Thermal Insulation Performance, American Society of Testing and Materials **718**, 272 (1980).

Bohren C.F. and Huffman D.R., Absorption and Scattering of Light by Small Particles (Wiley, 1983).

Bohren C.F. and Huffman D.R., Absorption and Scattering of Light by Small Particles, Wiley (1983)

Boulet P., Jeandel G. and Morlot G., Model of Radiative Transfer in Fibrous Media – Matrix Method, International Journal of Heat and Mass Transfer **36** (18), 4287 (1993).

Brewster M.Q., Thermal Radiative Transfer and Properties (Wiley, 1992).

Chandrasekhar S., Radiative Transfer (Dover Publications Inc., New York, 1960).

Clague D.S. and Phillips R.J., A Numerical Calculation of the Hydraulic Permeability of Three-dimensional Disordered Fibrous Media, Physics of Fluids **9**, 1562 (1997).

Coquard R., Baillis D., Radiative properties of Dense Fibrous Medium Containing Fibers in the Geometric Limit, Journal of Heat Transfer **128** (10), 926 (2005).

Coquard R., Baillis D., Radiative Properties of Dense Fibrous Medium Containing Fibers in the Geometric Limit, Journal of Heat Transfer-Transactions of the ASME, **128** (10), 1022 (2006).

Cunnington G. R., Lee S. C., Radiative Properties of Fibrous Insulations: Theory versus Experiment, Journal of Thermophysics and Heat Transfer **10** (3), 460 (1996).

Faessel M., Delisee C., Bos F., Castera P., 3D Modelling of Random Cellulosic Fibrous Networks Based on X-ray Tomography and Image Analysis, Composite Science and Technology **65 (**13), 1931 (2005).

Fu S. and Mai Y., Thermal Conductivity of Misaligned Short-fiber-reinforced Polymer Composites, Journal of Applied Polymer Science **88** (6), 1497 (2003).

Furmanski P., Influence of Different Parameters on the Effective Thermal Conductivity of Short-fiber Composites, Journal of Thermoplastic Composite Materials **4**, 349 (1991).

Houston R.L. and Korpela S.A., Heat Transfer through Fiberglass Insulation, Proceedings of the 7th International Heat Transfer Conference, Munchen, Federal Republic of Germany, 499 (1982).

Howell J.R., Siegel R. and Menguc M.P., Thermal Radiation Heat Transfer (CRC Press, Florida, 2011).

Hsieh C.K. and Su K.C., Thermal Radiative Properties of Glass from 0.32 to 206µm, Solar Energy **22**, 37 (1979).

Incropera F.P., DeWitt D.P., Bergman T.L., and Lavine A.S., Fundamentals of Heat and Mass Transfer (6th ed., Wiley, 2006)

Larkin B.K. and Churchill S.W., Heat Transfer by Radiation through Porous Insulations, AICHE Journal **5** (4)**,** 467 (1959).

Larkin B.K., A Study of the Rate of Thermal Radiation through Porous Insulating Materials, PhD. Dissertation, The University of Michigan 1957.

Lee S.C., Dependent vs. Independent Scattering in Fibrous Composites Containing Parallel Fibers, Journal of Thermophysics and Heat Transfer **8** (4), 641 (1994).

Lee S.C., Effect of Fiber Orientation on Thermal-Radiation in Fibrous Media, International Journal of Heat and Mass Transfer **32**, 311 (1989).

Lee S.C., Radiative Transfer through a Fibrous Medium: Allowance for Fiber Orientation, Journal of Quantitative Spectroscopy and Radiative Transfer **8** (4), 641 (1994).

Lee S.C., Scattering Phase Function for Fibrous Media, International Journal of Heat and Mass Transfer **33** (10), 2183 (1990).

Lind A.C. and Greenberg J.M., Electromagnetic Scattering by Obliquely Oriented Cylinders, Journal of Applied Physics **37** (8), 3195 (1966).

Liou K.N., Electromagnetic Scattering by Arbitrarily Oriented Ice Cylinders, Applied Optics **11** (3), 667 (1972).

Ljungdhal G., Fellman J. and Ribbing C. G., Infrared Optical Constants of Mineral Wool Raw Materials, *J. Non-Cryst. Solids* **136**, 137 (1991).

McKay N.L., Timusk T. and Farnworth B., Determination of Optical Properties of Fibrous Thermal Insulation, Journal of Applied Physics **55** (11)**,** 4064 (1984).

Milandri A., Asllanaj F. and Jeandel G., Determination of Radiative Properties of Fibrous Media by an Inverse Method – Comparison with Mie Theory, Journal of Quantitative Spectroscopy and Radiative Transfer **74**, 637 (2002).

Mohammadi M., Banks-Lee P. and Ghadimi P., Determining Effective Thermal Conductivity of Multilayered Nonwoven Fabrics, Textile Research Journal **73** (9), 802 (2003b).

Mohammadi M., Banks-Lee P. and Ghadimi P., Determining Radiative Heat Transfer Through Heterogeneous Multilayer Nonwoven Materials, Textile Research Journal **73** (10), 896 (2003a).

Spielman L., Goren S. L., Model for Predicting Pressure Drop and Filtration Efficiency in Fibrous Media, Environmental Science and Technology **2**, 279 (1968).

Tian M., Zhu S., Chen Q. and Pan N., Effects of Layer Stacking Sequence on Themperature Response of Multi-Layer Composite Materials Under Dynamic Conditions, *Appl. Therm. Eng.* **33-34**, 219 (2012).

Tong T.W. and Tien C.L., Analytical Models for Thermal Radiation in Fibrous Media, *J. Therm. Insul.* **4**, 27 (1980).

Vallabh R., Banks-Lee P. and Mohammadi M., Determination of Radiative Thermal Conductivity in Needlepunched Nonwovens, Journal of Engineered Fibers and Fabrics **3** (4), 46 (2008).

Vassal J-P., Orgeas L. and Favier D., Modelling Microstructure effects on the Conduction in Fibrous Materials with Fibre-fibre Interface Barriers, Modelling and Simulation in Materials Science and Engineering **16**, 35007 (2008).

Wang Q., Maze B., and Tafreshi H. V., and Pourdeyhimi B., "Simulating Through-plane Permeability of Fibrous Materials with Different Fiber Lengths," Modelling and Simulation in Materials Science and Engineering **15**, 855 (2007).

Zappe H., Fundamentals of Micro-Optics (1st ed., Cambridge University Press 2010).

Zhang B., Xie W., Du S., Zhao S., An Experimental Study of Effective Thermal Conductivity of High Temperature Insulations, Journal of Heat Transfer –Transactions of the ASME **130**, 34504 (2008).

Zhang B., Zhao S. and He X., Experimental and Theoretical Studies on High Temperature Thermal Properties of Fibrous Insulation, Journal of Quantitative Spectroscopy and Radiative Transfer **109**, 1309 (2008).

Zhang T. and Yi Y. B., Monte Carlo Simulations of Effective Electrical Conductivity in Short-fiber Composites, Journal of Applied Physics **103**, 014910 (2008).

Zhao S., Zhang B. and Du S., Effects of Contact Resistance on Heat Transfer Behaviors of Fibrous Insulation, Chinese Journal of Aeronautics **22**, 569 (2009).

Zhou W., Tang Y., Song R., Jiang L., Hui K.S. and Hui K.N., Characterization of Electrical Conductivity of Porous Metal Fiber Sintered Sheet Using Four-point Probe Method, Materials and Design **37**, 161 (2012).

Appendix A[5]

Two Flux Model

In the two flux model, it is assumed that rays scatter only in the forward and backward directions. The fraction of the energy in the forward and backward directions are represented by F_e and B_e, respectively, with the condition that $F_e + B_e = 1$. Let $i_{\lambda 1}$ and $i_{\lambda 2}$ represent the monochromatic radiant flux towards the sink and the source plates, respectively. If n represents the number of scattering bodies (fibers here) per unit volume, then the rate of change of $i_{\lambda 1}$ in the direction x is given as:

$$\frac{di_{\lambda 1}}{dx} = -n(S_{S\lambda} + S_{a\lambda})i_{\lambda 1} + nF_{e\lambda}S_{S\lambda}i_{\lambda 1} + nB_{e\lambda}S_{S\lambda}i_{\lambda 2} + n\varepsilon_{\lambda}A_f g_{\lambda}(T) \qquad \text{(A-1)}$$

where λ is the wavelength, A is the emitting area of a fiber in the insulation, ε_{λ} is the emissivity, and $g_{\lambda}(\lambda, T)$ is the Planck's radiation function, which provides the energy radiated at each wave length for a body. The scattering and absorption cross sections are shown by S_S and S_a. Scattering (or absorption) cross section is defined as the fraction of energy scattered (or absorbed) from a beam carrying a unit of energy per unit area normal to the direction of propagation. Integrating Eq. A-1 over all wavelengths, using the

[5] Contents of this appendix have been published in an article entitled "Analytical Monte Carlo Ray Tracing simulation of radiative heat transfer through bimodal fibrous insulations with translucent fibers", by R. Arambakam, H.V. Tafreshi, and B. Pourdeyhimi, *International Journal of Heat and Mass Transfer* **55**, 7234 (2012).

Kirchoff's law ($S_a = \varepsilon A_f$), and Planck's radiation function $\int_0^\infty g(\lambda,T)\,d\lambda = \sigma T^4$, we obtain the total flux transmitted from the sink to the source as:

$$\frac{dq_1}{dx} = -n(B_e S_S + S_a)q_1 + nB_e S_S q_2 + nS_a \sigma T^4 \qquad \text{(A-2)}$$

where $q_1 = \int_0^\infty i_1(\lambda)d\lambda$, which represents the radiant power per unit area traveling from the sink to the source. (Larkin, 1957) divided the radiative parameters into three groups defined as follows:

$$M = \left(nB_e S_S + S_a\right) \qquad \text{(A-3)}$$

$$N = nB_e S_S \qquad \text{(A-4)}$$

$$P = M - N = nS_a \qquad \text{(A-5)}$$

Here M, N and P are the interception, scattering, and absorption cross sections, for a unit volume of an insulation medium, respectively. Therefore:

$$\frac{dq_1}{dx} = -Mq_1 + Nq_2 + P\sigma T^4 \qquad \text{(A-6)}$$

By solving the flux equations in the absence of internal emission, (Larkin, 1957) developed an equation for the heat flux transmittance through an insulation material as follows:

$$q_1(0) = \frac{2\sqrt{M^2 - N^2}}{\sqrt{M^2 - N^2} + M} e^{-l\sqrt{M^2-N^2}} \sum_{n=0}^{\infty} (-1)^n \left[\frac{\sqrt{M^2 - N^2} - M}{\sqrt{M^2 - N^2} + M}\right]^n e^{-2nl\sqrt{M^2-N^2}} \qquad \text{(A-7)}$$

The values of N, M and P can be obtained from Figure A.1–A.3 respectively.

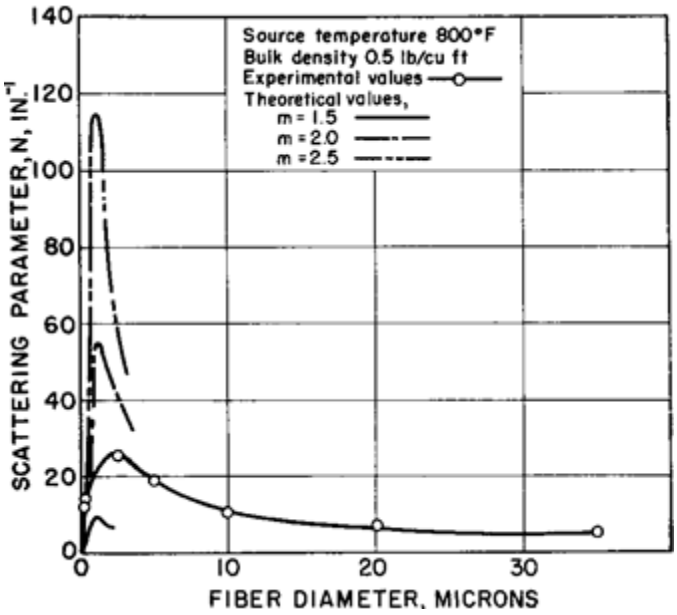

Figure A-1: Scattering parameter for glass fibers. This plot has been taken from the work of Larkin, 1957.

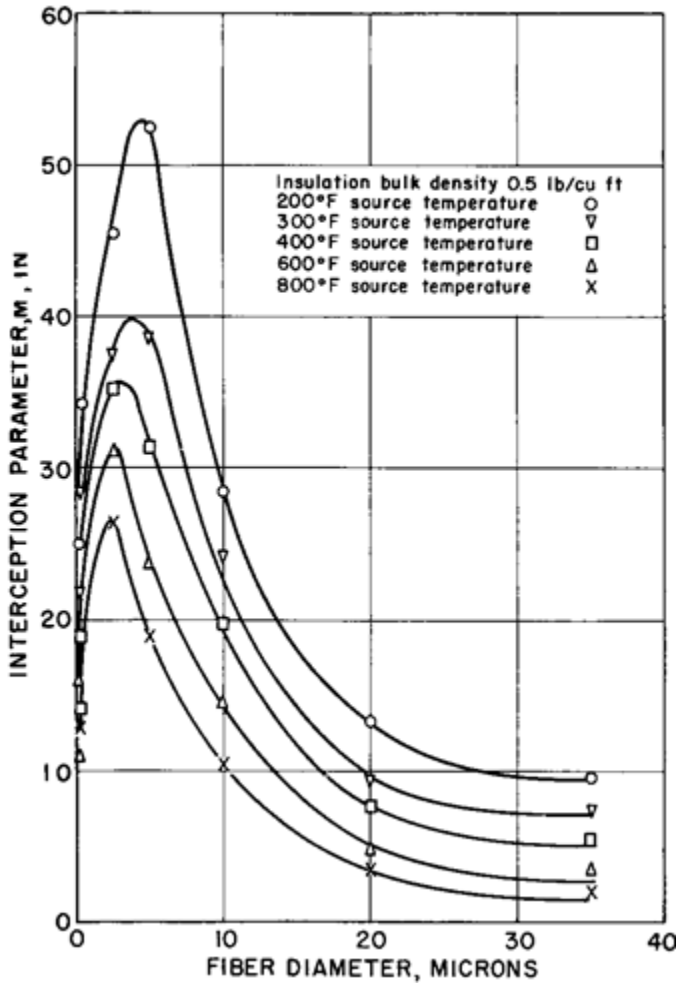

Figure A-2: Interception parameter for glass fibers. This plot has been taken from the work of Larkin, 1957.

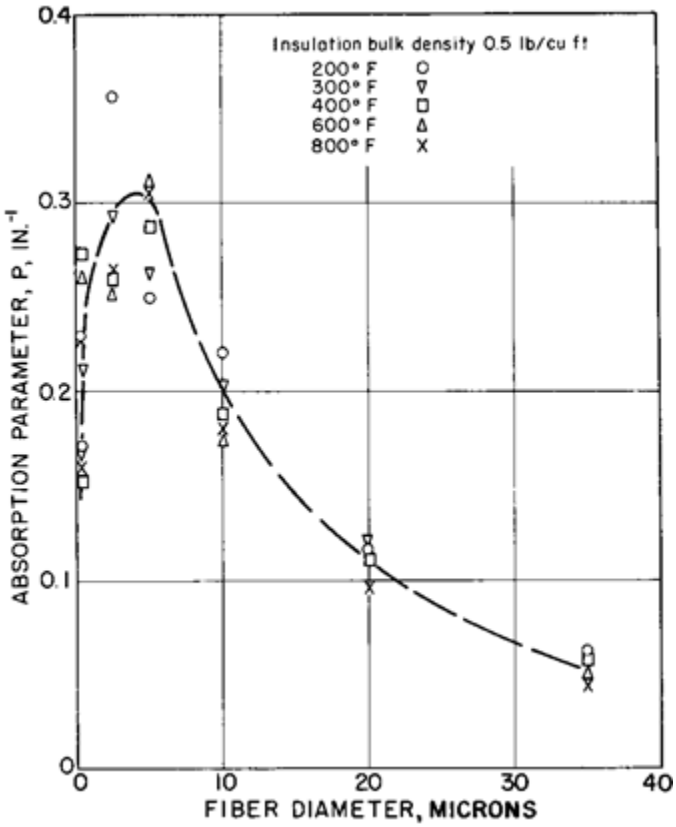

Figure A-3: Absorption parameter for glass fibers. This plot has been taken from the work of Larkin, 1957.

Appendix B[6]

Equations of Electromagnetic Theory

The scalar wave equation is a PDE and the solution of interaction of an IR wave with a cylinder can be mathematically found using separation of variables and is a function of the fiber diameter, fiber through-plane orientation angle, fiber refractive index, and wavelength (Bohren and Huffman, 1983). A polarized IR wave is composed of two mutually perpendicular electric and magnetic waves. A solution to the wave cylinder interaction for such cases is given by a set of vector cylindrical harmonics (Bohren and Huffman, 1983). The IR wave incident on a cylindrical fiber can be grouped into two cases depending upon whether the electric or magnetic component of the wave is polarized parallel or perpendicular to the fiber axis. The relation between incident and scattered intensity wave can be written in a matrix notation as, (Bohren and Huffman, 1983)

$$\begin{pmatrix} E_{Is} \\ E_{IIs} \end{pmatrix} = e^{i\frac{3\pi}{4}} \sqrt{\frac{2}{\pi kr \sin\phi_C}} e^{ik(r\sin\phi_C - z\cos\phi_C)} \begin{pmatrix} T_1 & T_4 \\ T_3 & T_2 \end{pmatrix} \begin{pmatrix} E_{Ii} \\ E_{IIi} \end{pmatrix} \tag{B-1}$$

where

$$T_1 = b_{0\mathrm{I}} + 2\sum_{n=1}^{\infty} b_{n\mathrm{I}} \cos(n\eta) \tag{B-2}$$

[6] Contents of this appendix have been published in an article entitled "Dual-Scale 3-D Approach for Modeling Radiative Heat Transfer In Fibrous Insulations", by R. Arambakam, H.V. Tafreshi, and B. Pourdeyhimi, *International Journal of Heat and Mass Transfer* **64**, 1109 (2013).

$$T_2 = a_{0\mathrm{II}} + 2\sum_{n=1}^{\infty} a_{n\mathrm{II}} \cos(n\eta) \tag{B-3}$$

$$T_3 = -2i\sum_{n=1}^{\infty} a_{n\mathrm{I}} \sin(n\eta) \tag{B-4}$$

$$T_4 = -2i\sum_{n=1}^{\infty} b_{n\mathrm{II}} \sin(n\eta) \tag{B-5}$$

are the elements of the scattering matrix given in Eq. B-1. This mathematical framework is built around the assumption that the fiber is infinitely long (length to diameter ratio is very high). The energy of scattered wave at large distance from the fiber, when the electric wave is parallel to the cylinder axis is given by the expression

$$E_{\mathrm{Is}} = -\sum_{n=-\infty}^{\infty} E_n \left[b_{n\mathrm{I}} N_n + i a_{n\mathrm{I}} M_n \right] \tag{B-6}$$

The expansion coefficients $a_{n\mathrm{I}}$ and $b_{n\mathrm{I}}$ can be expressed in terms of Henkel and Bessel functions as follows.

$$a_{n\mathrm{I}} = \frac{C_n V_n - B_n D_n}{W_n V_n + i D_n^2} \tag{B-7}$$

$$b_{n\mathrm{I}} = \frac{W_n B_n + i D_n C_n}{W_n V_n + i D_n^2} \tag{B-8}$$

The individual terms in the above equation are given as,

$$B_n = \tilde{\xi}\left[m^2 \tilde{\xi} J_n'(\tilde{\eta}) J_n(\tilde{\xi}) - \tilde{\eta} J_n(\tilde{\eta}) J_n'(\tilde{\xi}) \right] \tag{B-9}$$

$$C_n = n\cos\phi\tilde{\eta} J_n(\tilde{\eta}) J_n(\tilde{\xi}) \left(\frac{\tilde{\xi}^2}{\tilde{\eta}^2} - 1 \right) \tag{B-10}$$

$$D_n = n\cos\phi\tilde{\eta}J_n(\tilde{\eta})\tilde{H}_n(\tilde{\xi})\left(\frac{\tilde{\xi}^2}{\tilde{\eta}^2}-1\right) \tag{B-11}$$

$$V_n = \tilde{\xi}\left[m^2\tilde{\xi}J_n'(\tilde{\eta})\tilde{H}_n(\tilde{\xi}) - \tilde{\eta}J_n(\tilde{\eta})\tilde{H}_n'(\tilde{\xi})\right] \tag{B-12}$$

$$W_n = i\tilde{\xi}\left[\tilde{\eta}J_n(\tilde{\eta})\tilde{H}_n'(\tilde{\xi}) - \tilde{\xi}J_n'(\tilde{\eta})\tilde{H}_n(\tilde{\xi})\right] \tag{B-13}$$

where $\tilde{\xi} = x\sin\phi_C$, $\tilde{\eta} = x\sqrt{m^2-\cos^2\phi_C}$ and $x = kd_f/2$.

Similarly for the case where the magnetic component is parallel to the cylinder axis, the scattered wave is given by the expression

$$E_{\mathrm{IIs}} = \sum_{n=-\infty}^{\infty} E_n\left[ia_{n\mathrm{II}}M_n + b_{n\mathrm{II}}N_n\right] \tag{B-14}$$

Here M_n and N_n are the vector cylindrical harmonics and the corresponding expansion coefficients are given as

$$a_{n\mathrm{II}} = -\frac{A_nV_n - iC_nD_n}{W_nV_n + iD_n^2} \tag{B-15}$$

$$b_{n\mathrm{II}} = -i\frac{C_nW_n + A_nD_n}{W_nV_n + iD_n^2} \tag{B-16}$$

where $A_n = i\tilde{\xi}\left[\tilde{\xi}J_n'(\tilde{\eta})J_n(\tilde{\xi}) - \tilde{\eta}J_n(\tilde{\eta})J_n'(\tilde{\xi})\right]$.

Appendix C[7]

Experimental Results of Houston and Korpela

case	T_1 (K)	T_2 (K)	q_C	q_R	q_T	q_E	error (%)
1	308.8	285.2	16.41	10.94	27.35	28.49	4
2	337.3	285.3	37.78	28.5	66.28	68.86	3.7
3	365.2	285.6	59.49	52.75	112.24	116.66	3.8
4	392.7	285.7	83.36	83.36	166.72	173.56	3.9

Table C-1: Calculated contribution from conduction q_C (W/m^2) and radiation q_R (W/m^2) to the total flux q_T (W/m^2) compared to the experimentally measured heat flux q_E (W/m^2). T_1 and T_2 are the hot plate and cold plate temperature respectively. The values are for fiberglass with a bulk density of 8.82 kg/m^3 placed between two plates of emissivity 0.83 and with insulation thickness of 3.8 cm.

[7] The values of heat flux in this appendix are obtained from the paper, "Heat Transfer through Fiberglass Insulation", by R. L. Houston and S. A. Korpela, *Proceedings of the 7th International Heat Transfer Conference, Munchen, Federal Republic of Germany*, 499 (1982).

Appendix D[8]

Refractive Indices of Glass at Different Temperature

wavelength	temperature	n	k
2.5	1159.1074	1.492	1.13E-05
3	965.9228333	1.494	1.07E-04
4	724.442125	1.497	1.69E-04
4.95	585.4077778	1.5	1.60E-03
5.36	540.6284515	1.4	2.00E-02
5.77	502.2129116	1.31	4.00E-02
5.9	491.1472034	1.32	4.00E-02
6.05	478.97	1.33	5.00E-02
6.2	467.3820161	1.32	4.00E-02
6.36	455.623978	1.31	4.00E-02
6.52	444.4430215	1.28	3.00E-02
6.7	432.5027612	1.26	3.00E-02
6.89	420.5759797	1.23	3.00E-02
7.08	409.2893362	1.21	4.00E-02
7.29	397.4991084	1.17	5.00E-02
7.51	385.8546605	1.13	7.00E-02
7.75	373.9056129	1.07	1.20E-01
8	362.2210625	1	1.50E-01
8.26	350.819431	0.79	3.00E-01
8.55	338.9202924	0.78	5.80E-01
8.85	327.4314689	0.92	8.50E-01
9.18	315.6610566	1.05	1.08E-02
9.53	304.0680483	1.6	1.24E-02
9.92	292.1137601	1.85	9.50E-01
10.33	280.5196999	2.01	8.50E-01

Table D-1: Refractive indices of glass at different temperatures

[8] The values of refractive indices in this Appendix are obtained from the paper, "Thermal Radiative Properties of Glass from 0.32 to 206μm", by C.K. Hsieh and K.C. Su, *Sol. Energy* **22**, 37 (1979).

Appendix E[9]

Refractive Indices of Mineral Wool at Different Temperatures

wavelength	temperature	n	k
3	965.9228333	-	-
3.5	827.9338571	-	-
4	724.442125	-	-
4.5	643.9485556	-	-
5	579.5537	1.53	1.45E-02
6	482.9614167	1.526	2.32E-02
6.5	445.8105385	1.491	2.98E-02
6.8	426.1424265	1.458	3.29E-02
7	413.9669286	1.436	4.09E-02
7.2	402.4678472	1.411	4.74E-02
7.4	391.5903378	1.385	5.51E-02
7.6	381.2853289	1.348	6.15E-02
7.8	371.5087821	1.303	7.86E-02
8	362.2210625	1.26	9.98E-02
8.2	353.3864024	1.202	1.26E-01
8.4	344.9724405	1.137	1.70E-01
8.6	336.9498256	1.082	2.48E-01
8.8	329.291875	1.032	3.55E-01
9	321.9742778	1.001	4.93E-01
9.2	314.974837	1.009	6.53E-01
9.4	308.2732447	1.07	8.15E-01
9.6	301.8508854	1.178	9.47E-01
9.8	295.6906633	1.307	1.04E+00
10	289.77685	1.436	1.09E+00

Table E-1: Refractive indices of mineral wool at different temperatures (trial 1)

[9] The values of refractive indices in this Appendix are obtained from the paper, "Ribbing, Infrared Optical Constants of Mineral Wool Raw Materials", by G. Ljungdhal, J. Fellman and C. G. Ribbing, *J. Non-Cryst. Solids* **136**, 137 (1991).

wavelength	temperature	n	k
3	965.9228	-	-
3.5	827.9339	1.558	9.42E-03
4	724.4421	1.549	9.60E-03
4.5	643.9486	1.536	1.08E-02
5	579.5537	1.519	1.20E-02
6	482.9614	1.468	2.03E-02
6.5	445.8105	1.437	2.81E-02
6.8	426.1424	1.407	3.00E-02
7	413.9669	1.388	3.86E-02
7.2	402.4678	1.364	4.59E-02
7.4	391.5903	1.343	5.44E-02
7.6	381.2853	1.311	6.02E-02
7.8	371.5088	1.27	7.67E-02
8	362.2211	1.232	9.82E-02
8.2	353.3864	1.183	1.23E-01
8.4	344.9724	1.125	1.65E-01
8.6	336.9498	1.075	2.36E-01
8.8	329.2919	1.03	3.36E-01
9	321.9743	1.004	4.70E-01
9.2	314.9748	1.019	6.24E-01
9.4	308.2732	1.089	7.78E-01
9.6	301.8509	1.211	8.97E-01
9.8	295.6907	1.352	9.66E-01
10	289.7769	1.489	9.94E-01

Table E-2: Refractive indices of mineral wool at different temperatures (trial 2)

wavelength	temperature	n	k
3	965.9228	-	-
3.5	827.9339	1.567	7.89E-03
4	724.4421	1.56	8.44E-03
4.5	643.9486	1.547	8.94E-03
5	579.5537	1.532	1.01E-02
6	482.9614	1.483	1.69E-02
6.5	445.8105	1.453	2.34E-02
6.8	426.1424	1.424	2.45E-02
7	413.9669	1.406	3.24E-02
7.2	402.4678	1.383	3.93E-02
7.4	391.5903	1.362	4.73E-02
7.6	381.2853	1.331	5.31E-02
7.8	371.5088	1.291	6.97E-02
8	362.2211	1.255	9.03E-02
8.2	353.3864	1.208	1.15E-01
8.4	344.9724	1.151	1.55E-01
8.6	336.9498	1.104	2.22E-01
8.8	329.2919	1.062	3.17E-01
9	321.9743	1.036	4.44E-01
9.2	314.9748	1.049	5.95E-01
9.4	308.2732	1.117	7.48E-01
9.6	301.8509	1.235	8.65E-01
9.8	295.6907	1.374	9.36E-01
10	289.7769	1.512	9.64E-01

Table E-3: Refractive indices of mineral wool at different temperatures (trial 3)

wavelength	temperature	n	k
3	965.9228	-	-
3.5	827.9339	-	-
4	724.4421	1.568	1.61E-02
4.5	643.9486	1.553	1.83E-02
5	579.5537	1.534	2.05E-02
6	482.9614	1.481	2.78E-02
6.5	445.8105	1.443	3.31E-02
6.8	426.1424	1.414	3.85E-02
7	413.9669	1.392	4.30E-02
7.2	402.4678	1.368	4.81E-02
7.4	391.5903	1.339	5.44E-02
7.6	381.2853	1.304	6.26E-02
7.8	371.5088	1.263	7.44E-02
8	362.2211	1.219	8.67E-02
8.2	353.3864	1.156	1.03E-01
8.4	344.9724	1.073	1.35E-01
8.6	336.9498	0.997	2.12E-01
8.8	329.2919	0.915	3.30E-01
9	321.9743	0.853	4.96E-01
9.2	314.9748	0.846	6.88E-01
9.4	308.2732	0.902	8.87E-01
9.6	301.8509	1.024	1.063
9.8	295.6907	1.193	1.191
10	289.7769	1.377	1.263

Table E-4: Refractive indices of mineral wool at different temperatures (trial 4)

wavelength	temperature	n	k
3	965.9228	1.477	8.06E-03
3.5	827.9339	1.465	1.02E-02
4	724.4421	1.45	1.30E-02
4.5	643.9486	1.432	1.59E-02
5	579.5537	1.409	1.86E-02
6	482.9614	1.342	2.62E-02
6.5	445.8105	1.289	3.51E-02
6.8	426.1424	1.249	4.43E-02
7	413.9669	1.219	5.21E-02
7.2	402.4678	1.183	6.19E-02
7.4	391.5903	1.165	8.27E-02
7.6	381.2853	1.098	9.06E-02
7.8	371.5088	1.044	1.06E-01
8	362.2211	0.959	1.29E-01
8.2	353.3864	0.849	2.21E-01
8.4	344.9724	0.746	3.74E-01
8.6	336.9498	0.704	5.66E-01
8.8	329.2919	0.729	7.63E-01
9	321.9743	0.799	9.33E-01
9.2	314.9748	0.88	1.105
9.4	308.2732	1.018	1.297
9.6	301.8509	1.248	1.45
9.8	295.6907	1.533	1.497
10	289.7769	1.787	1.44

Table E-5: Refractive indices of mineral wool at different temperatures (average values of refractive indices given in Tables E-1– E-4). These values were used for the computations in Chapter 5.

VITA

RAGHU ARAMBAKAM

EDUCATION

Doctor of Philosophy, Mechanical and Nuclear Engineering December 2013

Virginia Commonwealth University, Richmond, Virginia, USA GPA: 3.75

Master of Science, Mechanical and Aerospace Engineering May 2010

Oklahoma State University, Stillwater, Oklahoma, USA GPA: 3.42

Bachelor of Technology, Mechanical Engineering May 2008

Jawaharlal Nehru Technological University, Hyderabad, India GPA: 3.90

TECHNICAL PUBLICATIONS

JOURNAL:

1. **R. Arambakam,** H.V. Tafreshi, and B. Pourdeyhimi, Modeling Performance of Multi-Component Fibrous Insulations against Conductive and Radiative Heat Transfer, *International Journal of Heat and Mass Transfer* (under review).
2. **R. Arambakam,** H.V. Tafreshi, and B. Pourdeyhimi, Dual-Scale 3-D Approach for Modeling Radiative Heat Transfer in Fibrous Insulations, *International Journal of Heat and Mass Transfer* 64, (2013) 1109-1117.
3. **R. Arambakam,** H.V. Tafreshi, and B. Pourdeyhimi, A Simple Simulation Method for Designing Fibrous Insulation Materials, *Materials and Design* 44, (2013) 99-106.

4. **R. Arambakam,** H.V. Tafreshi, and B. Pourdeyhimi, Analytical Monte Carlo Ray Tracing Simulation of Radiative Heat Transfer through Bimodal Fibrous Insulations with Translucent Fibers, *International Journal of Heat and Mass Transfer* 55, (2012) 7234-7246.
5. **R. Arambakam**, S.A. Hosseini, H.V. Tafreshi, and B. Pourdeyhimi, A Monte Carlo Simulation of Radiative Heat through Fibrous Media: Effects of Boundary Conditions and Microstructural Parameters, *International Journal of Thermal Sciences* 50, (2011) 935-941.

CONFERENCE:

1. **R. Arambakam,** S.A. Hosseini, and H.V. Tafreshi, A 2-D Monte Carlo Simulation of Radiative Heat in Fibrous Media, *NET Innovative Nonwovens Conference*, Raleigh NC, November 2010.
2. M.A. Tahir, H.V. Tafreshi, **R. Arambakam** and B. Pourdeyhimi, Modeling Radiative Heat Transfer in Fibrous Insulation Media, *NET Innovative Nonwovens Conference*, Raleigh NC, November 2010.

TECHNICAL SKILLS

CFD: Ansys Fluent 14 with knowledge of developing User Defined Functions (UDFs), Geodict

Math: MATLAB, Mathematica 8, Maple

CAD: Auto-CAD, CATIA, ProE, SolidWorks

Virtual Instrumentation: LabVIEW

Programming: C++, FORTRAN, and Python

TEACHING EXPERIENCE

Graduate Teaching Assistant August 2008 – May 2010

Oklahoma State University, Dept. of Mechanical and Aerospace Engineering OK, USA

- Assisted students in Measurements and Instrumentation Lab
- Provided assistance to students for using LabVIEW
- Graded homework, quizzes and exams

Graduate Teaching Assistant January 2013 – May 2013

Virginia Commonwealth Univ., Dept. of Mechanical and Nuclear Engineering VA, USA

- Administrated online classroom
- Graded homework, quizzes and exams

AWARDS

- Received special recognition for research excellence from School of Engineering at Virginia Commonwealth University for the year 2012-2013.
- Financial support for current research is provided by The Nonwovens Institute at NC State University.
- Financial support for Master of Science research was provided by Oklahoma State University.